INSTITUTO SUPERIOR TÉCNICO
Universidade Técnica de Lisboa

A Statistical 3D MIMO Radio Channel Model for UMTS

Filipe Miguel Gomes Leonardo

Dissertation submitted for obtaining the degree of
Master in Electrical and Computer Engineering

Jury

Supervisor: Prof. Luís M. Correia

President: Prof. António L. C. Topa

Members: Prof. Carlos Fernandes

September 2008

To my parents and sister

Acknowledgements

At first and the main thank goes to Professor Luis Correia, who gave me this unique opportunity to write my master thesis inserted in the international project NEWCOM++. I am thankful for all the valuable knowledge (professional and personal) he gave me as well for his time and mostly patience along the last year. This work was only possible to do with the demanded and desired quality given his orientation, help, constant support and useful guidelines. Discipline, hard work, perfectionism were few of many lessons that I have taken from him. A great thank for all.

I have also to thank to all the GROWers and the possibility to attend our periodic meetings. This allowed me to contact with several other areas of wireless and mobile communications and learn about them as well as to improve my speaking abilities. I would also to thank to Martijn Kuipers for his knowledge and availability that help me to do some decisions in the beginning of my work.

I also want to express my gratitude to my dear colleagues, Sara Duarte, Ricardo Preguiça, Vikash Mukesh, Armando Marques and Telmo Baptista for their critical suggestions and constant support. Their friendship and joy were really important in the development of this thesis. I have to thank too, to my dear friend Luís Gomes, who was a great help in several parts of this work, helping me to overcome some problems. His availability, friendship and good will are just a few of many reasons why I have a high regard for him. I am also grateful to my housemate, Adriano Andrade for his programming hints.

Special thank to a special and unique person, Catarina Varge, for her love, attention, support, friendship, encouragement and mainly for her patient along the last year. With her on my side, everything else is easier and could be overcome.

Finally, to the persons responsible for who I am, I send my acknowledgements to my parents and sister to whom I am very grateful to make this possible. It was their support, love and care who help me during the hardest times. Their incentive, motivation and encouragement were key factors to finish the work. I know I can always count on them. This achievement in not only mine but also of them.

Abstract

The aim of this work is to introduce a 3D single bounce MIMO radio channel model. The main motivation is that existing models, which account only for a 2D environment are not able to properly simulate a radio channel, in particular for indoor scenarios. As an indoor environment consists of many obstacles, which are really not deployed on the 2D plane, it seems vital to take a 3D environment into account. A comparison between the two models is done. Spatio-temporal radio channel parameters and relative capacity gain of MIMO were simulated for small-, medium- and large-sized rooms, as well for a street scenario. The analysis of the capacity gain of MIMO relative to SISO has been made for UMTS. The MIMO system was simulated for the several scenarios with a varying number of input and output antennas, and for time resolutions of the receiver of 0.1 and 260 ns. Results show that angular spread increases, when the 3D single bounce model is taken into account, for all the considered scenarios compared with the 2D one. For the street scenario, only with a street width factor of 2 in the 2D model, maximum delay and delay spread can be as large as 3D multipath components that exist in a real environment. The difference between the two models is significant, since for a 16×16 MIMO system a in street and medium-sized room scenarios, the relative MIMO capacity gain for the 3D model is over than 20% higher than in the 2D one. So, by using a 3D single bounce model, the radio environment can be more accurately simulated.

Keywords

Channel Models. Single bounce. MIMO. Delay spread. Angle spread. Capacity.

Resumo

O objectivo deste trabalho é introduzir o modelo de canal rádio MIMO 3D com refleção única. A motivação principal prende-se com o facto de os modelos existentes apenas tomarem em consideração um ambiente 2D que não simula o canal rádio de forma precisa, em particular para cenários interiores. Como um ambiente interior é constituído por muitos obstáculos, que não são verazmente representados num plano 2D, torna-se portanto fundamental levar em consideração o ambiente 3D. Desta forma, é feita uma comparação entre os dois modelos. Parâmetros do canal rádio espaço-temporais e o ganho da capacidade relativa do sistema MIMO foram simulados para salas de pequena, média e grandes dimensões bem como para um cenário de estrada. A análise do ganho do ganho do MIMO em relação ao SISO foi feita com referência ao sistema UMTS. O sistema MIMO foi simulado para os vários cenários com um número variável de antenas em ambos os terminais e para uma resolução temporal do receptor de 0.1 e 260 ns.

Os resultados mostram que o espalhamento angular aumenta, quando o modelo 3D de refleção única é considerado, para todos os cenários quando comparado com o mesmo modelo 2D. Para o cenário da estrada, apenas com um factor de largura da estrada de 2 no modelo 2D, o atraso máximo e o espalhamento do atraso podem ser alargados como as componentes multi-percurso 3D que existem num ambiente real.

A diferença entre os dois modelos é significante, uma vez que para um sistema MIMO 16×16 o ganho da capacidade relativa MIMO para o modelo 3D é mais do que 20% superior que no caso 2D para os cenários da estrada e da sala de dimensões medias. Assim, utilizando o modelo 3D de refleção única o ambiente 3D pode ser mais precisamente simulado.

Palavras-chave

Table of Contents

List of Figures

List of Tables

List of Acronyms

3GPP	Third Generation Partnership Project
AMC	Adaptive Modulation and Coding
AoA	Angle of Arrival
AoD	Angle of Departure
BER	Bit Error Rate
BPSK	Binary Phase Shift Keying
BS	Base Station
BTS	Base Transceiver Station
CIR	Channel Impulse Response
CN	Core Network
DB	Double Bounce
DL	Downlink
DoA	Direction of Arrival
DoD	Direction of Departure
E-DCH	Enhanced-Dedicated Channel
FDD	Frequency Division Duplex
GBMB	Geometrically Based Multibounce
GBSB	Geometrically Based Single Bounce
GROW	Group for Research On Wireless
GSCM	Geometry-based Stochastic Channel Model
HOM	Higher Order Modulation
HPBW	Half-Power Beamwidth
HSDPA	High-Speed Downlink Packet Access
HSPA	High-Speed Packet Access
HSUPA	High-Speed Uplink Packet Access
LoS	Line of Sight
LTE	Long Term Evolution
MB	Multiple Bounce
MIMO	Multiple-Input Multiple-Output
MMS	Multimedia Messaging Service
MPC	Multipath Component
MSC	Mobile Switching Centre
MT	Mobile Terminal

PDAP	Power Delay Angle Profile
PDCP	Packet Data Convergence Protocol
QAM	Quadrature Amplitude Modulation
QoS	Quality of Service
QPSK	Quadrature Phase Shift Keying
RAN	Radio Access Network
RCP	Radio Channel Parameter
RLC	Radio Link Control
RMG	Relative MIMO Gain
RMS	Root Mean Square
RNC	Radio Network Controller
RNS	Radio Network Sub-system
RRC	Radio Resource Control
RRM	Radio Resource Management
RT	Ray Tracing
Rx	Receiver
SB	Single Bounce
SC - FDMA	SC – Frequency Division Multiple Access
SCM	Spatial Channel Model
SISO	Single Input Single Output
SNR	Signal to Noise Ratio
SVD	Singular Value Decomposition
TDD	Time Division Duplex
ToA	Time of Arrival
TTI	Transmission Time Interval
Tx	Transmitter
UE	User Equipment
UL	Uplink
UMTS	Universal Mobile Telecommunications System
US	Uncorrelated Scatterers
UTRAN	UMTS Terrestrial RAN
VoIP	Voice over IP
WCDMA	Wideband Code Division Multiple Access
WSS	Wide Sense Stationary
WSSUS	Wide-Sense Stationarity Uncorrelated Scattering
XML	eXtensible Markup Language

List of Symbols

γ	Average power decay
γ_a	Array relative phase
Γ_s	Complex reflection coefficient of scatterer
δ	Phase shift
$\delta(t)$	Dirac delta distribution
θ	Elevation Angle
λ	Wavelength
ξ	SNR
ρ	Correlation
$\bar{\rho}$	Mean correlation among links in a MIMO system
σ_θ	RMS elevation spread
σ_τ	RMS delay spread
σ_φ	RMS azimuth spread
σ_Ω	RMS angle spread
$\mathbf{\Sigma}$	Matrix containing singular values of matrix $\boldsymbol{H}$
τ	Excess Delay
$\bar{\tau}$	Mean Excess Delay
τ_{max}	Maximum Delay
ϕ_S	Phase of the reflection coefficient
Φ_R	MPC phase
φ	Azimuth Angle
$\mathbf{\Omega}_r$	Direction of Arrival
$\mathbf{\Omega}_t$	Direction of Departure
A	Joint Direction P
$A_R(\bar{\tau},\varphi,\vartheta)$	Complex MPC normalised amplitude at the Rx
A_r	Receive Direction Power Spectrum
A_t	Transmit Direction Power Spectrum
b	Average gains of the channel transfer matrix elements
B_C	Coherence Bandwidth

C_L	Constant loss
C_{MIMO}	Capacity gain of a MIMO system
C_{SISO}	Capacity gain of a SISO system
d	Distance between Tx and Rx
d_a	Spacing between antennas
d_c	Cluster density
d_e	Deep of the environment
d_{max}	Maximum path length
d_{sr}	Distance between the Scatterer n and Rx
d_{ts}	Distance between Tx and the Scatterer n
D_a	Distance between dipoles
$f_{D_{max}}$	Maximum Doppler shift frequency
G_{int}	Interpolation antenna gain
G_{max}	Maximum linear gain of a $\lambda/2$ dipole
$G_{M/S}$	Relative capacity gain of MIMO system
G_R	Gain of the Rx
G_T	Gain of the Tx
$\boldsymbol{h}$	Normalised matrix containing CIRs
h_e	Height of the environment
$\boldsymbol{H}$	Normalised channel transfer matrix
H_r	Horizontal antenna rotation
$\boldsymbol{n}$	Vector containing the noise power received by each antenna
N_a	Number of dipoles in the array
N_c	Number of clusters
N_{MPC}	Number of MPCs
N_{sc}	Number of scatterers within cluster
N_R	Number of Rx antennas
N_{run}	Number of simulations
N_T	Number of Tx antennas
$P(\tau)$	Power-Delay Spectrum
P_h	Power-Delay Joint Direction Spectrum
P_{LoS}	Received power level of LoS component
Pr	Received power
P_{Rx}	Received power in reference to LoS component
P_T	Transmitted power
$\boldsymbol{r_R}$	Position of the Receiver
$\boldsymbol{r_S}$	Position of the Scatterer n
$\boldsymbol{r_T}$	Position of the Transmitter
s_e	Shape of the scattering region

$\boldsymbol{T}$	Non-normalised channel transfer matrix
T_C	Coherence Time
$\boldsymbol{U}$	Unitary matrix containing the singular vectors of matrix $\boldsymbol{H}$ after SVD
v	Velocity of the Tx or Rx
$\boldsymbol{V}$	Unitary matrix containing the singular vectors of matrix $\boldsymbol{H}$ after SVD
V_{min}	Sensitivity of the Rx
V_r	Vertical antenna rotation
$V_R(\bar{\tau})$	Complex amplitude at the Rx in the continuous time-domain
w_{DCIR}	Channel richness
w_e	Width of the environment
$\boldsymbol{x}$	Vector of transmitted symbols for a particular T_X antenna
$\boldsymbol{X}$	Fourier transform of the $\mathbf{x}$
$\boldsymbol{y}$	Vector of received symbols for a particular R_x antenna
$\boldsymbol{Y}$	Fourier transform of the $\mathbf{y}$
Z_A	Impedance of Rx antenna

List of Software

Microsoft Word	Text editor tool
Microsoft Excel	Calculation tool
Microsoft Visio	Design tool (e.g. flowcharts, diagrams, etc)
Matlab	Computational math tool
Dev C++	Bloodshed Software, GNU General Public License

Chapter 1

Introduction

This chapter gives a brief overview of the work. Before establishing work targets and original contributions, the scope and motivations are brought up. The current State-of-the-Art in relation to the scope of the work is also presented. At the end of the chapter, the work structure is provided.

1.1 Overview and Motivation

"Imagine a world without wires; a world where verbal and visual communication is simple, convenient and reliable", Rob Conway.

Nowadays, this "old-fashionable" vision is turned into reality by the communications industry and what was in the past single and remarkable achievements (as voice and visual calls) is something that millions of people take daily for granted. In fact, a new wide diversity of services is emerging and consumers are likewise driving the mobile content for entertainment, advertising and MMS services. As these applications proliferate, voice is becoming a secondary factor when purchasing a mobile device. High-speed wireless data services have elevated the device formerly known as the cell phone to much more. Wireless-phone makers offer a new generation of handsets that combine a variety of functions in a single device. Handsets can send email, store music on removable memory, store video clips, check satellite positioning and even monitor a user's stress level. A wireless device is now a must-have device for lifestyle–conscious consumers as well as world travellers and business people.

For achieving higher and reliable data rate on wireless communications, cellular systems have been developing rapidly. Universal Mobile Telecommunications System (UMTS), a third-generation digital cellular system, provides the voice service, but also the desirable Mbps data rates for demanding applications such as broadband Internet access, interactive gaming, and high-quality audio and video entertainment. Using the standard Wideband Code Division Multiple Access (WCDMA) developed by the Third Generation Partnership Project (3GPP), higher peak data rates have been achieved – namely, up to 7Mbps – within a 5MHz bandwidth. According to [UMTS07], there are about 170 millions of UMTS subscribers all over the world.

High Speed Downlink Packet Access (HSDPA) was set as a standard in 3GPP Release 5 with the first specifications made available in March 2002. The initial peak data rate was 1.8 Mbps, increased to 3.6 Mbps during 2006. By the end of 2007, 7.2 Mbps were available, with the maximum peak data rate of 14.4 Mbps in a near future, starting the mobile IP revolution, [HoTo06]. Following the success accomplished by HSDPA, in December 2004, 3GPP launched Release 6 with Enhanced-Dedicated Channel (E-DCH), also known as High Speed Uplink Packet Access (HSUPA), first specifications. HSUPA started to be deployed at the end of 2007, with expected peak data rates up to 1.45 Mbps and around 3-4 Mbps in later releases [HoTo06].

HSDPA and HSUPA together are referred to as High Speed Packet Access (HSPA). HSPA is deployed on top of 3G networks, minimising equipment upgrade, with practical data rates beyond 2 Mbps in the Downlink (DL) and up to 1 Mbps in Uplink (UL), while keeping latency under 100 ms. This characteristics make HSPA attractive to low data rate applications that require low latency, like Voice over IP (VoIP), which can be the driver application to the migration to an all-IP scenario, as well as to new packet-based applications to go wireless in an efficient way. Further HSPA evolution is specified in 3GPP Release 7, and its commercial deployment is expected by 2009. HSPA evolution is also known as HSPA+.

In general HSPA Evolution consists of introduction of Multiple Input Multiple Output (MIMO), Higher Order Modulation (HOM), protocols optimisation and optimisations for voice over IP. The deployment of existing HSPA should be, from the point of view of the operators, easily updated. HSPA+ does not support soft handover. HSPA evolution uses MIMO in order to transmit two separately encoded streams to a Mobile Terminal (MT). Therefore, the process of successive interference cancellation receiver becomes more attractive, which allows a better performance of the system compared with linear receivers. As a consequence, the streams are modulated and spread separately, and the spreading codes can be reused over both streams. The link adaptation has two types of components: spatial and temporal ones.

Release 6 HSPA systems support the use of 16 Quadrature Amplitude Modulation (16QAM) in the downlink and Quadrature Phase Shift Keying (QPSK) in the uplink. The peak rate with the addition of 64QAM increases to 21.6 Mbps compared with the 16QAM case. The combination of MIMO and 64QAM increases the peak rate to 43.2 Mbps. The former combination is already being considered for future releases.

3GPP is also working to specify a new radio system called Long Term Evolution (LTE). Release 7 and 8 solutions for HSPA evolution, will be worked in parallel with LTE development, and some aspects of LTE work are also expected to reflect on HSPA evolution. LTE has expected peak data rates of 100 Mbps in DL and up to 50 Mbps in UL, which will further improve the end user experience [HoTo06].

LTE will enable high mobile broadband capacity and services, providing an even higher cost efficiency mobile coverage. Future releases will offer DL peak data rates up to 326 Mbps and UL data rates up to 86 Mbps, with 20 MHz bandwidth in both UL and DL. It will allow operability in Frequency Division Duplex (FDD) and Time Division Duplex (TDD) modes, scalability to operate in a range of bandwidth from 1.4 to 20 MHz, reduced latency and transaction time from inactive to active. In January 2008, LTE technical specifications were approved by 3GPP, being included in Release 8.

In this context, MIMO systems can enhance radio systems and wireless network operators see a need for it due to its many advantages. Wireless systems using MIMO represent an economical way to increase user capacity, range and throughput in a variety of environments, most notably those that are enclosed and having low radio interference, such as small and/or isolated cells.

The use of multiple antennas at both transmitter and receiver allows:
- Multiplicative increase in peak data rate;
- Significantly higher spectrum efficiency, especially in low-interference environments;
- Increased system capacity (number of users).

In UMTS, operators see a great need for MIMO in "contained environments" such as:
- Hot spots similar to those serviced by today's WiFi systems (airports, hotel lobbies, etc.);
- Academic campuses, in various self-contained areas (quads, auditoriums, cafeterias, etc.);
- Stadiums and arenas, again, which offer self-contained environments;

- Shopping centres and shopping areas, favoured by large numbers of younger, internet-savvy users;
- Mass transportation (trains, etc.) with users looking for interaction and entertainment;
- Enclosed parks and recreation areas;
- Residential homes, supplanting DSL/Cable services;

A MIMO system cannot be treated as an antenna array where all antenna elements are treated as a single system. The MIMO approach is to use spatial diversity by applying multiple antennas on both ends of the radio link and to establish parallel links between them. If the links are independent, a gain of the radio channel can be observed and achieve results that are a few times greater than those for Single-Input Single-Output (SISO) systems. The independence of the links between input and output is related to propagation conditions in the radio channel (i.e., the correlation between Channel Impulse Responses (CIRs)), thus, the gain of MIMO systems is possible only in multipath environments, and depends on how strong the multipath phenomenon is. The MIMO system gain is related to some parameters, as numbers of input and output antennas and spacing between them and time resolution of the Receiver (Rx). An increase of the antenna separation gives a greater decorrelation among links, because the influence of each obstruction is more significant, while an increase of the time resolution allows to distinguish more Multipath Components (MPCs).

The propagation conditions determine the channel capacity that can be expected for a MIMO system. It is of great interest to characterise and model the MIMO channel for different conditions in order to predict, simulate, and design high performance communication systems. Among other advantages, the simulation of MIMO propagation channel can assist in the choice of efficient modulation schemes under different scenarios and system performance can be accurately predicted. As a consequence, the most important task is the selection of an appropriate channel model in order to develop accurate and efficient simulators of radio channel. So, the chosen model should be analysed under different aspects, such as: implementation complexity, runtime cost and results accuracy. This means that a trade-off between accuracy and complexity should be made in order to choose the most appropriate channel model. A specific phenomenon, the process of grouping a set of physical or abstract objects into classes of similar objects – clustering, is used in order to simplify MIMO channel models. Instead of describing a large number of individual paths, only their superset, the clusters, need to be parameterised. For this reason, clusters became very popular. Even more, several studies have shown that MIMO channel models disregarding clustering effects might significantly overestimate capacity.

Many channel models for MIMO systems have appeared in the literature. However, with the exception of a few recent results, they are largely focused on two dimensional propagation, i.e., propagation in the horizontal plane, and the impact of elevation angle is not considered. The assumption of 2D propagation breaks down when in some propagation environments the elevation angle distribution is significant. Consequently, the estimation of capacity assuming a 2D channel coefficient alone can lead to erroneous results [SZSM06].

Geometrically Based Single Bounce (GBSB) channel models have been used for many years, because of their low complexity and quite good accuracy, [MaCo04]. In this model, the multipath signal is the result of signal bounce over numerous reflectors placed randomly in the environment, while the distribution and features of the reflectors depend on considered scenario. The GBSB model applied to the simulation of a MIMO system was presented in [KoKo05], while in [Mack07], Multiple Bounces (MBs) were introduced to the geometrically based model and the comparison with Single Bounce (SB) was made. The novel aspect of this work is to introduce a 3D approach of the GBSB channel model and compare it with the old 2D one, since this cannot be found in the literature. In reality, a signal arriving at Rx is a combination of SB and MB MPCs that are reflected over obstacles in the propagation environment. Even though, the SB MPCs are dominant and for the purpose of this work multiple bounce MPCs are not taken into account.

1.2 Structure of the Dissertation

This work consists of six chapters, followed by a set of annexes. In Chapter 2, systems like UMTS and LTE and aspects related with channel modelling are described. Some parameters describing radio channels are introduced and examples of various channel models are given. This work is related to MIMO systems, so basic information about this technique is presented. Moreover, the main advantages of this system are discussed and considerations related to the capacity of MIMO systems can be found. In this chapter, a review of MIMO channel models as well the 3D models are done and at the end, three types of scenarios are introduced.

As the developed model is based on the GBSB one, this one is well described at the beginning of Chapter 3. This chapter is focused on the development of the 3D GBSB MIMO channel model. All the aspects concerning the 3D approach are discussed and considered, like the radiation pattern of the antennas.

Chapter 4 presents all issues related to the implementation of the model in the simulator. At first, the simulator architecture is explained and the way it cooperates with other applications is pointed out. The data flow in the simulator is presented as well. This chapter finishes with the assessment of the simulator implementation and the study of relations between input and output parameters.

Chapter 5 begins with the description of the scenarios that were taken for simulations. In the following parts of the chapter, results of simulations are presented; first, the study of the SISO channel for different input parameters and for different scenarios is examined, next some correlations aspects in MIMO systems are presented and at the end, the MIMO capacity for different scenarios is calculated and the comparison with the 2D model made.

In Chapter 6, the final conclusions of the work are drawn. Some clues related to further developments of 3D GBSB models can also be found in the chapter.

Annexes consist of supplement to all chapters, where results, not presented in previous parts of the work, can be found. The information needed to run the simulator and the description of generated

output files can be found in the annexes. The tables of Radio Channel Parameters (RCPs) for various situations and for different scenarios and graphs illustrating results for the SISO systems can be found. At the end, graphs showing correlation between links in the MIMO systems and plots with relative and MIMO capacity gain for scenarios can also be found.

Chapter 2

Basic Concepts

This chapter provides an overview of some systems that use MIMO, like UMTS and LTE, and addresses different approaches to radio channel modelling. The MIMO system is described and a classification of MIMO channel models is discussed according with the state of the art. Some aspects related with single and multi bounces channel modelling are presented and finally the different main scenarios are explained.

2.1   Basic System Description

2.1.1   UMTS

UMTS consists of a number of logical network elements that each has a defined functionality. For the purpose of this work, it is only necessary focus on the network elements that handle all radio-related functionality, the Radio Access Network (RAN). UMTS Terrestrial RAN (UTRAN) architecture is highlighted in Figure 2.1.
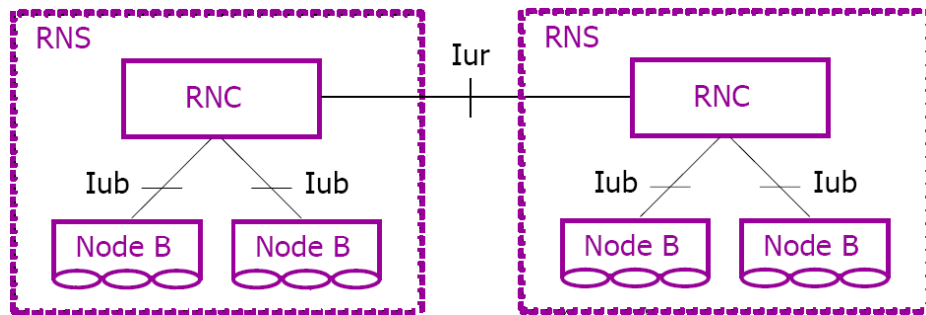
Figure 2.1. UTRAN architecture (extracted from [3GPP00]).

UTRAN consists of one or more Radio Network Sub-systems (RNS), [HoTo04]. An RNS is a sub-network within UTRAN and consists of one Radio Network Controller (RNC) and one or more Node Bs. RNCs may be connected to each other via an Iur interface. RNCs and Node Bs are connected with an Iub interface. The functionality of these two distinct elements can be summarised in:

- The Node B converts the data flow between the Iub and the WCDMA radio interfaces (the interface through which the User Equipment (UE) accesses the fixed part of the system). It also participates in radio resource management;

- The RNC owns and controls the radio resources in its domain (the Node Bs connected to it). RNC is the service access point for all services UTRAN provides the Core Network (CN), for example, management of connections to the UE.

The interfaces between the logical network elements have been well defined in the UMTS standards and within UTRAN there are two different open interfaces:

- Iub interface. The Iub connects a Node B and an RNC. In UMTS the Controller-Base Station interface is standardised as a fully open interface;

- Iur interface. The open Iur interface allows soft handover between RNCs from different manufacturers, and therefore complements the open Iu interface (that connects the UTRAN to the CN).

WCDMA was selected for the UTRAN air interface. UMTS WCDMA is a Direct Sequence CDMA system where user data is multiplied with quasi-random bits derived from WCDMA Spreading codes. In UMTS, in addition to channelisation, codes are used for scrambling. The operation mode of UMTS is FDD with different frequency bands: [1920 - 1980] MHz for UL and 2110 - 2170] MHz for DL. The frequency split in FDD causes a distinct channel behaviour depending on the link. By this simple fact, channel modelling should be considered separately. Also, UMTS radio channels have a bandwidth of

4.4 MHz, being separated by 5 MHz.

HSDPA improves capacity and spectral efficiency, sharing all network elements, requiring only a software upgrade at the Node B and at the Mobile Switching Centre (MSC) on the network side, but a new terminal on the user side. Although designed for non-RT (non-real time) traffic, simulations show that HSDPA provides enough capacity for low bit rate and low latency applications, like VoIP.

The idea of the HSDPA concept is to increase DL packet data throughput by means of fast physical layer (L1) retransmission and transmission combining, as well as fast link adaptation controlled by the Node B, i.e., the Base Station (BS).

While in Release 99 the scheduling control is based on the RNC, and Node B only has power control functionality, in HSDPA, scheduling and fast link adaptation based on physical layer retransmissions were moved to the Node B, minimising latency and changing the RRM architecture. With HSDPA, RNC-based retransmission can still be applied on top of physical layer, using Radio Link Control/Acknowledgment (RLC/ACK) in case of physical layer failure.

Another substantial change is the fact that HSDPA does not support soft handover. Higher data rates are accomplished through the use of a new higher order modulation, the 16QAM with 4 bits per symbol - that can only be used under good radio signal quality, due to additional decision boundaries: phase and amplitude estimations. QPSK modulation is mainly used to maximise coverage and robustness. HSDPA introduces Adaptive Modulation and Coding (AMC) which adjusts the modulation and coding scheme to the radio channel conditions, and, together with 16QAM, allows achieving higher data rates.

HSDPA performance depends on network algorithms, deployment scenarios, traffic generated, Quality of Service (QoS) and MT receiver performance and capability. It uses a fixed spreading factor of 16. From these 16 available codes, only 15 can be allocated for data transmission, as one code is needed for the signalling and control information. From the BS point of view, all the 15 codes can be allocated. However, for the MT, the allocated codes can vary, depending on the MT category. Terminals supporting HSDPA are divided into 12 categories with different maximum DL bit rates, between 0.9 and 14.4 Mbps.

After the improvement of HSDPA in DL, the same approach was taken in UL. HSUPA main objectives are to improve UL's capacity and to achieve higher data rates, compared to Release 99 384 kbps, reaching 1 to 2 Mbps in early phases. HSUPA improves the radio interface, maintaining all other network elements unchanged. Power control is essential for HSUPA operation as well as support for soft handover.

As in HSDPA, in HSUPA, a faster physical layer, shorter Transmission Time Interval (TTI) of 2 and 10 ms and Node B scheduling were introduced. The main difference between HARQ used in HSDPA and HSUPA is the fact that for the latter, it is fully synchronous, avoiding the need for sequence numbering, and can operate in soft handover. The modulation used, Binary Phase Shift Keying (BPSK), was left unchanged since transmission with multiple channels was adopted, instead of using higher order modulation, avoiding complex implementations at the MT side.

In HSUPA, similarly to HSDPA, performance depends on network algorithms, deployment scenarios, traffic generated, QoS and MT receiver performance and capability. There are six MT categories, with UL bit rates between 69 kbps and above 4 Mbps.

Table 2.1. HSDPA, HSUPA and WCDMA comparison table (extracted from [HoTo06]).

Feature	Release 99	HSDPA	HSUPA
Variable Spreading Factor	Yes	No	Yes
Fast Power Control	Yes	No	Yes
Adaptive Modulation	No	Yes	No
Fast L1 HARQ	No	Yes	Yes
Soft handover	Yes	No	Yes

2.1.2 LTE

LTE was created with the purpose of providing data services over a network originally conceived for mobile voice services, and will provide high data rates with MIMO antenna techniques in flexible sub-channelisation schemes. LTE in DL is based on OFDM/OFDMA and on the use of SC – Frequency Division Multiple Access (SC-FDMA) with cyclic prefix in UL.

Similar to HSDPA and HSUPA, more intelligence is being added to the BS. Radio-related functionalities are all located in the BS, compared to HSDPA/HSUPA the new functionalities are Radio Link Control (RLC) Layer, Radio Resource Control (RRC) and Packet Data Convergence Protocol (PDCP).

Another difference from WCDMA is the use of different bandwidths, from 1.4 MHz up to 20 MHz. The parameters have been chosen such that the FFT lengths and sampling rates are easily obtained for all operation modes, and at the same time ensuring the easy implementation of dual mode devices with a common clock reference.

The LTE physical layer is designed for maximum efficiency of the packet-based transmission. For this reason there are only shared channels in the physical layer to enable dynamic resource utilisation.

The resulting data rate for a particular user will depend on:
- Number of resource blocks allocated,
- Modulation applied,
- Rate of the channel coding,
- Whether MIMO is used or not
- Amount of overhead, including whether long or short cyclic prefix is used.

The achieve downlink peak bit rates are shown in Table 2.2. QPSK modulation carries 2 bits per symbol, 16QAM 4bits per symbol and 64QAM 6 bits, and 2x2 MIMO further doubles the peak bit rate. Therefore, QPSK ½ rate coding carries 1bps/Hz, and 64QAM without any coding and with 2x2 MIMO carries 12 bps/Hz. The bandwidth is included in the calculation by taking the corresponding number of sub-carriers for each option: 72 per 1.4 MHz and 180 per 3.0 MHz bandwidth. For the bandwidths 5 MHz, 10 MHz and 20 MHz there are 300, 600 and 1200 subcarriers respectively, and there are 13 data symbols per 1 ms sub-frame. The highest theoretical data rate is approximately 170 Mbps.

Table 2.2. Downlink peak bit rates (extracted from [HoTo07]).

Modulation Coding		Peak bit rate per sub-carrier/bandwidth combination [Mbps]				
		72/1.4 MHz	180/3.0 MHz	300/5.0 MHz	600/10 MHz	1200/20 MHz
QPSK ½	Single Stream	0.9	2.2	3.6	7.2	14.4
16QAM ½	Single Stream	1.7	4.3	7.2	14.4	28.8
16QAM ¾	Single Stream	2.6	6.5	10.8	21.6	43.2
64QAM ¾	Single Stream	3.9	9.7	16.2	32.4	64.8
64QAM 4/4	Single Stream	5.2	13.0	21.6	43.2	86.4
64QAM ¾	2x2 MIMO	7.8	19.4	32.4	64.8	129.6
64QAM 4/4	2x2 MIMO	10.4	25.9	43.2	86.4	172.8

For the uplink the achieve peak data rates are shown in Table 2.3. The peak data rates are lower in uplink than in downlink since single user MIMO is not specified in uplink. MIMO can be used in uplink as well to increase cell data rates, not single-user peak data rates.

Table 2.3. Uplink peak bit rates (extracted from [HoTo07]).

Modulation Coding		Peak bit rate per sub-carrier/bandwidth combination [Mbps]				
		72/1.4 MHz	180/3.0 MHz	300/5.0 MHz	600/10 MHz	1200/20 MHz
QPSK ½	Single Stream	0.9	2.2	3.6	7.2	14.4
16QAM ½	Single Stream	1.7	4.3	7.2	14.4	28.8
16QAM ¾	Single Stream	2.6	6.5	10.8	21.6	43.2
16QAM 4/4	Single Stream	3.5	8.6	14.4	28.8	57.6
64QAM ¾	Single Stream	3.9	9.0	16.2	32.4	64.8
64QAM 4/4	Single Stream	5.2	13.0	21.6	43.2	86.4

Table 2.4 summarises the basic aspects of the LTE.

Table 2.4. Summary of LTE features (adapted from [WiMF06b]).

Attributes	LTE
Duplex Mode	FDD

Downlink	OFDMA
Uplink Multiple Access	SC-FDMA
Channel Bandwidth	1.4,3,5,10,15,20 MHz
Frame Size	1 ms FDD
Modulation	QPSK, 16QAM, 64QAM
Coding	CTC
DL Peak Data Rate	172.8 Mbps (20 MHz BW)
UL Peak Data Rate	86.4 Mbps (20 MHz, Single Antenna)
Scheduling	Fast Scheduling in the DL
Spectral Efficiency - DL [bps/Hz]	2.73
Spectral Efficiency - UL [bps/Hz]	0.7

2.2 Generic Channel Models

It is usual to distinguish among three types of channel models: empirical (statistical), deterministic and mixed. Stochastic models characterise channels in a statistical way, and do not rely on site-specific descriptions [SBMS04]; these models are described by numerous parameters, which are obtained from the analysis of many measurement sessions and despite the fact that this group of channel models is very flexible, their accuracy is not very high. In the deterministic models, the knowledge of the environment is needed (and the accuracy of the results strongly depends on a precise description of the environment) and two main techniques are known: solving electromagnetic formulas and ray tracing. The former is highly complicated, and the latter needs a huge computer power. The combination of the two previously mentioned approaches results in a mixed category. As presented in [MaCo04], arriving signals can result from geometric contributors – just like in the deterministic model, but some properties of the contributors (e.g., localisation, physical characteristics) can be modelled statistically. Radio channel models in this category are able to meet a good accuracy-complexity compromise.

In order to capture the statistics of the channel, it is usually to do some assumptions about the physics of the channel [Moli05]. The most frequently used assumptions are the so-called Wide Sense Stationary (WSS) assumption and the Uncorrelated Scatterers (US), which lead to the Wide-Sense Stationarity Uncorrelated Scattering (WSSUS) model. Physically speaking, WSS means that the statistical properties of the channel do not change with time. The US assumption is defined as "contributions with different delays are uncorrelated". So, the WSSUS model assumes that the statistics of the channel are time and frequency independent and with no correlation between

multipath components (which in practice is not always fulfilled).

By the fact that UMTS radio channels have a bandwidth of 4.4 MHz, one assumes a wide band approach, which means that the radio channel is not flat (it introduces dispersion to signal spectral components, passing channel with different amplitude gains). The range of frequencies within which the radio channel is flat is defined by the coherence bandwidth, usually defined for a correlation coefficient of 0.5, which gives [Corr08]:

$$B_{c[Hz]} \approx \frac{1}{2\pi\sigma_\tau} \tag{2.1}$$

- σ_τ - RMS delay spread

Given the purpose and scope of this work, it can be considered that there are no changes in the radio channel in time, i.e., a static channel. This means that there are no concerns with the coherence time because the Channel Impulse Response (CIR) is invariant. Usually the coherence time has the following form (correlation above 0.5 assumed) [Corr08]:

$$T_{C[s]} \approx \frac{9}{16\pi f_{D_{max}}} \tag{2.2}$$

where:

- $f_{D_{max}}$ - a maximum Doppler shift frequency

$$f_{D_{max}} = \frac{v}{\lambda} \tag{2.3}$$

- v - velocity of the Transmitter (Tx) or Rx
- λ - wavelength

Several power spectra are largely used in channel modelling. To obtain those spectra, one can consider the assumptions made before (WSSUS model and static channel). So the power-delay spectrum is given by [OeCl07]:

$$P(\tau) = \iint P_h(\tau, \mathbf{\Omega}_t, \mathbf{\Omega}_r) d\mathbf{\Omega}_t d\mathbf{\Omega}r \tag{2.4}$$

where:

- $P_h(\tau, \mathbf{\Omega}_t, \mathbf{\Omega}_r)$ - power-delay joint direction spectrum of the channel at any time t
- τ - excess delay
- $\mathbf{\Omega}_t$ - direction of departure (DoD)
- $\mathbf{\Omega}_r$ - direction of arrival (DoA)

It is worth to notice that $\mathbf{\Omega}_t$ and $\mathbf{\Omega}_r$ represent, respectively, the DoD and DoA (both in 3-D space). The

directional vectors are defined as follows. $\boldsymbol{\Omega}_t$ and $\boldsymbol{\Omega}_r$ are uniquely determined by their spherical coordinates (i.e., the azimuth $\varphi_{t,r}$ and elevation $\theta_{t,r}$) on a sphere of unit radius according to the relationship:

$$\boldsymbol{\Omega}_{t,r} = [\cos\varphi_{t,r}\sin\theta_{t,r}, \sin\varphi_{t,r}\sin\theta_{t,r}, \cos\theta_{t,r}]^T \tag{2.5}$$

The joint direction power spectrum is given by:

$$A(\boldsymbol{\Omega}_t, \boldsymbol{\Omega}_r) = P_h(\tau, \boldsymbol{\Omega}_t, \boldsymbol{\Omega}_r)d\tau \tag{2.6}$$

The transmit/receive direction power spectrum can be written by:

$$A_{t,r}(\boldsymbol{\Omega}_{t,r}) = \iint P_h(\tau, \boldsymbol{\Omega}_t, \boldsymbol{\Omega}_r)d\tau d\boldsymbol{\Omega}_{r,t} \tag{2.7}$$

It is worth to notice that the Root Mean Square (RMS) delay and transmit/receive directional spreads are the square-root of the second-order moments of $P(\tau)$, $A_t(\boldsymbol{\Omega}_t)$ and $A_r(\boldsymbol{\Omega}_r)$, respectively. The RMS delay-spread is therefore given by:

$$\sigma_\tau = \sqrt{\frac{\int_0^\infty (\tau - \overline{\tau})^2 P(\tau)d\tau}{\int_0^\infty P(\tau)d\tau}} \tag{2.8}$$

Where the mean excess delay is:

$$\overline{\tau}_{[s]} = \frac{\int_0^\infty \tau P(\tau)d\tau}{\int_0^\infty P(\tau)d\tau} \tag{2.9}$$

In the direction domain, RMS directional spreads are expressed similarly, at the transmit and receive side respectively:

$$\overline{\boldsymbol{\Omega}}_{t,r} = \frac{\int \boldsymbol{\Omega}_{t,r} A_{t,r}(\boldsymbol{\Omega}_{t,r})d\boldsymbol{\Omega}_{t,r}}{\int A_{t,r}(\boldsymbol{\Omega}_{t,r})d\boldsymbol{\Omega}_{t,r}} \tag{2.10}$$

$$\sigma_{\Omega_3 t,r} = \sqrt{\frac{\int \left\|\boldsymbol{\Omega}_{t,r} - \overline{\boldsymbol{\Omega}}_{t,r}\right\|^2 A_{t,r}(\boldsymbol{\Omega}_{t,r})d\boldsymbol{\Omega}_{t,r}}{\int A_{t,r}(\boldsymbol{\Omega}_{t,r})d\boldsymbol{\Omega}_{t,r}}} \tag{2.11}$$

It is worth to notice that the average direction $\overline{\boldsymbol{\Omega}}_{t,r}$ is a vector, while $\sigma_{\Omega_3 t,r}$ is a scalar (but not in angular units), corresponding to a RMS Euclidean distance.

The solid angles $\mathbf{\Omega}_t$ and $\mathbf{\Omega}_r$ may also be divided into azimuth and elevation angles, (φ_t, θ_t) and (φ_r, θ_r). Spreads are then defined for each of these four angles, transmit/receive elevation-spreads being respectively given by:

$$\sigma_{\theta\, t,r} = \sqrt{\frac{\int_0^{2\pi} (\theta_{t,r} - \overline{\theta}_{t,r})^2 A_{t,r}(\theta_{t,r}) d\theta_{t,r}}{\int_0^{2\pi} A_{t,r}(\theta_{t,r}) d\theta_{t,r}}}$$

(2.12)

where average transmit/receive elevation angles are:

$$\overline{\theta}_{t,r} = \frac{\int_0^{2\pi} \theta_{t,r} A_{t,r}(\theta_{t,r}) d\theta_{t,r}}{\int_0^{2\pi} A_{t,r}(\theta_{t,r}) d\theta_{t,r}}$$

(2.13)

Transmit/receive azimuth-spreads $\sigma_{\varphi\, t,r}$ and average transmit/receive azimuth angles, $\overline{\varphi}_{t,r}$ being given by expressions similar to the previous ones.

The radio channel model in a multipath environment can also be described by the average power decay, given by:

$$\gamma = \log_{10}\left(\frac{P_T G_T G_R}{P_R d}\right) + \log_{10}\left(\left(\frac{\lambda}{4\pi}\right)^2 \frac{C_L}{d}\right)$$

(2.14)

where:

- P_T : transmitted power
- P_R : received power
- d: distance between Tx and Rx
- G_T : transmitted gain
- G_R : received gain
- C_L : Constant loss

The channel richness, which is an indication of the quantity of relevant AoA per relevant time unit, is given by [GiCo06]:

$$W_{DCIR[rad/\mu s]} = \frac{\sigma_{\Omega[rad]}}{\sigma_{\tau[\mu s]}}$$

(2.15)

where:

$$\sigma_{\Omega_2} = \sqrt{\sigma_\theta^2 + \sigma_\varphi^2}$$

(2.16)

In wireless communications, the mechanisms of radio propagation are include the impulse response of

the channel between the positions r_T of the Tx and r_R of the Rx. With the assumption of ideal omnidirectional antennas, the impulse response consists of contributions of all individual MPCs. Disregarding polarisation, the temporal and angular dispersion effects of a static (time-invariant) channel are described by the double-directional channel impulse response, [ABBC07]:

$$h(\boldsymbol{r_T}, \boldsymbol{r_R}, \tau, \boldsymbol{\Omega}_t, \boldsymbol{\Omega}_r) = \sum_{k=0}^{N_{MPC}} h_k(\boldsymbol{r_T}, \boldsymbol{r_R}, \tau, \boldsymbol{\Omega}_t, \boldsymbol{\Omega}_r) \tag{2.17}$$

where N_{MPC} is the total number of MPCs (typically those above the noise level of the system considered).

2.3   Multiple-Input Multiple-Output

In a multipath propagation environment, the Rx antenna is reached by many copies of the transmitted signal. The difference in each component propagation path results in diversity of Time of Arrival (ToA), Angle of Arrival (AoA), signal amplitude and phase. In order to achieve a better performance, MIMO systems take advantage of all arriving arrays. However the MIMO scheme, which is the result of parallel deployment of several space-separated antennas at input and output, does not only improve the Bit Error Ratio (BER) performance but also causes an increase of channel capacity [Mack07]. Nevertheless, the capacity in such system strongly depends on the propagation conditions in the radio channel and can vary significantly [Dziu04].

In contrast to conventional communication systems with one transmit and one receive antenna, MIMO systems are equipped with multiple antennas at both link ends, Figure 2.2. As a consequence, the MIMO channel has to be described for all transmit and receive antenna pairs.
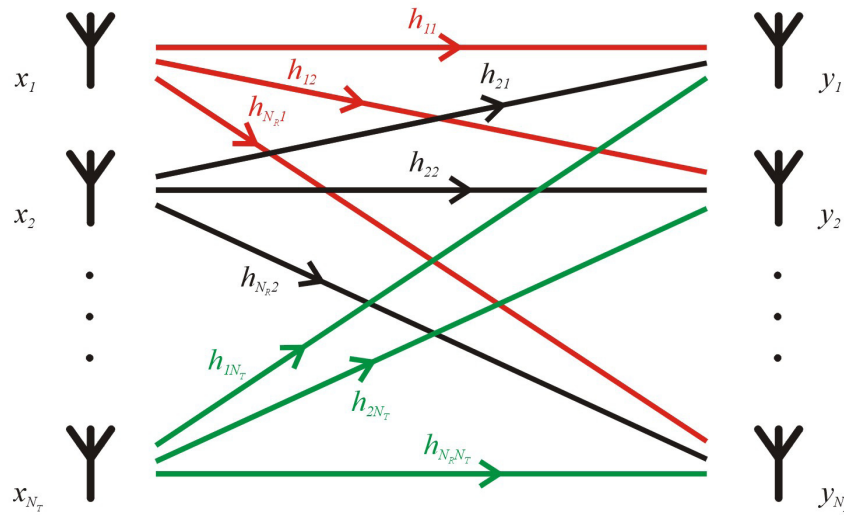
Figure 2.2. MIMO System (extracted from [Mack07]).

The relation between input and output is, [FoGa98]:

$$\boldsymbol{y} = \boldsymbol{h} * \boldsymbol{x} + \boldsymbol{n} \tag{2.18}$$

where

- $\textbf{x} = [\ x_1,\ x_2,\ ...,\ x_{N_T}\ ]$ - vector of symbols transmitted from the input antennas   (2.19)

- $\textbf{y} = [\ y_1,\ y_2,\ ...,\ y_{N_R}\ ]$ - vector containing symbols on the receiving side   (2.20)

- $\textbf{n}$ - noise vector   (2.21)

Considering an $N_R \times N_T$ MIMO system, where N_R and N_T are the number of transmit and receive antennas, respectively, from a system level perspective, the MIMO channel matrix is:

$$\textbf{h} = \left[h_{N_R N_T} \right] \tag{2.22}$$

Matrix $\textbf{h}$ describes the total CIR of a MIMO channel, where h_{ij} are CIRs between signals from the kth Tx antenna to the lth Rx one. The mean correlation between links in a MIMO system, $\overline{\rho}$, can be defined as:

$$\overline{\rho} = \frac{1}{(N_T N_R)^2} \sum_{k=1}^{N_T} \sum_{l=1}^{N_R} \sum_{m=1}^{N_T} \sum_{n=1}^{N_R} \rho(h_{kl}, h_{mn}) \tag{2.23}$$

The equation of the MIMO system (2.18) can also be written, after a Fourier transform:

$$\textbf{Y} = \textbf{H}\,\textbf{X} + \textbf{N} \tag{2.24}$$

where:

- $\textbf{X}$: Fourier transform of $\textbf{x}$ (2.19)
- $\textbf{Y}$: Fourier transform of $\textbf{y}$ (2.20)

The MIMO system equation (2.18) can also be transformed into [Dziu04]:

$$\textbf{Y}' = \Sigma\,\textbf{X}' + \textbf{N}' \tag{2.25}$$

where:

- $\textbf{Y}' = \textbf{U}^{-1}\textbf{Y}$
- $\textbf{X}' = \textbf{V}^{H}\textbf{X}$
- $\Sigma = \text{diag}[\sigma_1, \sigma_2, \ldots, \sigma_{\min(NT,\ NR)}]$: are the singular values of matrix $\textbf{H}$
- $\textbf{U},\textbf{V}$: unitary matrices containing the singular vectors of matrix $\textbf{H}$ after Singular Value Decomposition (SVD)
- $[]^{H}$: Hermitian operation

which can be interpreted as parallel independent subchannels between Tx and Rx. The number of parallel subchannels depends on the rank of matrix $\textbf{H}$ (the number of non-zero singular values). In an environment rich in scatterers (rich in MPCs), it leads to a possibly high number of uncorrelated subchannels, in which case a maximum system performance is observed.

The main advantage of MIMO systems is the ability to achieve higher data rates (the ambitious goal of up to 1000Mbit/s has been set by ITU). In principle, the information-theoretic capacity of these systems can increase linearly with the number of antennas. So, the capacity of MIMO systems is greater than the capacity of a SISO one. According to the general principles of information theory, the capacity of a SISO radio channel, C_{SISO}, is bounded by Shannon's rule [Proa01]:

$$C_{SISO[bps/Hz]} = \log_2(1 + \xi)$$ (2.26)

where:

- ξ : Signal to Noise Ratio (SNR).

This means that, in MIMO systems, it is possible to establish multiple parallel subchannels, which operate simultaneously on the same frequency band and at the same time. With some assumptions, the theoretical capacity of such a system has been presented in [FoGa98]:

$$C_{MIMO[bps/Hz]} = \log_2\left[\det\left(\mathbf{I}_{N_R} + \frac{\xi}{N_T}\mathbf{H}\mathbf{H}^H\right)\right]$$ (2.27)

where:

- $\mathbf{I}_{N_R}$: N_R dimensional identity matrix

- ξ : defined at each Rx antenna as:

$$\xi = \frac{P_{Total}}{n^2} b$$ (2.28)

- P_{Total} : the total Tx power

- n : the noise power at the Rx antenna

- $\mathbf{H}$: normalised channel transfer matrix related to $\mathbf{T}$ as:

$$\mathbf{H} = \frac{\mathbf{T}}{b}$$ (2.29)

- $\mathbf{T}$: non-normalised channel transfer matrix, containing the channel transfer gains for each par of antennas

- b : defined as:

$$b^2 = E\left[|\mathbf{T}|\right]^2 = \frac{1}{N_T N_R}\sum_{m=1}^{N_R}\sum_{n=1}^{N_T}|T_{mn}|^2$$ (2.30)

It is possible to derive the upper and lower bounds for capacity, from (2.27), since the correlation of a channel is between zero and one. When all subchannels are totally dependent ($\rho=1$), the minimum capacity of a MIMO channel occurs:

$$C_{MIMO_{\rho=1}} = \log_2\left(1 + N_{min}\frac{\xi}{N_T}\right)$$ (2.31)

where:

- $N_{\min} = \min(N_T, N_R)$ (2.32)

On the contrary, if there is no correlation (ρ=0) between parallel paths, the maximum capacity is achieved:

$$C_{MIMO_{\rho=0}} = N_{\min} \log_2(1 + \frac{\xi}{N_T})$$ (2.33)

Since the correlation between the subchannels is known (CIR matrix **H**) at the Tx, a power distribution known as waterfilling [ATEM02] can be performed, allowing to achieve maximum capacity in specified conditions.

A good way to have a notion of how MIMO can increase capacity is to use the Relative MIMO Gain (RMG), since it can be defined as the relation between the capacity of a MIMO system relative to the SISO one [KuMC08]:

$$G_{M/S} = \frac{C_{MIMO}}{C_{SISO}}$$ (2.34)

2.4   MIMO Channel Models

A variety of MIMO channel models have been developed in the last years. A potential way of distinguishing the individual models is with regard to the type of channel that is being considered [ABBC06]. So, it is possible to distinguish narrowband (flat fading) from wideband (frequency selective) models. Narrowband MIMO channels are completely characterized in terms of their spatial structure and in contrast, wideband (frequency-selectivity) channels require additional modelling of the multipath channel characteristics. One can also distinguish time-invariant from time-varying models. The latter requires a model for the temporal channel evolution according to certain Doppler characteristics. Despite these several MIMO channel models classifications, according to [ABBC06], the fundamental distinction is between physical and analytical models (see Figure 2.3).

Physical channel models characterise an environment on the basis of electromagnetic wave propagation by describing the double-directional multipath propagation between the locations of the Tx and Rx arrays.

These models explicitly model wave propagation parameters like the complex amplitude, DoD, DoA, and delay of an MPC; and also allow for an accurate reproduction of radio propagation. In addition, physical models are independent of antenna configurations (antenna pattern, number of antennas, array geometry, polarisation, mutual coupling) and system bandwidth.

Physical propagation models are termed "deterministic" if they aim at reproducing the actual physical radio propagation process for a given environment. There are two classes of deterministic models: ray tracing (RT) and stored measurements. RT models use the theory of geometrical optics to treat reflection and transmission on plane surfaces and diffraction on rectilinear edges.
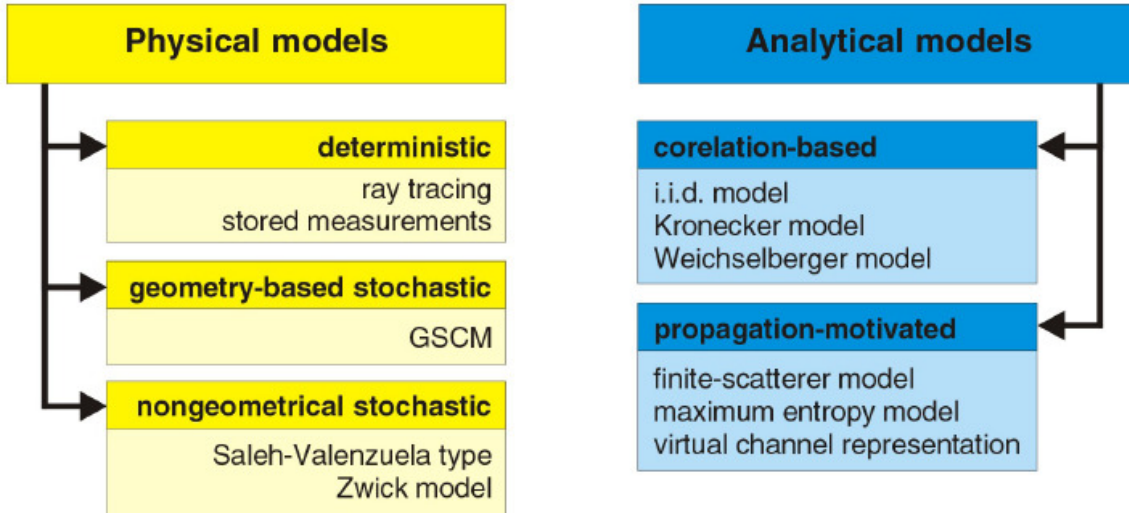
Figure 2.3. MIMO Channel Models (extracted from [Mack07]).

Initially the Tx and Rx positions are specified and then all possible paths (rays) from the Tx to the Rx are determined according to geometric considerations and the rules of geometrical optics. Stored measurements models use environment databases (obtained from measurements) and then simulate the corresponding propagation process through computer programs. Deterministic models are physically meaningful, and potentially accurate. However, they are only representative for the environment considered.

Geometry-based Stochastic Channel Models (GSCM) characterise the impulse response by the laws of wave propagation applied to specific Tx, Rx, and scatterer geometries. In the predecessor of the GSCM, Lee's model [Lee73], scatterers are placed in a deterministic way on a circle around the MT while in GSCM their position is chosen in a stochastic (random) manner. This random placement reflects physical reality much better.

The main difference among the various versions of the GSCM is the proposed scatterer distributions, because all information is inherent to the distribution of the scatterers. The simplest GSCM is obtained by assuming that scatterers are spatially uniformly distributed. However, more complex scatterer distributions approaches are analysed in order to describe reality better.

When the distribution of scatterers is set and only single bounce scatterer occurs, the calculation of output parameters is extremely simple. Firstly, apart from the Line of Sight (LoS) component, all paths consisting of two subpaths connecting the scatterer to the Tx and Rx respectively, are calculated. These subpaths characterise the DoD, DoA, and propagation time.

A GSCM has a number of important advantages, according to [MKLH03]:

- it has an immediate relation to physical reality; important parameters (like scatterer locations) can often be determined via simple geometrical considerations;
- many effects are implicitly reproduced: small-scale fading is created by the superposition of waves from individual scatterers; DoA and delay drifts caused by MT movement are implicitly included;

- Tx/Rx and scatterer movement as well as shadowing and the (dis)appearance of propagation paths (e.g., due to blocking by obstacles) can be easily implemented; this allows to include long-term channel correlations in a straightforward way.

An example of a GSCM is the Geometrically Based Single Bounce MIMO Channel Model [Koko05]. The main assumption of this model is that the MIMO system can be treated like n independent SISO ones. It means that each pair of input and output antennas can be treated separately, therefore, the GBSB radio channel model can be used without significant modifications. It is worth to notice that cluster of scatterers are common for the pairs of antennas. Because each pair has its own set of multipath components, the delays, signal phase and amplitude are different. The number of the generated MPCs by the scatterer is related to the number of antenna pairs between transmit and receive sides. The total number of MPCs is equal to the number of scatterers multiplied by the number of antennas pairs. Despite small spacing between antennas, the CIR for each multipath link is different if the number of scatterers is significant. Another example of a GSCM is the Geometrically Based Multibounce MIMO Channel Model [Mack07]. The great feature of this model from the previous one is the MB approach introduced.

In contrast, nongeometric stochastic models describe and determine physical parameters (DoD, DoA, delay, etc.) in a completely stochastic way by prescribing underlying probability distribution functions without assuming an underlying geometry. It means that the paths from Tx to Rx are described by statistical parameters only, without reference to the geometry of a physical environment. Two classes of stochastic nongeometrical models are reported in the literature:
- Extended Saleh-Valenzuela [SaVa87]: in this model clusters of MPCs are used.
- Zwick model [ZwFW02]: the MPCs are treated individually.

In contrast to physical models, analytical channel models characterise the impulse response (equivalently, the transfer function) of the channel between the individual Tx and Rx antennas in a mathematical/analytical way without explicitly accounting for wave propagation. Analytical models can be further subdivided into propagation-motivated models and correlation-based ones.

Propagation-motivated channel models, deal with the channel matrix via propagation parameters. Examples of these models are: the finite scatterer [Burr03], maximum entropy [DeMu05] and virtual channel representation [Saye02].

The fundamental assumption of the finite scatterer model [Burr03] is that propagation can be modelled in terms of a finite number of MPCs. For each of the components, an AoA, AoD, complex amplitude, and delay are specified. The model allows for single and multiple bounces scattering, which is in contrast to GSCMs that usually only incorporate single and Double Bounces (DBs) scattering. Finite scatterer models even allow for split components, which have a single AoD but subsequently split into two or more paths with different AoAs. The split components can be treated as multiple components having the same AoD.

In maximum entropy model [DeMu05], the question of MIMO channel modelling based on statistical inference was addressed. The maximum entropy principle was proposed to determine the distribution

of the MIMO channel matrix based on a priori information that is available. This a priori information might include properties of the propagation environment and system parameters (e.g., bandwidth, AoAs, etc.). The maximum entropy principle was justified by the objective to avoid any model assumptions not supported by the prior information. In [Saye02], a MIMO model called virtual channel representation was proposed, and in essence, this model corresponds to a spatial sampling that collapses all physical DoAs and DoDs into fixed directions determined by the spatial resolution of the arrays.

Correlation-based MIMO channel models characterise the MIMO channel matrix statistically in terms of the correlation between the matrix entries. Within the correlation-based models, one can distinguish the following: independent and identically distributed (i.i.d.), Kronecker [OzCB05] and Weichselberger [WHOB06]. These models have been used for the theoretical analysis of MIMO system capacity.

In order to compare different MIMO systems and algorithms, various organisations have defined reference MIMO channel models, which establish reproducible channel conditions. It is worth to notice that these models are not a model implementation as such, but rather a framework that allows assessing the benefits of different techniques for enhancing capacity and improving performance. Five standardized directional MIMO channel models can be mentioned:

- 3GPP Spatial Channel Model (SCM) [3GPP08]
- COST 259 [Corr01] and 273 [Corr06]
- IEEE 802.11n [ErSK04]
- IEE 802.16a,e [ErHS01]
- WINNER [ISTW08]

Despite the fact that in real life, propagation is dominated by single bounce, neglecting MB MPCs is insufficient [HoMC06] for modelling MIMO system performance. The main restriction of single bounce scattering is that the position of a scatterer completely determines AoA, AoD, and delay; in other words, only two of these parameters can be chosen independently. Thus, single bounce models are well applicable for antenna systems with an antenna array only at one link end.

The reason of the strongly interest in decouple AoA, AoD, and delay, is that many environments (e.g., micro- and pico-cells) feature multiple bounce scattering, for which the mentioned parameters are uncorrelated. In case the BS is below rooftop height, multiple reflections and diffractions are the consequence of the waveguiding through street canyons [Suzu77]. Moreover, measurement campaigns have shown that multiple reflections or scattering instants are important in indoor environments [MKLH99]. These environments are at the same time also the most likely locations for high speed wireless systems [Svan02].

When the directional channel properties need to be reproduced only for one link end (i.e., multiple antennas only at the Tx or Rx), multiple bounce scattering can be incorporated into a GSCM via the concept of equivalent scatterers [ABBC06]. These are virtual single bounce scatterers, whose positions and path loss are chosen such that they mimic multiple bounce contributions in terms of their delay and AoA. This concept is always possible, because the delay and azimuth of a single bounce

scatterer are in one-to-one correspondence with its geometric position.

Another approach to incorporate multiple bounce scattering into GSCM models is the twin cluster concept, which was introduced in COST 273 [HoMC06]. Here, the BS and MT views of the scatterer positions are different, and a coupling is established in terms of a stochastic link delay. This concept indeed allows for decoupled AoD, AoA, and delay statistics.

2.5   Two vs. Three Dimensional Models

The MIMO channel models proposed in [Koko05] and [Mack07], which are the support of this work, were done assuming that waves only arrive from the azimuth direction (two-dimensional model) and all elements of the environment are deployed on a 2D plane. However, it is commonly accepted that scattered electromagnetic waves do not strictly travel in azimuth but in elevation too [MPSF08]. In general there is a real scarcity of published models for the elevation spectrum, channel models and parameters for propagation that includes a 3D component [SZSM06]. Hence, it is highly important to investigate the sensitivity of key MIMO parameters, especially capacity, to the specifics of the propagation environment, especially in indoor environments consisting of many obstacles.

In [SZSM06], for cross polarized channels, a composite channel model has been defined, based on the 3GPP spatial channel model (SCM), and channel coefficient that takes into account both 2D and 3D propagation. The total propagation channel is modelled as the sum of a 2D and a 3D components, which are scaled via a g parameter (the ratio of powers of the 3D to 2D components) to form the composite channel. The 3D component captures the environments when the elevation angle power spectrum is significant.

It has been shown [SZSM06], that capacity is very sensitive to the value of the g parameter especially when the MT is in an environment with low angular spread. Also, the consideration of elevation angle distributions is also important since differences in the concentration of elevation power can lead to significant changes in capacity. Similarly, different 2D azimuth AoA distributions can lead to different capacity values, especially for large angular spread values. Finally, omission of a significant 3D component in the channel can result in a significant underestimation of the capacity.

Also, in order to evaluate the performance of the developed 3D model some measurements are presented to compare the results obtained from the 3D simulator. In [Czin07], in case of an indoor scenario, Figure 2.4, for a 2.55 GHz centre frequency, an average number of 10 MPCs was concluded to be the most probable. Related with the cluster angular spread for the AoA and AoD two important properties were identified: first, the AoA and AoD spreads seem to have similar statistics, which comes from the fact that Rx and Tx were in the same room; second, the cluster angular spreads are usually smaller in LoS situations. Also, it was concluded that a small cluster spread is correlated with a large number of clusters and vice-versa. Moreover, a typical number of clusters within [3-12] was observed. A cluster spreading within [5º-30º] was found to be the most probable. For the mean cluster delay and the cluster delay spread [50-100] ns and [5-17] ns were identified to be the most probable,

respectively.
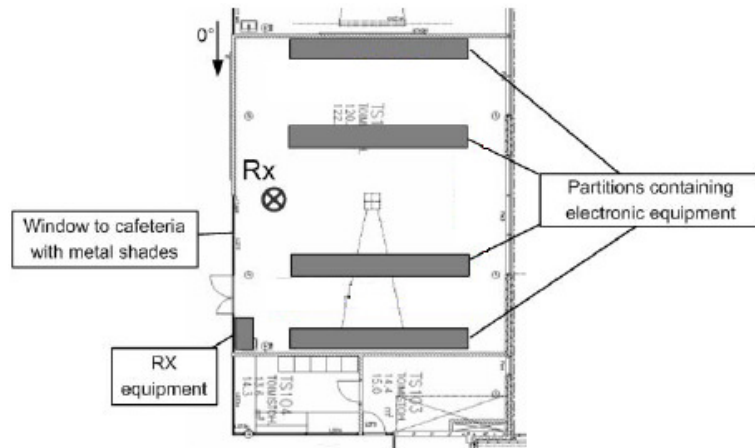
Figure 2.4. Measurement route in the medium-sized laboratory (extracted from [Czin07]).

2.6 Scenarios

To model the behaviour of MIMO channels, the different types of scenarios must be correctly defined. Usually three main typical scenarios are considered: pico-, micro- and macro-cells. The cell size, the location of the BS and MT with reference to the deployment of scatterers and the shape of the region of influence are the main features that distinguish these scenarios [MaCo04]. According to the definition of Prasad [Pras98], the pico-cell has radius smaller than 200 m, the micro-cell has radius within [200, 1000] m, and the macro-cell is larger than 1 km. The cell type not only depends on the cell radius but also on the height of the antennas.

In the micro-cell scenario, it is usual to assume that the BS is placed below rooftops, e.g., a street in the urban area (whereas in the macro-cell scenario the BS is placed above rooftops). The consequence of having a BS placed below rooftops is essentially the fact that, as the MT, it will also be surrounded by multipath contributors. Also, all scatterers are shared by all links between transmit and receive sides, because the distances between antennas are not significant in comparison with the dimensions of the propagation environment. Therefore, scattering will occur in the surroundings of both the BS and the MT, and in the region between them - with the same density. The chosen region shape is an ellipse, as Figure 2.5 shows [MaCo04].
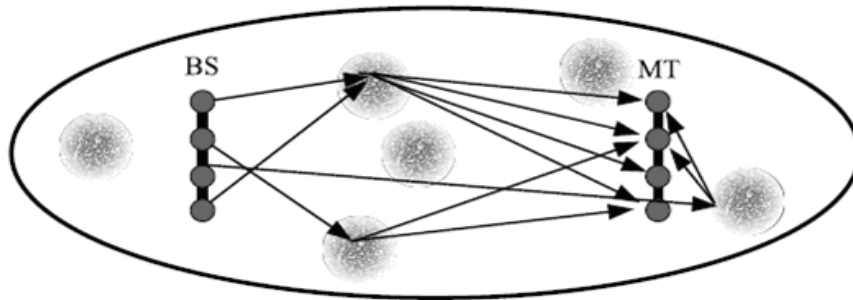
Figure 2.5. Micro-cell scattering model (extracted from [KuMC08]).

In the macro-cellular environment, it is assumed that the BS antenna height is relatively large in

comparison to that of the MT, therefore, scattering contributors will essentially exist in the vicinity of the MT. Consequently, the region of influence has the shape of a circle, Figure 2.6, which means that scattering contributors in the area near to the BS will be disregarded [MaCo04].
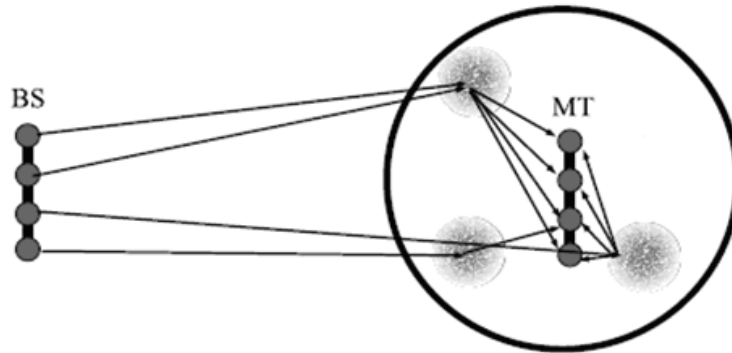
Figure 2.6. Macro-cell scattering model (extracted from [KuMC08]).

The area of the pico-cell is bounded by a circle, with the indoor BS at its centre, Figure 2.7. The dimension of the circle is determined by the size of the room, where the pico-cell is placed. The location of the MT and the amount of scattering contributions are specific to each individual environment. Needless to say, the Line of Sight (LoS) component exists in the pico-cellular environment.
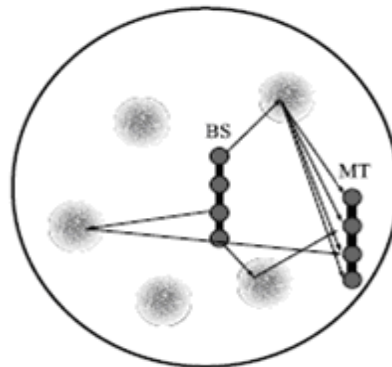
Figure 2.7. Pico-cell scattering model (extracted from [KuMC08]).

Chapter 3

Model Development

This chapter describes the Geometrically Based Single Bounce Model in detail, and discusses the main approaches in the development of the 3D Model. The chapter finishes with a discussion of system parameters and procedures to obtain channel impulse response between transmit and receive antennas.

3.1 Geometrically Based Single Bounce Channel Model

The Geometrically Based Single Bounce (GBSB) model is now presented in detail. This model was developed by the Group for Research On Wireless (GROW) of Instituto Superior Técnico (IST) [MaCo04].

The main idea behind the GBSB model is that the multipath characteristic of a radio channel is the result of signal bounce over numerous scatterers. Additionally, every scatterer is a source of one multipath component. Each scatterer is described by random, complex reflection coefficient, which determines the influence on the multipath component. It is worth to notice that scatterers reflection coefficients are generated randomly.

$$\Gamma_s = \left|\Gamma_s\right| e^{j\phi_S} \tag{3.1}$$

where:

- $\left|\Gamma_s\right|$: the magnitude of the reflection coefficient, which has a Uniform distribution in [0, 1]

- ϕ_S : the phase of the reflection coefficient, which has a Uniform distribution in [0, 2π]

After bouncing off the scatterer, the MPC changes its magnitude and phase.

Despite the fact that output parameters (amplitude, phase, AoA, AoD, and ToA) for each MPC are calculated according to the positions of Tx and Rx antennas and the distribution of the scatterers, Figure 3.1, this method is not a ray-tracing technique.
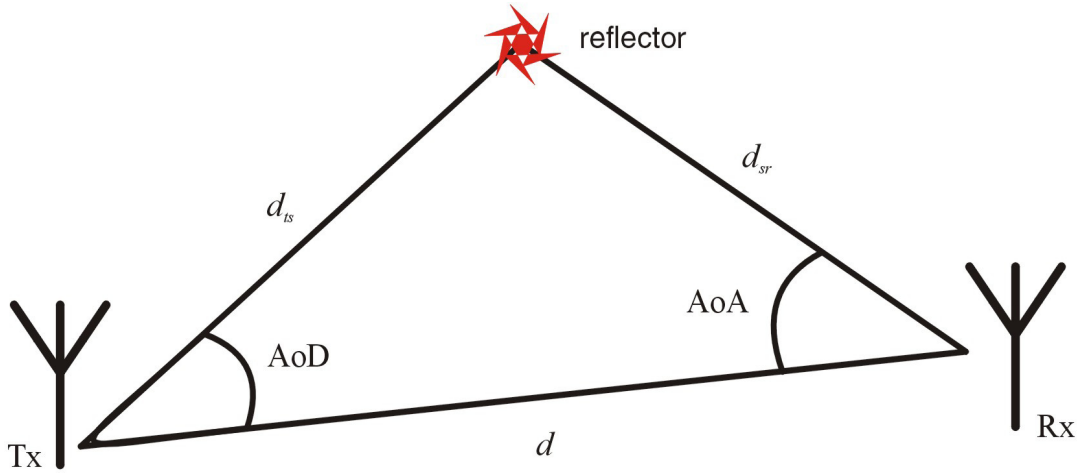
Figure 3.1. Calculation of some output parameters (extracted from [Mack07]).

A specific phenomenon was observed by Saleh and Valenzuela [SaVa87], i.e., that scatterers can be grouped into clusters. This means that in an area of a cluster there is a dense deployment of reflectors. Also, deployment and shape of clusters depends on the considered scenario.

To simplify calculations in this model, scattering of rough surface, diffraction, MB and other aspects of propagation are not included [LiRa99], despite the real zone of propagation is not modeled in a perfect way. Multipath rays, which are the result of a bounce over a scatterer, are presented on Figure 3.2).
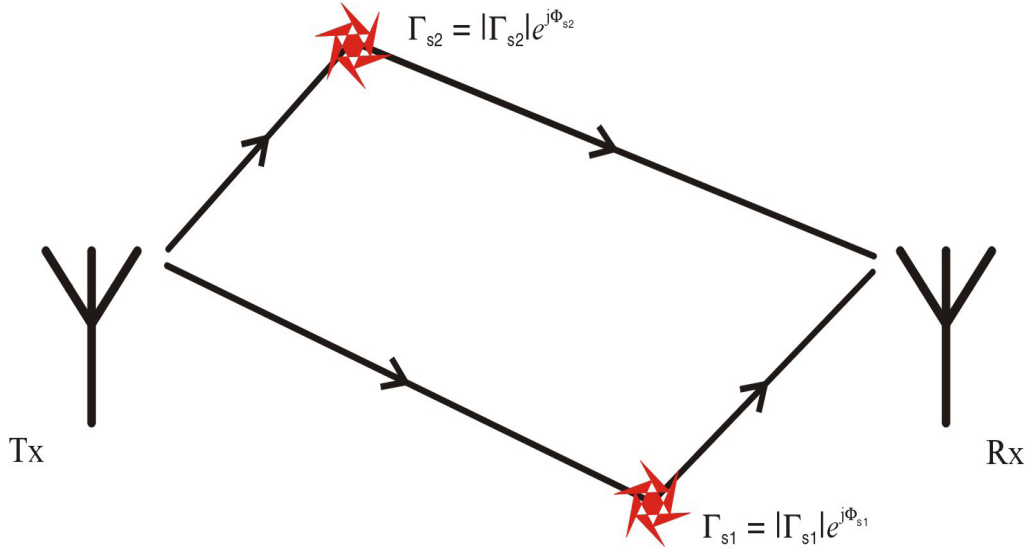
Figure 3.2. Scatterers in GBSB model (extracted from [Mack07]).

In conclusion, the GBSB model can be considered as a combination of deterministic (parameters like AoA, AoD and ToA are computed based on environment geometry) and statistical features (coordinates of scatterers are generated randomly, and each scatterer is described by a random reflection complex coefficient).

3.2 3D Model

3.2.1 General Structure

In this part, the main approaches in the development of the 3D model are discussed. In a real environment situation, the radiated wave is propagating by constantly bouncing over numerous reflectors. For simplification reasons, only single bounce will be considered. Also, reflections can be modelled in two ways: as specular reflection or as diffuse scattering. Admitting only single bouncing, it makes no sense consider diffuse scattering.

The model can be described by certain global input parameters, which can be organized in three different groups. The first group includes the parameters that determine the propagation environment and the type of scenario:

- number and distribution of clusters;
- number and distribution of scatterers within each cluster;
- values of scatterers reflection coefficients;
- geometry of the environment (i.e. considered scenario).

The follow group describes Tx properties, as:

- 3D antenna radiation pattern;
- radiate power.

Within the last group, there are the parameters related to the Rx:

- 3D antenna radiation pattern;
- sensitivity;
- resolution (i.e., receiver bandwidth);
- maximum delay (i.e., system time slot).

The above mentioned parameters are the information available in order to design the most accuracy and efficiency 3D algorithm.

The 3D model architecture can be divided into two different processes. On the one hand, there is a component performing the 3D algorithm, which implementation depends only on environment parameters; on the other hand, there is a component responsible for system specification. The results obtained from the 3D algorithm are then post processed by the receiver according to system specifications. The implementation of the 3D algorithm does not depend on any system parameter.

The model introduced above is used to describe the radio channel in SISO systems, but it can also be used to simulate MIMO systems. In that case, each pair of input and output antennas can be treated separately, and because the distance between antennas in each set is small, some generalisations can be made. The position of clusters of scatterers are common for the pairs of antennas, but their properties (e.g., reflection coefficient) can be chosen independently. For each pair of antennas, the LoS component is calculated as in free space, however, because of a specific deployment of Tx and Rx antennas, i.e., sets of antennas are placed on parallel lines, some of them have the same LoS component. Finally, having N_T input and N_R output antennas in the MIMO system means that the result of the algorithm has $N_T \cdot N_R$ sets of MPCs with different amplitudes, delays, azimuth and elevation AoAs and azimuth and elevation AoDs.

3.2.2 3D Approach

Any 3D point, is determined by its spherical coordinates (r, φ, θ) with $0^\circ \leq \theta \leq 180^\circ$, $0^\circ \leq \varphi \leq 360^\circ$. The 3D model requires a spherical coordinate system as illustrated in Figure 3.3. In this figure, is only represented the angles of departure (azimuth and elevation) as well just one scatterer.

So each receiver, transmitter and scatterer position in the 3D domain, r_R, r_T and r_S respectively, will be converted in terms of spherical coordinates according to:

$$x = r\cos(\varphi)\sin(\theta)$$
$$y = r\sin(\varphi)\sin(\theta) \qquad (3.2)$$
$$z = r\cos(\theta)$$
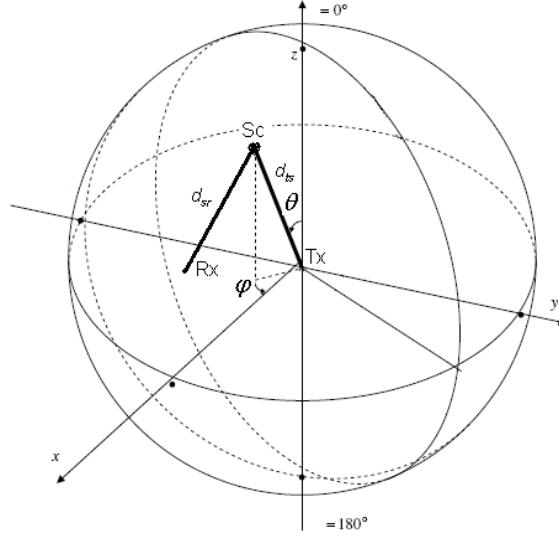
Figure 3.3. Spherical coordinate system for the 3D model (adapted from [SZSM06]).

The elevation and azimuth AoD/AoA can be obtained according to geometrical considerations:

$$\theta_{AoD[deg]} = \cos^{-1}\left(\frac{(z_{Scn} - z_{Tx})}{d_{ts}}\right) \tag{3.3}$$

$$\varphi_{AoD[deg]} = \tan^{-1}\left(\frac{(y_{Scn} - y_{Tx})}{(x_{Scn} - x_{Tx})}\right) \tag{3.4}$$

$$\theta_{AoA[deg]} = \cos^{-1}\left(\frac{(z_{Rx} - z_{Scn})}{d_{sr}}\right) \tag{3.5}$$

$$\varphi_{AoA[deg]} = \tan^{-1}\left(\frac{(y_{Rx} - y_{Scn})}{(x_{Rx} - x_{Scn})}\right) \tag{3.6}$$

where:

- d_{ts} - distance between Tx and Scatterer n

$$d_{ts} = \sqrt{(x_{Scn} - x_{Tx})^2 + (y_{Scn} - y_{Tx})^2 + (z_{Scn} - z_{Tx})^2} \tag{3.7}$$

- d_{sr} - distance between Scatterer n and Rx

$$d_{sr} = \sqrt{(x_{Rx} - x_{Scn})^2 + (y_{Rx} - y_{Scn})^2 + (z_{Rx} - z_{Scn})^2} \tag{3.8}$$

- d - distance between the Tx and Rx

$$d = \sqrt{(x_{Rx} - x_{Tx})^2 + (y_{Rx} - y_{Tx})^2 + (z_{Rx} - z_{Tx})^2} \tag{3.9}$$

- (x_{Tx}, y_{Tx}, z_{Tx}) - positions in 3D of the Tx
- $(x_{Scn}, y_{Scn}, z_{Scn})$ - positions in 3D of the Scatterer n
- (x_{Rx}, y_{Rx}, z_{Rx}) - positions in 3D of the Rx

As a result of the physical location of the scatterers will be represented in three dimensions, a MPC can arrive from any azimuth co-elevation pair of angles defined by the scatterer's position within the propagation path. Each MPC is characterised by seven different parameters, by its delay τ, amplitude, phase, azimuth AoD φ_{AoD}, elevation AoD θ_{AoD}, azimuth AoA φ_{AoA} and elevation AoA θ_{AoA}. The delay of a MPC corresponds straightforward to path length, and is measured in reference to the delay of the LoS component. Normalised (i.e., making the assumption that transmitted power is equal to 1W) MPC amplitude and phase only depends on the scatterer reflection coefficient and the phase of the scatterer reflection coefficient. The MPC normalised amplitude, A_R, is equal to:

$$A_R = \frac{|\Gamma_s|}{\sqrt{4\pi}.(d_{ts} + d_{sr})} \tag{3.10}$$

and the MPC phase, Φ_R is equal to:

$$\Phi_R = \left(\frac{(d_{ts} + d_{sr})}{\lambda} - \left\lfloor \frac{(d_{ts} + d_{sr})}{\lambda} \right\rfloor \right) \cdot 2\pi + \phi_S \tag{3.11}$$

3.2.3 3D Antenna Radiation Pattern

The problem of obtaining the 3D antenna radiation pattern also needs the attention on the development the 3D radio channel model. In almost all cases, antenna manufacturers do not make available full three-dimensional radiation patterns, but only the patterns in the horizontal and vertical planes (or, perhaps only the half-power beamwidth (HPBW) for the vertical plane). So, two main approaches are considered and taken into account:

- "Real" 2D antenna patterns;
- Theoretical 3D antenna patterns.

In the first case, it is used 2D antenna patterns files (available from the manufacturers), which contains the gains (for a given angle) of the horizontal and vertical plane and then it is done a 3D interpolation base on [GCFP01], with a small relative error. Figure 3.4 shows the diagram used. The calculation of the gain using this interpolation is done according to (3.12).

$$G_{\text{int}[dB]} = \frac{\left[\phi_1 G_{\phi 2} + \phi_2 G_{\phi 1} \right] \dfrac{\theta_1 \theta_2}{\left(\theta_1 + \theta_2 \right)^2} + \left[\theta_1 G_{\theta 2} + \theta_2 G_{\theta 1} \right] \dfrac{\phi_1 \phi_2}{\left(\phi_1 + \phi_2 \right)^2}}{\left[\phi_1 + \phi_2 \right] \dfrac{\theta_1 \theta_2}{\left(\theta_1 + \theta_2 \right)^2} + \left[\theta_1 + \theta_2 \right] \dfrac{\phi_1 \phi_2}{\left(\phi_1 + \phi_2 \right)^2}} \tag{3.12}$$

In the second case a theoretical $\lambda/2$ dipoles radiation pattern is considered and also arrays of $\lambda/2$ dipoles. In both cases, the vertical radiation pattern is symmetric, having only a unique lobe. Also, it is the vertical plane that depends on the considered angle, contrary to the horizontal plane (which is constant for all the angles).
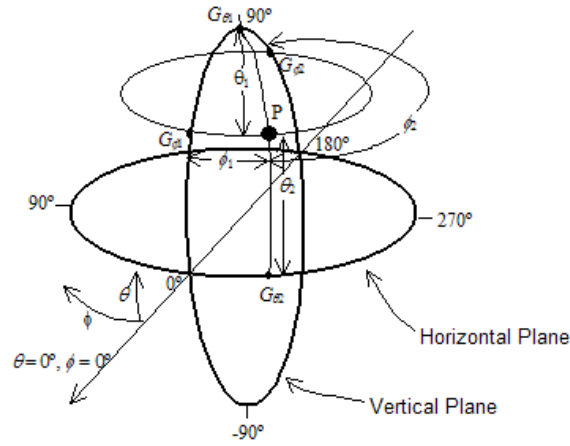
Figure 3.4. 3D diagram used for the interpolation of the antenna gain in the P point direction (extract from [GCFP01]).

For the case of $\lambda/2$ dipole, the linear gain depends on the elevation angle, θ and is equal to:

$$G_{dipole}(\theta) = G_{max} \frac{\cos^2(\frac{\pi}{2}\cos(\theta))}{\sin^2(\theta)} \tag{3.13}$$

where:

- G_{max} - maximum linear gain of a $\lambda/2$ dipole, 1.64.

The linear gain of an array of $\lambda/2$ dipoles is equal to:

$$G_{array}(\theta) = G_{array\,max} \frac{\cos^2(\frac{\pi}{2}\cos(\theta))\sin^2(N_a\gamma_a/2)}{\sin^2(\theta)\sin^2(\gamma_a/2)N_a^2} \tag{3.14}$$

where:

- N_a – number of dipoles in the array,

- $G_{array\,max}$ - maximum gain of a $\lambda/2$ dipole array:

$$G_{array\,max[dB]} = 2.15 + 10.63\log_{10}(N_a) \tag{3.15}$$

- γ_a - array relative phase:

$$\gamma_a = d_a \frac{2\pi}{\lambda}\cos(\theta) + \delta \tag{3.16}$$

where:

- $d_{a[m]}$ – distance between the dipoles,

- $\delta_{[rad]}$ - phase shift.

3.3 System

After the collection of the information from the environment, the signal is then processed by the Rx, Figure 3.5, according to input system specifications.
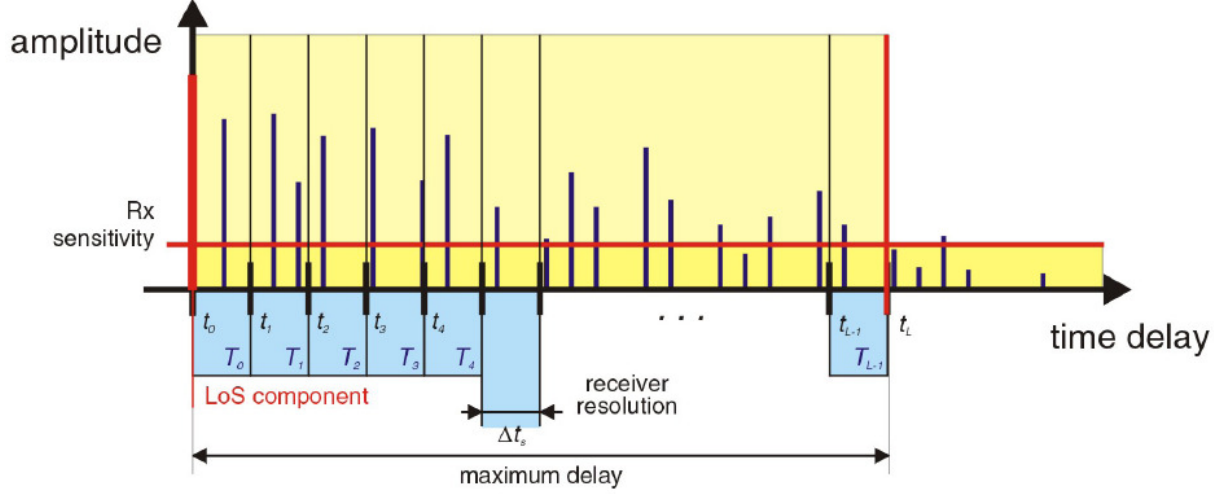
Figure 3.5. Signal processed by Rx. (extracted from [Mack07])

First of all, the amplitude of each MPC is adjusted according to 3D Rx and Tx antenna radiation patterns, AoA and AoD. Then, the amplitude of the MPCs is adjusted according to the power level of the Tx. As a result, it is obtained:

$$V_R(\bar{\tau}) = \frac{A_R(\bar{\tau}, \varphi, \vartheta) \lambda \sqrt{G_T} \sqrt{G_R} \sqrt{P_T}}{Z_A}$$

(3.17)

where:

- $V_R(\bar{\tau})$: is the complex amplitude at the Rx in the continuous time-domain
- $A_R(\bar{\tau}, \varphi, \vartheta)$: is the complex MPC normalised amplitude at the Rx,
- Z_A : is the impedance of Rx antenna.

Based on Rx time-domain resolution or Rx frequency bandwidth, rays are grouped and cumulated. At the same time, the rays which delay exceed the receiver maximum one are neglected. So the operation that transforms signals from the continuous time-domain into the discrete one can be written as:

$$V_R(\bar{\tau}_i) = \sum_{i=0}^{M-1} V_R(\bar{\tau}) \text{, for } \bar{\tau} \in [\bar{\tau}_i, \bar{\tau}_i + \Delta t_s]$$

(3.18)

where:

- $V_R(\bar{\tau}_i)$: is the filtered complex amplitude at the Rx in the discrete time-domain.

At the end, the rays which power is below the Rx sensitivity are also neglected:

$$V_R(\bar{\tau}_i) = 0 \text{, for } V_R(\bar{\tau}_i) < V_{R_{min}}$$

(3.19)

where:

- $V_{R_{min}}$: is the sensitivity of the Rx.

The CIR between the Tx and the Rx has the form:

$$h(t) = \sum_{i=0}^{M-1} \left| V_R(\overline{\tau_i}) \right| . \delta(t - \overline{\tau_i}) . e^{j\phi_{R,\overline{\tau_i}}}$$

(3.20)

where:

- $\delta(t)$: is the Dirac delta distribution.

3.4   Considered Scenarios

In the 3D model one distinguishes between two different types of environments:

- Room/Closed Space, which allows bounces from all over the place. In this specific case, one should differentiate two main situations: an office room, with a metallic roof, Figure 3.6, (magnitude reflection coefficient $\left| \Gamma_s \right|$ =1, and phase ϕ_S =π) and a regular room in which there will not be no restrictions in the magnitude and phase of the reflection coefficient, according to (3.1).
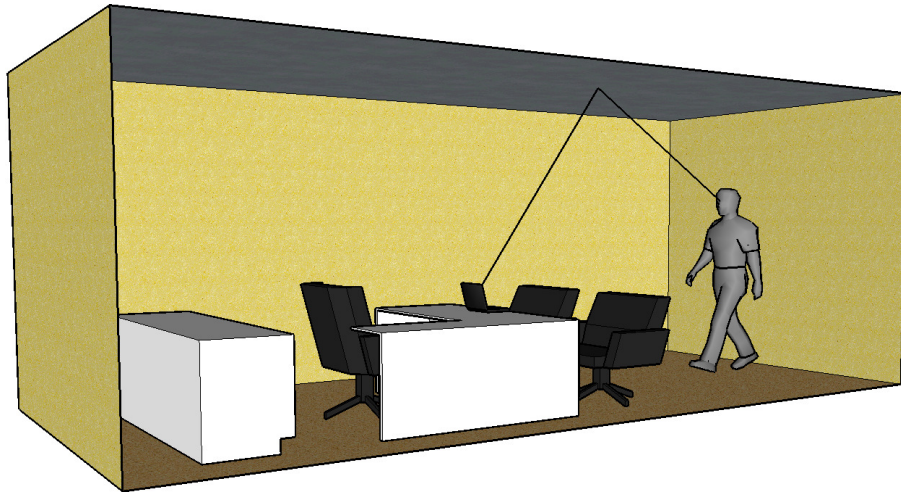
Figure 3.6. Typical office room scenario.

- Street, in which there is no upper bound, like the room. So scatterers are mainly in the lateral sides of the street, e.g., buildings. Also in this scenario, one considers the illumination poles along the street or other reflecting object (in which reflections can occur), according to Figure 3.7.
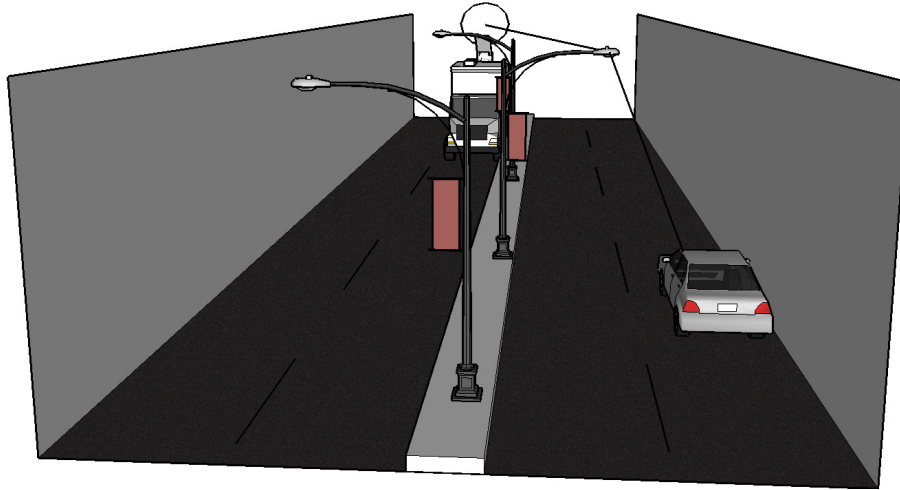
Figure 3.7. Typical street scenario.

In the first type of environment, the main objective is to evaluate the differences between them. Nevertheless, large differences between office and normal room are not expected. This first type of environment, closed space, is a specific type of pico-cell scenario. In this scenario, the BS is located in the centre of the scattering surface (a sphere, or even a spheroid) and the MT can take any position in the room. Still, in the case of large-sized rooms (hundreds of metres), this type of environment can also be assumed as a micro-cell scenario. In this situation, maybe LoS cannot occur due to the high distance between Rx and Tx. The shape of the scattering surface in this case is an ellipse or a spheroid.

For the last type of environment, an urban street, one consideres a micro-cell scenario with the BS and the MT in the beginning and end, respectively, or vice-versa, of the scattering surface (an ellipse in this case). Thus, scattering can occur in the surroundings of both BS and the MT, as well along the street due the multipath contributors presented in the environment.

Chapter 4

Simulator Development

This chapter includes the description of the implementation of the simulator. Input and output parameters, a structure of the code, and the assessment can be found in this chapter as well. At the end, comparison with measurements is done.

4.1   General Structure

The aim of the application is to simulate a physical radio link between multiple input and output antennas, considering 3D single bounces. The needed parameters to describe physical conditions in an environment and the specification of the system are given by the user. These configuration parameters are introduced using an eXtensible Markup Language (XML) file. Annex A presents in detail how this XML configuration file is structured. Moreover, in order to calculate statistics and average results, the simulator can be run automatically as many times as the user wants. The simulator can also cooperate with other applications, like Matlab, in order to automatically present the results. The simulator has been programmed in object oriented C++, which allows to keep each logical module in a different class, in order to make implementation easy and to enable further extensions of the functionalities. The structure of the simulator is as flexible as possible and its general structure can be decomposed into four independent routines, as depicted in Figure 4.1.
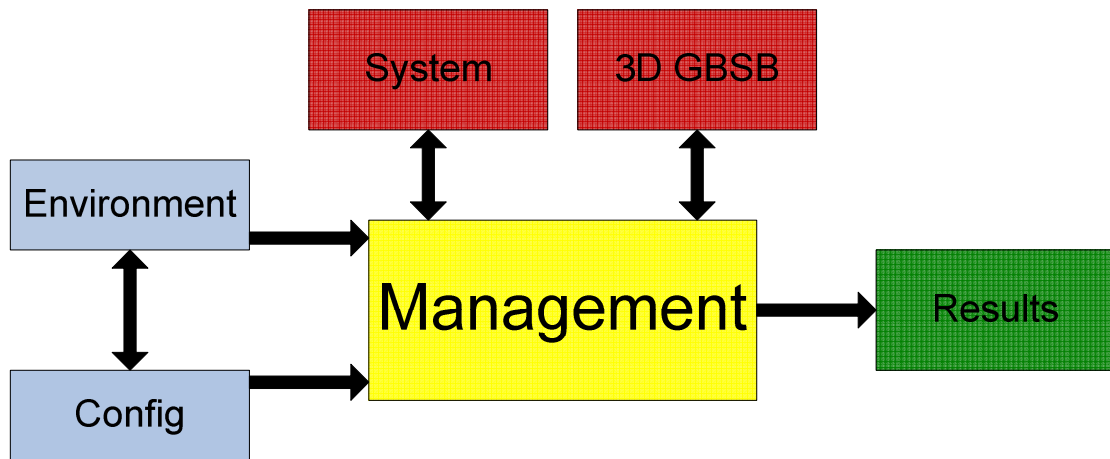
Figure 4.1. General structure of the simulator.

The dark red blocks (the heart of the program), are the ones that use the input parameters from the blue blocks, where the physical radio channel is simulated, and the output signals are calculated. These blocks establish the relation between input parameters and the CIR. The green block calculates parameters of the CIR from each run of the simulator and exports them as Matlab files and the management block gives more control on the data flow in the simulator. Figure 4.2 illustrates the flow of information during a simulator run.
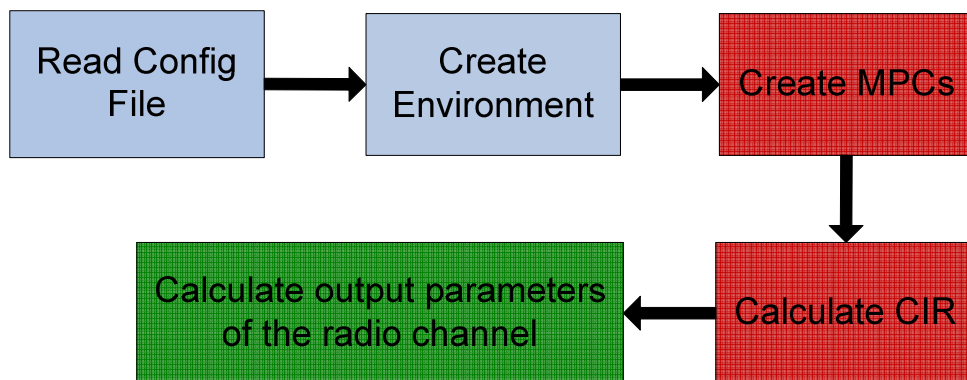
Figure 4.2. Data flow during a simulator run.

After the creation of the environment (from the input parameters), MPCs are created and their output parameters calculated. Then, the MPCs are summed up according to system parameters and the CIR between particular pairs of input and output antennas is calculated. The calculation of the CIR is performed for all combinations of input and output antennas. Finally, output parameters of the radio channel are evaluated.

4.2 Main Simulator Modules

The creation of the environment is prepared by the Environment Module. This module is prepared according to different ways: generated as a reference to input parameters (from the config file) or read from a XML file (a specific scenario previously created). The main idea behind this module is to set clusters and scatterers distributed within a specific region, described by their reflection coefficients. This distribution was done using uniform and gaussian random generators. Also, in order to perform simulations in the same conditions (with the same deployment of clusters and scatterers), export functions are implemented, generating the respectively XML environment file. Figure 4.3 illustrates the procedure of environment generation.
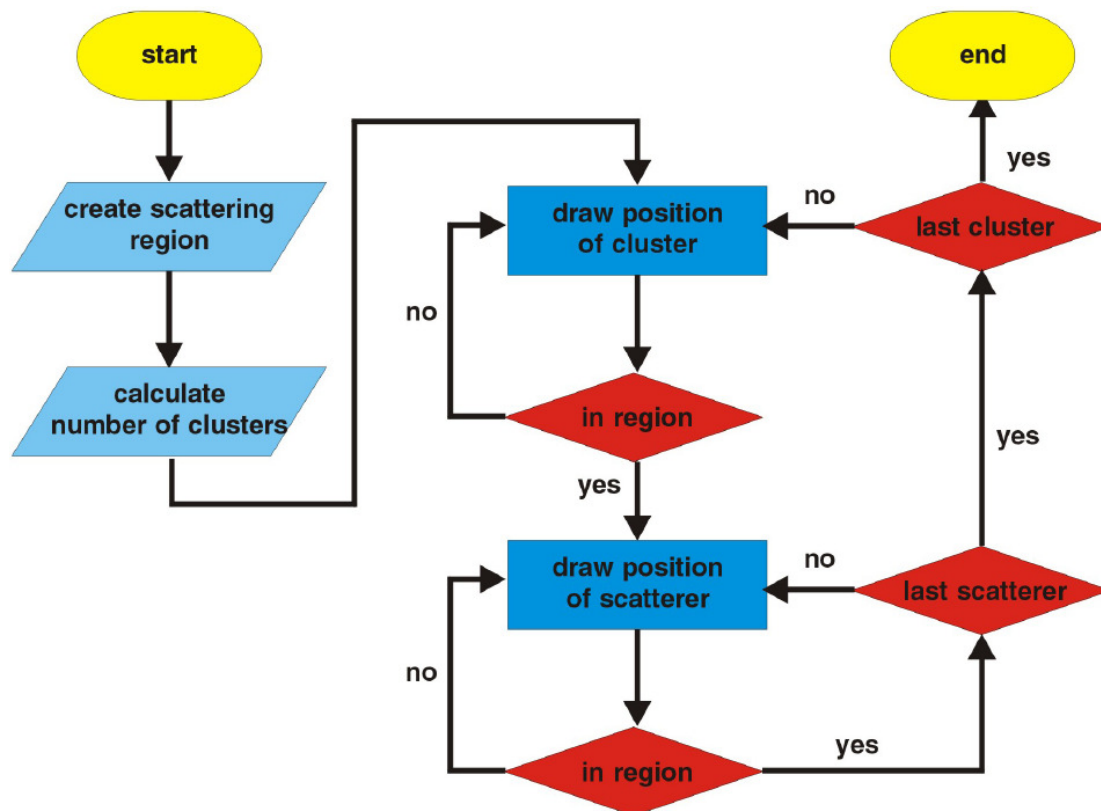
Figure 4.3. Algorithm of environment generation.

First of all, the whole environment is bounded according to the input environment parameters. Then, the specific shape of the environment – sphere, spheroid or ellipsoid – is defined. The clusters coordinates are drawn, according to the Uniform distribution and is always checked if the position of the generated cluster is within the region defined by the environment shape. One neglects the generated scatterer when it is outside the region and the procedure is repeated. Next, the scatterers

are deployed around the centre of the cluster with a Gaussian distribution, where the standard deviation is determined by the radius of the cluster.

The calculation of the output signal is made by two different modules: the 3D GBSB and the system one. The 3D GBSB module is responsible not only for the generation of the LoS path but also for the single bounce paths. First, the parameters for the LoS path are calculated relative to the position of Tx and Rx, and then the calculation of path parameters is done for single bounce paths. The total path length for single bounce paths is the sum of the distance between Tx and the scatterer, and Rx and the scatterer. Also, based on Tx, Rx and scatterer positions azimuth and elevation AoA and AoD are calculated for all the MPCs according to Section 3.2.2. The output of the 3D GBSB module is a list of all the MPCs generated by the environment.

Subsequently, the System module (based on Section 3.3) processes the set of calculated MPCs and transforms them into CIRs, according to system configuration input parameters, such as: maximum delay, Rx time resolution, transmitted power and 3D radiation pattern of antennas. The list of CIRs is also created separately for different azimuth and elevation AoA and AoD. This approach allows to keep the angular information about the received signal, as these data will then be evaluated by the results module. It is also in this module that azimuth and elevation spreads are calculated as well the delay spread, later used by the module responsible for the output of the simulator. The system module handles also the antenna properties in the calculation of the CIR. If Tx and Rx antennas are aligned, antennas radiation patterns are set to their maximum in reference to the LoS path. Then the reference angles (reference Azimuth/Elevation AoD and AoA) are calculated according to the angles to which corresponds the maximum of the Tx/Rx radiation patterns and Tx/Rx LoS angles, previously obtained. Basically, a change in the coordinates system is done. So, for each MPC new Azimuth/Elevation AoA and AoD are calculated according to the reference angles. Moreover, before the amplitude calculation of the CIR between each pair of input and output antennas, one accounts for horizontal or/and vertical rotations in antennas radiation pattern according to input parameters (which are well described in the following section).

The relationship between the previous explained modules and how they cooperate with each other is depicted in Figure 4.4. It is worth to notice, that this is a flowchart which looks into the macro-processes of each main module.

4.3   Input Parameters

The config module is responsible for reading the input parameters from the XML file and store them into memory, to be used by other modules. Moreover, the input parameters of the simulator are organised into four main groups: Simulator, Environment, System and Antenna. It is also worth to notice that the last group (Antenna) is stored in a different XML file. This choice was made regarding the possibility of having different types of Tx or Rx antennas. Besides that, each scenario is described by its name and type, which are the information needed to choose the name of output files and directories. This allows to perform many simulations without the risk of output overwriting by different scenarios.
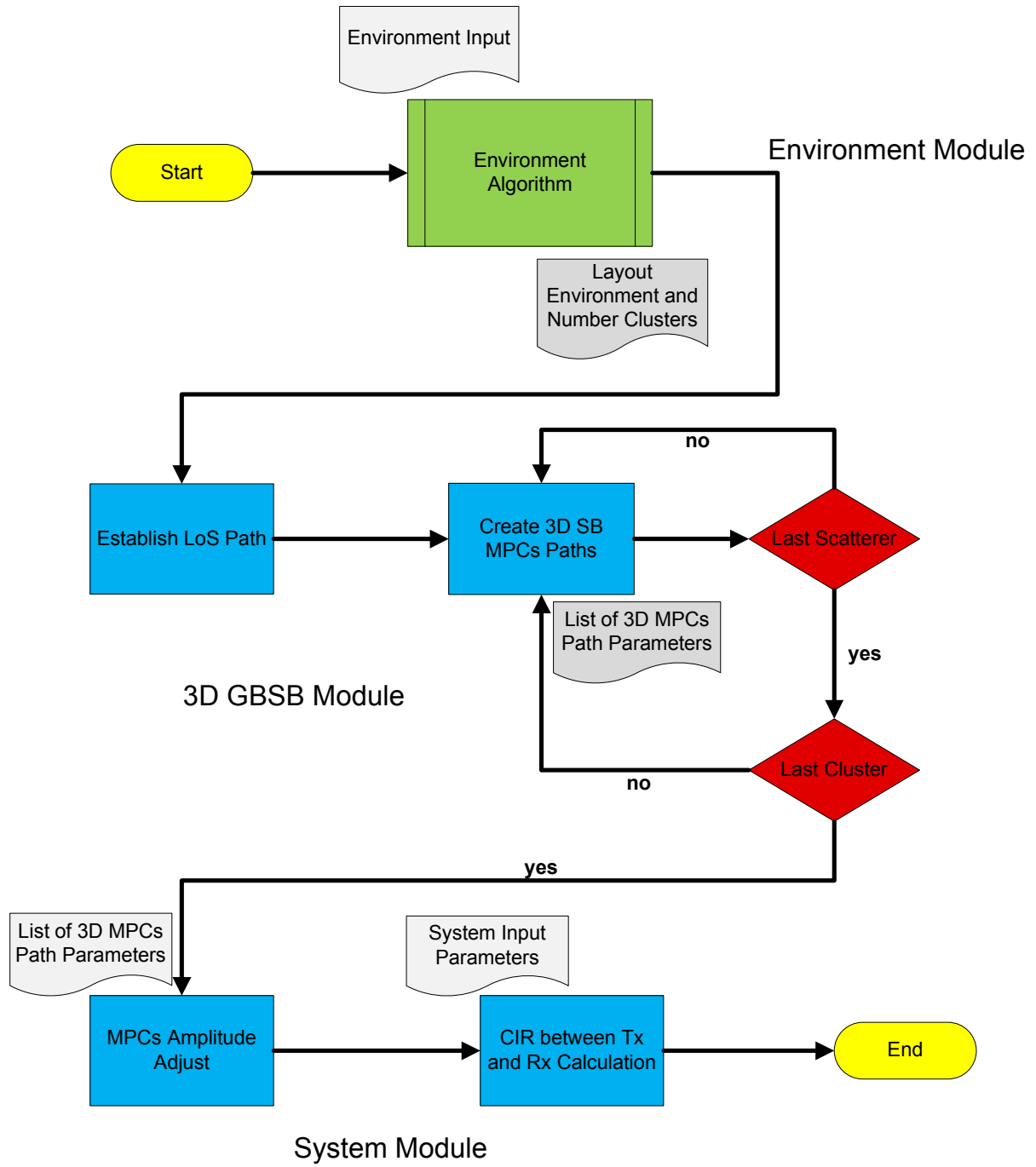
Figure 4.4. Main simulator modules scheme.

The simulator can be controlled by the following parameters:

- N_{run}: number of simulations,
- d_{max}: maximum path length,
- angle resolution,
- mask with the mode of environment generation.

Calculations are repeated N_{run} times for each pair of input and output antennas. Each time, the environment is changed according to the mode of the environment flag, Table 4.1.

Table 4.1. Binary mask of the environment.

mode	randomise position of scatterers	randomise reflection coefficients
decimal value	2	1
mask	ON/OFF	

For the environment, the following input parameters can be defined:

- $d_{c[m^{-3}]}$: cluster density,

- N_{sc}: number of scatterers per cluster,

- $w_{e[m]}$: width of the environment,

- $h_{e[m]}$: height of the environment,

- $d_{e[m]}$: deep of the environment,

- s_e: shape of the scattering region (sphere, spheroid or ellipsoid).

Three different shape types of the scattering region are available in the simulator: sphere, spheroid and ellipsoid. The sphere is described by its radius and centre position, while for the ellipsoid, centre position is defined as well dimension of all axis in order to set up ellipsoid dimensions; for the spheroid, centre position, dimension of large and small axis are defined. Therefore, the number of clusters for a specific scenario is determined by the cluster density and the volume of the scattering region. The volume of the scattering region is calculated according to its type. For the system part, the following input parameters can be defined:

- $f_{[Hz]}$: carrier frequency,

- $\tau_{Max[s]}$: maximum delay,

- $V_{min[V/m]}$: sensitivity of Rx,

- N_R : number of Rx antennas,

- N_T : number of Tx antennas,

- (x_T, y_T, z_T) : coordinates of first Tx antenna from the array,

- (x_R, y_R, z_R) : coordinates of first Rx antenna from the array,

- $d_{a[m]}$: spacing between antennas,

- Rx time resolution,

- Rx position random generated,

- Aligned antennas,

- Mode of Tx power.

The positions of all input and output antennas are calculated relative to the position of first Tx and Rx antennas, being determined by the spacing between antennas. The user has also the possibility to choose if each Tx antenna or all Tx antennas are fed by Tx power. Moreover, the Rx position can be randomly generated in order to transmit the normal variation of the Rx position in a specific scenario. Antenna parameters consist of:

- 3D radiation pattern of antennas,

- Type of antenna,

- N_a : number of dipoles in the array,

- $\delta_{[rad]}$: array phase shift,

- $d_{a[m]}$: distance between the dipoles,

- $H_{r[deg]}$: horizontal antenna rotation,

- $V_{r[deg]}$: vertical antenna rotation.

The properties of the Tx and Rx antennas can be loaded from an XML file according to the input parameters previously presented. Having such structure allows to define the most suitable properties of Tx/Rx antennas for a considered scenario. The mutual coupling between antennas in the array is not taken into account.

4.4 Output Parameters

Output parameters are grouped into four distinct groups: MPCs, CIRs, radio channel statistics and environment. Each MPC is described by the following parameters: Azimuth and Elevation AoA, Azimuth and Elevation AoD and path length. The output parameters of the MPCs are calculated by the 3D GBSB Module.

In what concerns CIRs, the calculated parameters are: delay, amplitude and phase of a ray. Nevertheless, the list of CIRs is not only created for the total arriving signal but it also creates distinct lists for different azimuth and elevation AoA and AoD. This approach allows to keep the angular information about the received signal, in order to be exported as Matlab scripts to create Power Delay Angle Profiles (PDAPs) for Tx and Rx. PDAPs are created isolated for the azimuth and elevation angles and finally the full PDAP of the specific scenario is generated.

After each run of the simulator, some results related to the radio channel can be obtained. Moreover, when all simulations are performed, results are averaged, and for each one, the maximum and minimum values and standard deviation are calculated. Two different groups of output parameters can be obtained from the radio channel: spatio-temporal and power. The first group consists of:

- $\tau_{max[s]}$: maximum delay,

- $\sigma_{\tau[s]}$: RMS delay spread, from (2.8),

- $\bar{\tau}_{[s]}$: mean excess delay, from (2.9),

- $\sigma_{\Omega[\text{º}]}$: RMS angle spread, from (2.11),

- $w_{DCIR[rad/\mu s]}$: channel richness, from (2.15)

while for the latter:

- $P_{LoS[dBm]}$: received power level of LoS component,

- $P_{Rx[dB]}$: single bounce power level in reference to LoS component,

- $Pr_{[\%]}$: percentage of power within single bounce,

- γ : average power decay, from (2.14).

It is also possible to export the layout of the environment as a Matlab script. On the plot, Rx and Tx are depicted and its respective coordinates and the shape of the scattering region is drawn with the respective clusters and scatters randomly generated. An XML file with all information about the environment is always created. This allows the user to load a specific environment previously created in order to perform other simulations with unchanging environment conditions. In addition to the previously output parameters, a Matlab script with the information of antennas radiation patterns is generated. On the plot, the horizontal and vertical planes of the Tx/Rx radiation pattern are depicted. This allows to make a relationship between the obtained results with the type of antenna. In detail, the output files given by the simulator are:

- Config.txt, with the resulting data (input parameters, flags, etc.) from the simulator code,
- RCP.txt, with the statistics about the RCPs of the simulator run,
- CIR.txt, with the CIR parameters between each pair of input and output antenna,
- MPC.txt, with the list of MPCs generated in the environment,
- Environment.xml, with the layout of the environment created in the simulation,
- Environment.m, 3D plot were Rx/Tx position, scatterers and clusters coordinates as well the shape of the scattering region used on the considered scenario are deployed,
- CIR.m, creates a plot of the normalised (in reference to LoS) amplitudes of the CIRs,
- PDAP.m, creates three different plots: Azimuth PDAP, Elevation PDAP and the full PDAP,
- Antenna.m, creates two plots with Rx and Tx antenna radiation pattern used on the simulation,
- Correlation.m, creates a plot with the correlation between links as well a txt file with the numeric data of the correlation among links between input and output antennas and its mean.

4.5   Implementation Assessment

In order to assess the simulator, a specific simple situation was analysed, Figure 4.5. In this case, the environment has only two scatterers, the Tx and Rx. The coordinates of the scatterers are (25, 10, 20) and (35, 20, 30) and the reflection coefficients are:

- $\left|\Gamma_s\right| = 0.5,$
- $\phi_S = \pi.$

Moreover, the scatterers were set to be in the centre of the clusters.

The path parameters obtained are presented in Table 4.2, which were obtained by using the equations presented in Section 3.2.2. Since only two scatterers are assumed in this assess, the result of the signal bouncing in the scattering environment is as expected by two MPCs plus the LoS component.

Table 4.2. Output path parameters.

No.	length [m]	Azimuth AoD[º]	Elevation AoD[º]	Azimuth AoA[º]	Elevation AoA[º]	bounce
1	46.37	45	49.68	45	130.32	LoS
2	48.71	26.57	48.19	71.57	57.69	1
3	49.50	0	45	59.04	55.55	1
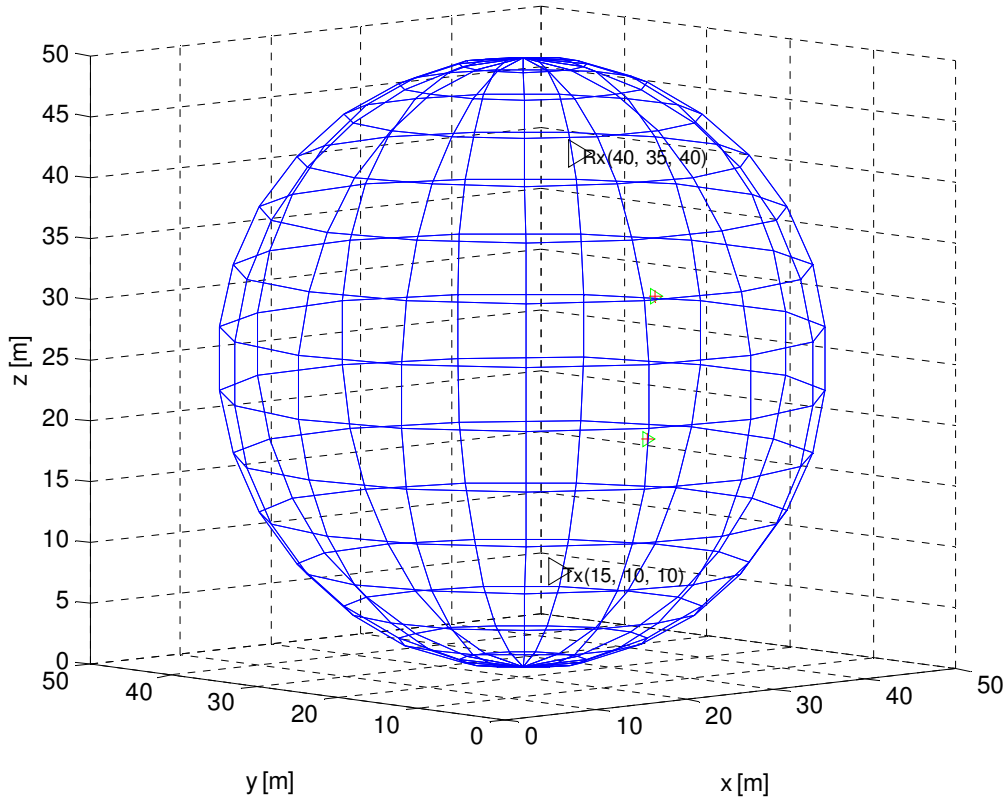
Figure 4.5. Example of the simulator assessment.

Next, one presents the parameters of the CIRs between Rx and Tx, Table 4.3, which are characterized by the following parameters: delay, amplitude and phase. Section 3.2.2 presents the theoretical explanation in order to get these values. To obtain this results the transmitted power was set to $P_T = 1$ W, and the carrier frequency was set to 2 GHz, which gives a wavelength of 0.1499 m. Moreover, the Rx and Tx antennas were set as a $\lambda/2$ dipole. Delay is calculated relative to the LoS component, for which this value is equal to 0. After calculations, comparing the results with the ones in Table 4.2 and Table 4.3, it was confirmed that the modules of the 3D GBSB and system work correctly.

Table 4.3. Output CIR rays parameters.

No.	delay [ns]	amplitude [μV/m]	phase [º]	bounce
1	0	201.24	120.46	LoS
2	7.81	106.47	520.82	1
3	10.44	94.91	256.18	1

Next, one presents the environment assessment. Two different types of tests were done in order to assess the correct environment generation:

- Gaussian scatterer generation within cluster,
- Uniform cluster generation within scattering region.

Figure 4.6 presents the assessment of scatterer generation within a cluster. It was simulated for a specific environment, with only a cluster but 1000 scatterers within the cluster.
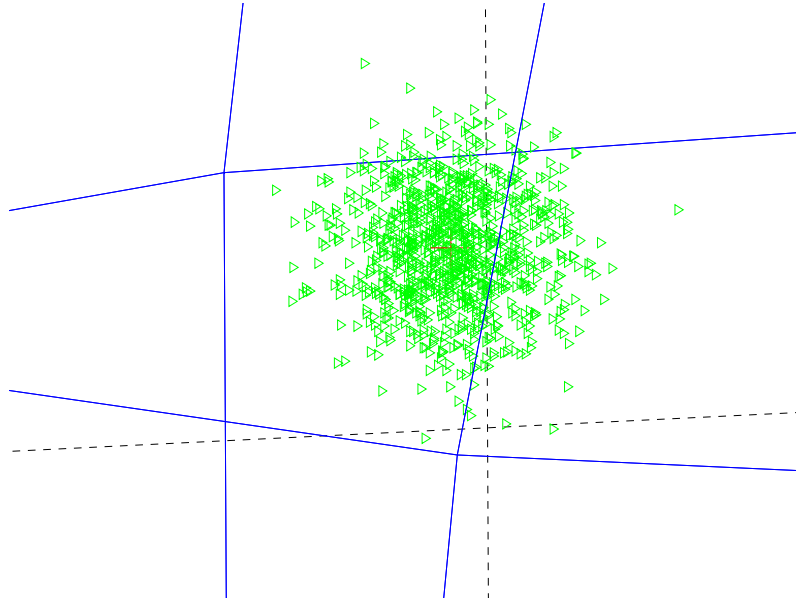
Figure 4.6. Zoom in, on the Gaussian scatterer generation.

A mean value of coordinates of all scatterers was calculated: $(\bar{x}, \bar{y}, \bar{z}) = (26.01\ m, 46.36\ m, 63.19\ m)$.

The ideal mean coordinates should be (26.00 m, 46.40 m, 63.20 m), which is the centre of the cluster. The obtained results have an insignificant error, (0.04 %, 0.08 %, 0.01 %), which confirms the correct distribution of the scatterers.

Table 4.4 presents the full results obtained for both tests, for the previous one and for the Uniform clusters generation. It is worth to notice that the scattering region in the tests was set as a sphere, in which the localisation of the generated clusters and scatterers positions in terms of the coordinates system were accounted for.

Table 4.4. Scatterers and clusters deployment.

side	N_{sc}	N_{sc} error [%]	N_c	N_c error [%]
xyz - bottom	130	4.83	253	3.68
xy-bottom z-up	121	2.41	247	1.22
xz- bottom y- up	114	8.06	227	6.96
x- bottom yz- up	120	3.22	256	4.91
xyz- up	129	4.03	254	4.09
xy- up z- bottom	113	8.87	240	1.63
xz- up y- bottom	125	0.8	236	3.27
x- up yz- bottom	140	12.9	240	1.63

Figure 4.7 presents the Uniform clusters generation in an environment with 2000 clusters.
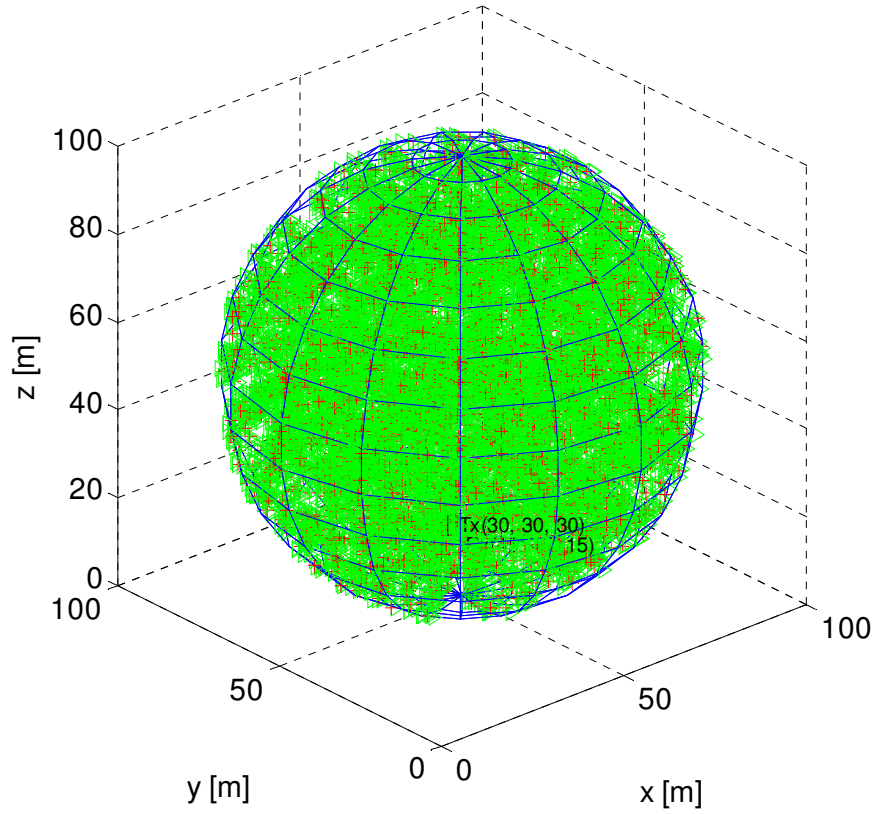
Figure 4.7. Assessment of clusters generation.

A mean value of coordinates of all clusters was calculated: $(\overline{x}, \overline{y}, \overline{z}) = (49.95\ m, 49.97\ m, 50.63\ m)$. The ideal mean coordinates should be (50 m, 50 m, 50 m) which is the centre of the sphere. The obtained results have an insignificant error of (0.09 %, 0.06%, 1.26%), which confirms the correct uniformly distribution of the clusters. The previous tests show the correct generation of the environment.

4.6   Influence of Parameters

In order to check the simulator with a real life situation, an indoor scenario was defined, a medium-sized room (length ~ 12m) based on the measurement campaign conducted within the cooperation of Elektrobit,   Vienna University of Technology, and University of Oulu / Centre for Wireless Communications [Czin07]. The measurements were done with LoS between Rx and Tx, with a carrier frequency 2.55 GHz and a Tx power equal to 0.4 W. Tx antenna height was set at 1.53m and Rx antenna at 0.82m. For Tx antenna an omni-directional patch array was used and for Rx antenna an uniform circular monopole array. The Rx and Tx antenna radiation patterns used to perform the simulations are presented in Figure 4.8.

Measurement results obtained were evaluated using pdfs. The following results were found: RMS delay spread $\sigma_\tau \in$ [5 - 18] ns, RMS angle spread $\sigma_\Omega \in$ [5º - 30º], number of clusters $N_c \in$ [2 - 12] and number of paths, $N_{MPC} \in$ [5 - 15]. In order to setup the input parameters for this scenario, some

simulations were performed. The output parameters (i.e., RMS delay spread σ_τ, RMS angle spread σ_Ω and received power relative to the LoS component P_{Rx}) were calculated for different number of clusters N_c in the environment and for different numbers of scatterers N_{sc} (2, 4 and 6) within the cluster.

(a) Rx pattern (b) Tx pattern
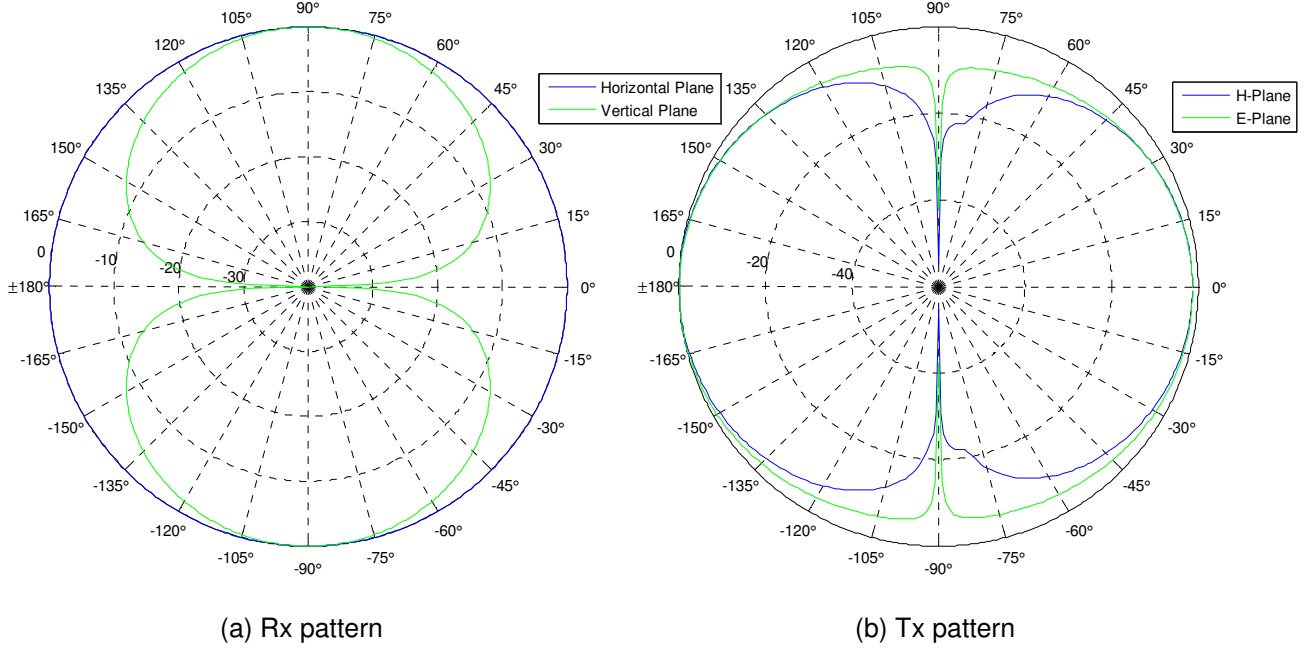
Figure 4.8. Rx and Tx antenna radiation patterns.

The analysis of the RCP obtained from simulations with a varying number of clusters and scatterers, led to some general conclusions. From Figure 4.9, the RMS delay spread increases gradually when more clusters or scatterers are present in the scattering region and their values are in conformity with the measurements for all the numbers of clusters and scatterers.
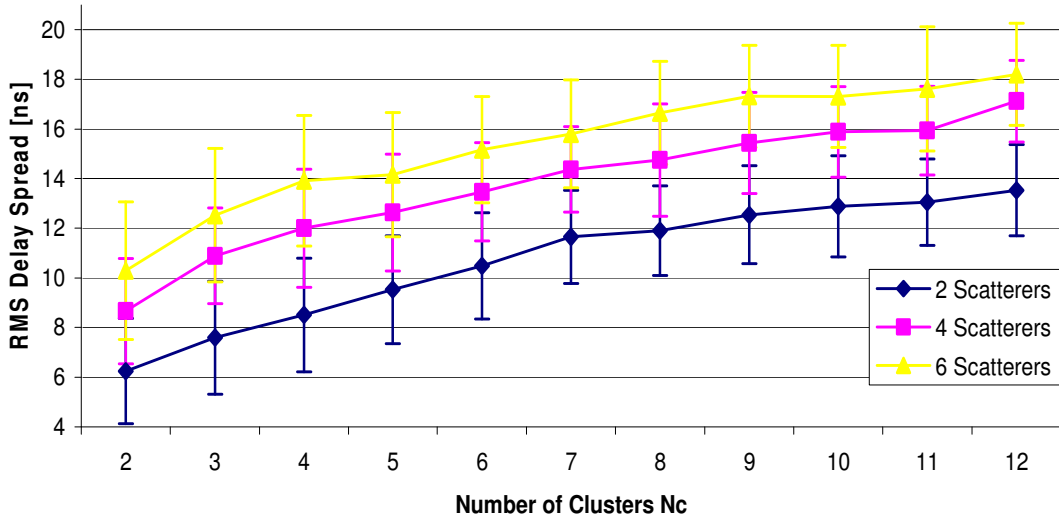
Figure 4.9. RMS delay spread for different number of clusters and scatterers.

Figure 4.10 presents the RMS AoA spread, where a significant variation on the angular spread for different number of clusters and scatterers is observed. Angular properties are related mostly to the dimensions and shape of the scattering region. As expected, with a higher number of scatterers a

higher value of the RMS angle spread is observed. For this particular RCP, not all the values are in conformity with measurements. Only for the following situations one obtains acceptable values for the RMS angle spread: two clusters, three clusters (with 2 and 4 scatterers), four, five and six clusters (with 2 scatterers).
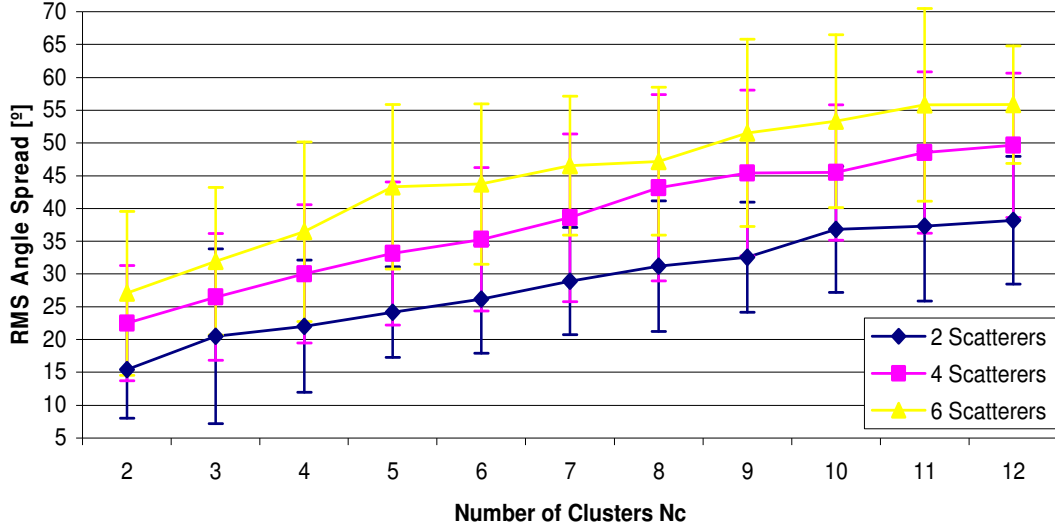
Figure 4.10. RMS Angle spread for different number of clusters and scatterers.

In order to choose the cluster density and number of scatterers for this scenario from the previous options, in concordance with measurements, the number of MPCs was also evaluated for each option. The average number of MPC measured was equal to 10. Moreover, the number of clusters measured with a probability density function over 0.1 was between 5 and 8. Additionally, the authors of [YLCP04] found cluster sizes (the whole extent of a cluster) ranging between 6º and 36º and identified 4-5 clusters (for each individual data set) for comparable indoor scenarios. The authors of [CWTN07] identified 4.4 clusters and a RMS delay spread of 10 ns, on average, for similar indoor scenarios. So, based on the previous measured data, 5 clusters with 2 scatterers were picked.

Each path carries a portion of radiated power and at the Rx all MPCs are summed up in a coherent way. Thus, more paths give higher values of received power, which is illustrated in Figure 4.11.

Moreover, it is observed that the LoS path is the responsible for the received power, because Rx and Tx are at small distances. Nevertheless, when the number of clusters increases, single bouncing has a greater participation on the received power. Particularly, for 12 clusters and 6 scatterers, it is almost 50% the total amount of received power carried by single bounce paths.

Based on the observations presented above, input parameters for the Vienna scenario were chosen, Table 4.5.
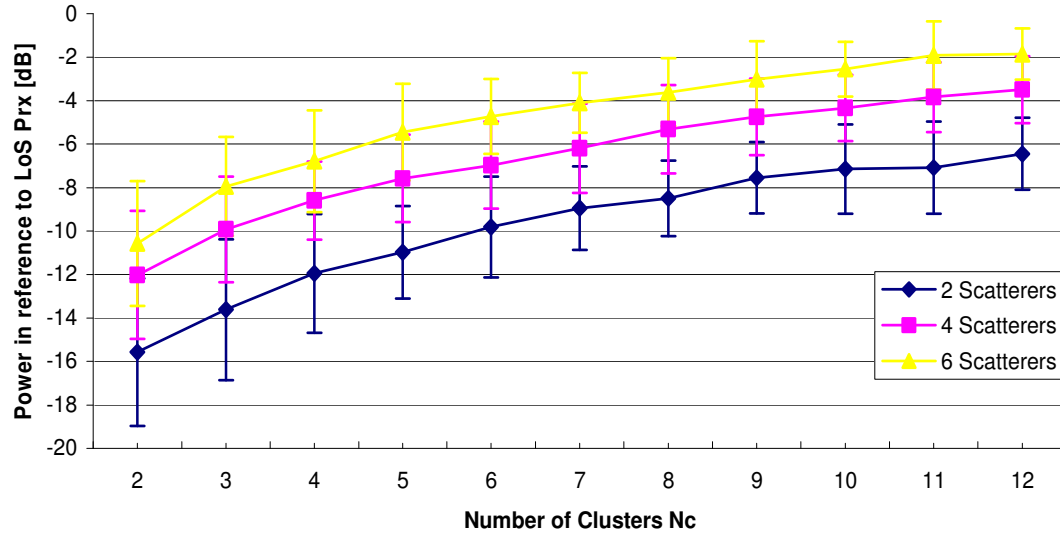
Figure 4.11. Received power for different number of clusters and scatterers.

Table 4.5. Input parameters for Vienna scenario.

Name	Vienna	
scenario type	Pico-cell	
propagation conditions	LoS	
shape of scattering region	Sphere	
radius of scattering region [m]	6	
distance between Tx and Rx [m]	3	
single bounce	cluster density $\left[\dfrac{1}{m^3}\right]$	0.007
	number of clusters	5
	number of scatterers	2
frequency [GHz]	2.55	
wavelength [m]	0.117647	
Tx Power [W]	0.4	

Chapter 5

Analysis of Results

This chapter consists of descriptions of the used scenarios and results of simulations. Radio Channel Parameters for the SISO channel are calculated for different scenarios. Next, the correlation properties between links in MIMO systems are examined. At the end, the relative MIMO capacity gain is calculated and the 3D approach is compared with the 2D one.

5.1 Scenarios Description

In order to make a realistic investigation into differences introduced by 3D SB, it is necessary to choose appropriate scenarios for the simulations. This approach helps to find places where the influence of 3D SB on MIMO capacity is most significant. In particular, indoor scenarios are the object of this investigation.

The following scenarios were taken for simulations:

- Small-sized (length ~ 6m) office room (pico-cell), Figure 3.6,
- Small-sized (length ~ 6m) normal room (pico-cell),
- Large-sized (length ~ 100m) room (micro-cell),
- City street scenario, Figure 3.7, (micro-cell).

Scenarios have been defined for the SB case. The cluster density and number of scatterers were taken from [Mack07], [Koko05] and from the values available in the literature, [Czin07]. The small-sized office room is a specific case of a room with a metallic roof (magnitude reflection coefficient $|\Gamma_s|$ =1, and phase ϕ_S =π), Section 3.2. The shape of scattering region used for this scenario is the sphere. The height of this room was set equal to 3m. An example of a deployment of clusters for the typical office room is depicted on Figure 5.1.
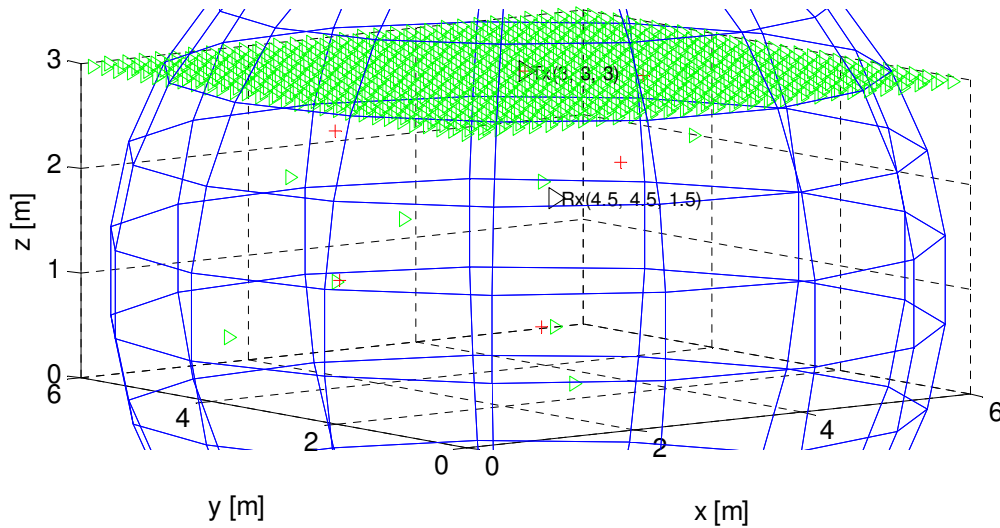
Figure 5.1. An example of a deployment of clusters for the typical office room.

The scenario of the small-sized normal room is very similar to the previous one, with the exception of the roof. An example of a deployment of clusters for the small-sized normal room scenarios is depicted on Figure 5.2. The type of the roof is, concrete, without the previous reflection properties. So, this environment has less scattering richness comparing with the first one. In this specific type of environment, a group of tests was performed in order to see the differences in the RCPs with the variation of some parameters, like:

- density of scatterers within the cluster,
- Tx position,

- room dimensions.

Figure 5.2. An example of a deployment of clusters for the typical normal room.

For the variation of the density of scatterers within the cluster, one considered clusters with 2, 4, 6, 8 and 10 scatterers. Next, when the Tx position was changed, three different groups of coordinates were set, all of them at the ceiling:

- Position 1: at the middle of the room; $\{x, y, z\} = \{3, 3, 3\}$, reference position,

- Position 2: at the beginning of the room; $\{x, y, z\} = \{0, 3, 3\}$,

- Position 3: at the end of the room; $\{x, y, z\} = \{0, 6, 3\}$.

For these 3 positions, the Rx position is fixed, $\{x, y, z\} = \{4.5, 4.5, 1.5\}$, but one also presents the values of the RCPs for the Tx reference position with the Rx position randomly generated. At last, room dimensions were changed. Four different room dimensions were simulated:

- Dimension 1: reference room dimension with $\{x, y, z\} = \{6, 6, 3\}$,

- Dimension 2: decreasing the length of the room, $\{x, y, z\} = \{6, 3, 3\}$,

- Dimension 3: increasing the length of the room, $\{x, y, z\} = \{6, 9, 3\}$,

- Dimension 4: increasing the length of the room, $\{x, y, z\} = \{6, 12, 3\}$.

Dimension 4 has 4 times the room length of dimension 2 room, which allows to see the differences between the RCPs when the dimension of the room is changed. These simulations were performed with the Tx reference position and Rx position set equal to $\{x, y, z\} = \{4.5, 1.5, 1.5\}$. Consequently, the distance between Rx and Tx was set constant.

The large-sized scenario is a specific case of an airport or a shopping centre. Even though this situation can be treated as a pico- or a micro-cell, for the purpose of this work only the micro-cell is considered.

Active users can be located in many locations: outside the building, on the platform ready to embark

and in other facilities, e.g., waiting rooms, shops, etc.. This scenario may be enhanced to more complicate radio situations, by combination of a few scenarios, but for the purpose of this work, the micro-cell consists of a BS located in its centre (placed on the main hall). The radius of the scattering region (spheroid) is set to 50m. An example of a deployment of clusters for these scenarios is presented in Figure 5.3. In this specific type of environment, a group of tests was performed in order to see the differences in the RCPs with the variation of some parameters, like:

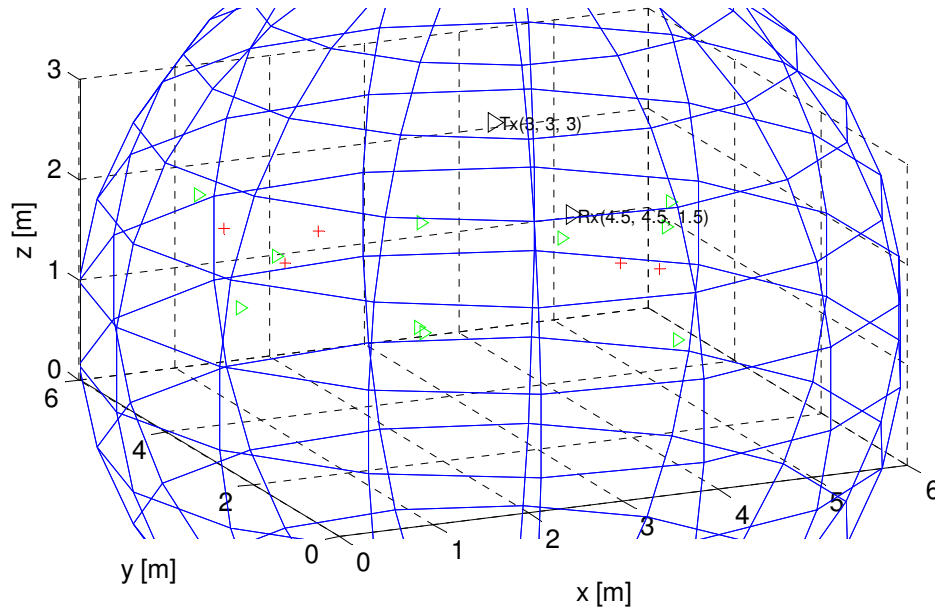- density of scatterers within the cluster,
- α_{3dB},
- Rx sensitivity,
- system time resolution.

For the variation of the density of scatterers within the cluster, one considered clusters with 10, 15 and 20 scatterers. It is also interesting to see the variation of the RCPs (namely the delay spread and the angle spread) with the variation of α_{3dB}. For this study, a $\lambda/2$ dipole and an array of (2, 4, 6, 8 and 10) $\lambda/2$ dipoles were used in order to reduce the α_{3dB}. Results show the variation of RCPs for the respective angles: 48º, 25.4º, 12.7º, 8.5º, 6.3º and 5.1º. Next, one changed Rx sensitivity. By default, it was assumed in all simulations an Rx sensitivity equal to 0 W. However, it should also be considered better values of Rx sensitivity, like $10^{-4}, 2\times10^{-4}, 3\times10^{-4}$ and 10^{-3} W. As a direct consequence of increasing Rx sensitivity, less rays will be detected by the Rx. Finally, it is taken system time resolution into account, which influences the number of MPCs that can be distinguished at the Rx. For this test, the following values of system time resolution were used: 1, 10, 100 and 260 ns. It makes sense to perform the tests of the Rx sensitivity and system time resolution in the environment with the highest number of generated MPCs, the large-sized room scenario, in order to get reliable conclusions.
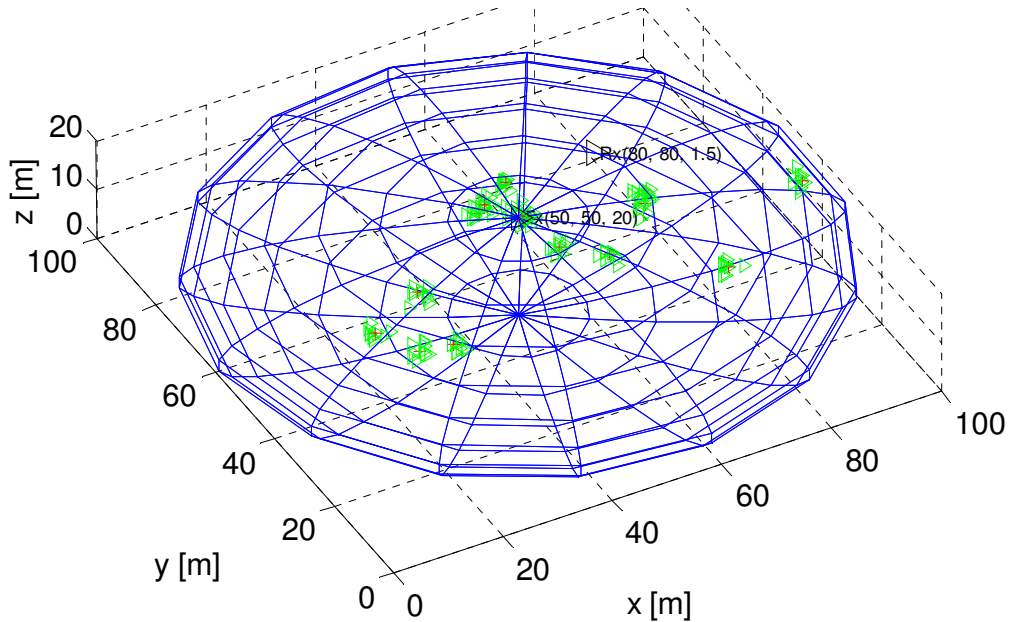
Figure 5.3. An example of the deployment of clusters for the large-sized room.

The street scenario is a scenario typical for an urban environment. The street has a grid pattern and is bounded by buildings, which are the reason for wave guiding along the street canyons. Reflections

mainly occur in buildings (on the lateral sides of the street), but also can happen on other reflection objects, such as: illumination poles, cars (this is very relevant during a traffic jam situation), etc.. The typical shape of the scattering region used for this scenario is the ellipsoid with MT and BS at its foci. An example of a deployment of clusters for the city scenarios is shown in Figure 5.4. For this specific scenario, the density of scatterers within the cluster was varied. One considered clusters with 10, 15 and 20 scatterers.
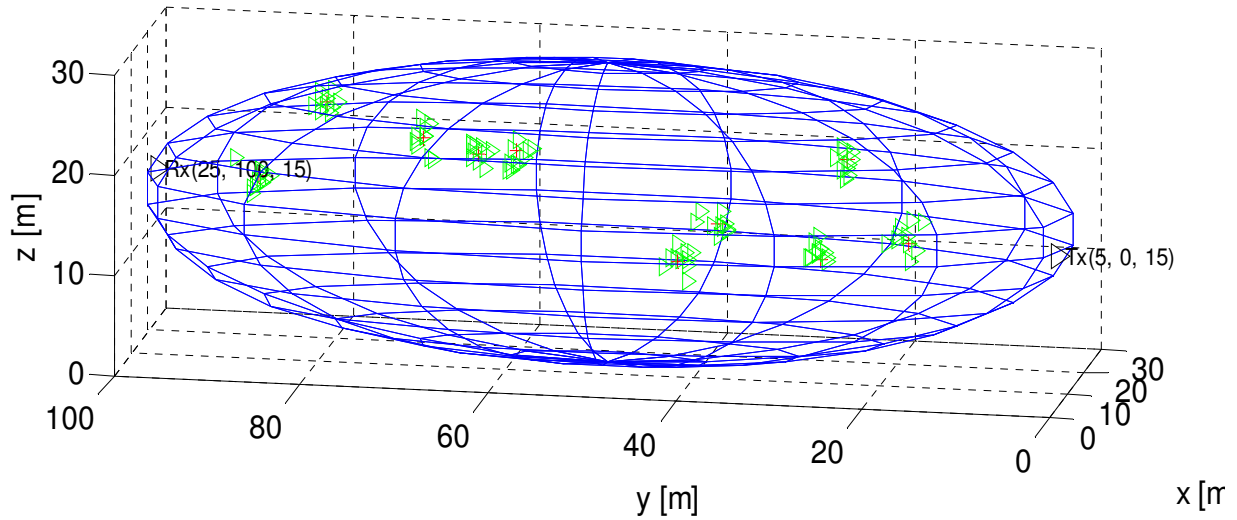
Figure 5.4. An example of the deployment of clusters for the city street scenario.

All parameters for the scenarios can be found in Table 5.1, providing all the information for the conditions of the radio environment. The system in consideration is UMTS, thus the spacing between antennas equals 0.15m, λ, which is sufficient to give enough decorrelation between CIRs.

Table 5.1. Input parameters.

Simulation				
name	small office room	small normal room	large room	street
scenario type	pico-cell		micro-cell	
Environment				
propagation conditions	LoS			
shape of environment	Sphere		spheroid	ellipsoid
cluster density $\left[\dfrac{1}{m^3}\right]$	0.02		0.00015	0.00005
number of clusters	5		15	10
number of scatterers	2		10	10
Tx - Rx distance [m]	2.5		45	100
System				
carrier frequency [GHz]	2			
bandwidth [MHz]	5			
wavelength [m]	0.149896			
Tx power [W]	1			

5.2 SISO Channel

The aim of this research is to check how 3D SB influences RCP (i.e., spatio-temporal and power parameters), depending on the considered scenario. When RCPs for simulations are calculated, CIRs are not filtered in the time domain, thus, results are not dependent on system parameters. All presented values of output parameters are the average of 200 simulations in order to make the statistics of the RCPs reliable. Also, to compare the RCPs obtained with the ones of the 2D model developed in [Mack07], the statistics of the 2D GBSB model are presented too. Nevertheless, it is worth to notice that the Rx/Tx antennas used in the 2D GBSB model are isotropic antennas. So with this restriction on the antennas type, to do a consistent comparison between the two models, the simulations of the 3D one were performed also with isotropic antennas. Even though, others simulations were also performed with Tx/Rx antennas being $\lambda/2$ dipoles as well with different antennas types.

At the beginning, the study of the small-sized room was performed. One presents in Table 5.2 the results of the RCPs of a normal and office room as well the 2D results for a normal room. The RCPs and how they can be obtained are explained in Section 4.4.

Table 5.2. RCP for small room for 2D and 3D and for different type of room.

	small normal room				small office room	
	2D		3D		3D	
	mean	std	mean	std	mean	std
τ_{max} [ns]	16.01	2.51	17.71	3.15	18.19	3.31
σ_τ [ns]	3.83	0.90	4.50	0.97	4.68	1.01
σ_Ω [º]	38.90	14.10	60.94	10.72	63.98	10.18
$w_{DCIR}\left[\dfrac{rad}{\mu s}\right]$	192.86	101.21	251.43	85.91	252.52	79.25
Pr [%]	49.34	11.02	48.58	9.50	55.03	8.56
γ	1.06	0.30	1.28	0.20	1.14	0.20

In the case of the small normal room, the major difference between 2D and 3D RCPs is the angle spread, as expected. This can be explained by the simple fact of considering a 3D domain. One extra dimension has the effect of increasing the angle spread since the shape of the scattering region goes from a circle in the 2D case to a sphere in the 3D one. One also observes a slight increase on the delay spread for the 3D case also related with the previous explaination. Another interesting difference is the channel richness. The 3D model presents a higher channel richness than the 2D one, which was also expected since the angle spread is over 36% higher in the new model than the old one.

The major difference between normal and office rooms is the fact that the latter has an extra MPC due the reflection on the roof. This means a higher received power due to single bounce relative to to LoS. This fact is well shown on the difference of Pr [%] between the two difference scenarios. Having one more reflecting object, increases also the angle spread as well the delay spread, even though the differences are small.

The average power decay indicates indirectly the value of the overall attenuation of the radio link, being also called the path loss exponent. The obtained values, assume a constant loss, C_L, equal to 1. However, more than the absolute values, the interest on this RCP is to analyse its variation along different situations. The lower the value of the average power decay, the more rich in reflectorsthe environment is. This conclusion is well proved by the lower value in the small office room than in the small normal room.

The results of two RCPs when the density of scatterers within the cluster is changed are presented next. Rx and Tx antennas radiation patterns used to perform these simulations were the same as the ones presented in Figure 4.8. The all set of RCPs for this test and for all others is presented in Annex B. Figure 5.5 shows the variation on these two RCPs when one changes the density of scatterers within the cluster.
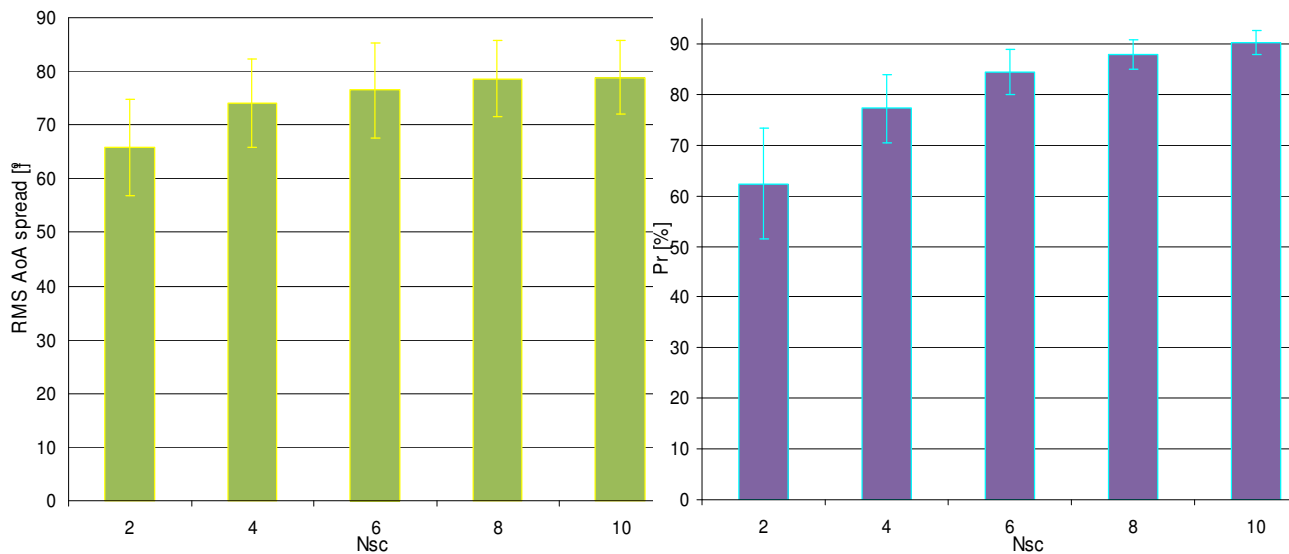
Figure 5.5. RCPs for different number of scatterers within the cluster.

Analysing the obtained results, almost no variation is obtained on the delay spread. This happens, because there are no changes in the room dimensions, despite the slightly increase in maximum delay. So increasing the number of scatterers in the cluster has no influence on delay spread. A gradually increase on the received power due to single bounce relative to LoS is observed, since there are more interfering objects. So, if the multipath phenomenon gets stronger, the received power due LoS decreases. Angle spread is also affected by the variation of scatterers within the cluster, since in the same environment conditions more interfering objects are added on, increasing the channel richness.

For the variation of Tx position, Table 5.3 presents the RCPs for this study and considering the same room scenario.

Table 5.3. RCPs for the small normal room for different Tx positions.

	Tx position variation							
	Position 1		Position 2		Position 3		Rx position rand.	
	mean	std	mean	Std	mean	std	mean	std
τ_{max} [ns]	17.88	2.98	12.08	2.96	17.27	3.77	17.77	3.55
σ_τ [ns]	4.83	1.14	4.24	0.93	4.53	1.16	4.59	1.29
σ_Ω [º]	65.79	9.06	69.24	10.15	64.09	10.42	72.90	22.27
$w_{DCIR}\left[\dfrac{rad}{\mu s}\right]$	255.17	87.79	405.78	99.49	267.55	98.56	306.01	96.60
Pr [%]	62.33	10.96	69.77	9.44	55.63	11.27	66.07	16.94
γ	0.93	0.32	1.23	0.19	1.47	0.16	0.59	0.56

From these results, it is concluded that the Tx position has influence on the RCPs. Still, delay spread is almost not affected by Tx positions. It is in Position 2 that one obtaines the higher values of the AoA spread and the received power due to SB relative to the LoS component. This happens, for the reason that Tx and Rx are at opposite sides of the room and their distance is higher than in the other cases. Also, as expected, when the Rx position is randomly generated, higher values on the standard deviation of the RCPs are observed.

When room dimensions were changed, it is worth to notice that in face of the decrease/increase of the scattering area (due the variation in room dimensions), cluster density has to be adjusted in order to maintain the same value of clusters as the reference room dimension. This was done to keep the room with the same characteristics in order to do a reliable comparison among the several rooms. Table 5.4 shows the obtained results. This study leads to some conclusions: enlarging room dimensions increases the delay spread on the one hand, but decreases the angular spread and the channel richness on the another. Obviously, RCPs are influenced by the size and shape of the scattering area, which varies with different room dimensions. Moreover, analysing rooms Dimension 1 and 4, one observes an increase on the delay spread of approximately 40%. It is worth to notice that room Dimension 4 has the double of length than room Dimension 1, so, doubling room length almost increases the delay spread 40%. As Rx-Tx distance was set constant, 2.6m, enlarging room dimensions increases the power carried by the LoS component just because the interfering objects become more disperse, delocalised in the environment. For room Dimension 4, the receiver power due to single bounce is just 34.17% of the total received power, approximately 45% less than in the

reference dimension room.

Table 5.4. RCPs for different room dimensions.

	Dimension 1		Dimension 2		Dimension 3		Dimension 4	
	mean	std	mean	std	mean	std	mean	std
τ_{max} [ns]	17.81	3.17	13.85	3.18	21.86	3.78	32.39	4.80
σ_τ [ns]	4.81	1.20	3.74	1.03	5.38	1.12	7.88	1.33
σ_Ω [º]	66.09	10.64	62.94	11.82	61.95	8.08	53.21	8.21
$w_{DCIR}\left[\dfrac{rad}{\mu s}\right]$	257.70	84.38	320.88	120.97	211.96	61.00	121.87	31.62
Pr [%]	62.74	11.45	62.53	11.88	54.41	13.66	34.17	13.09
γ	0.91	0.34	0.92	0.35	1.13	0.33	1.54	0.23

In Annex B, one presentes the full RCPs for three different types of the Tx antenna radiation pattern. These are three different examples of antenna radiation patterns used by mobile operators, nowadays. In spite of the few differences among them, the RCPs stay almost unchangeable.

The analysis of the large room scenario as well the values of the RCPs is presented in Table 5.5. The examples of CIR and Power Delay Angle Profiles (PDAPs) for this scenario are presented in Figure 5.6, and others, can be found in Annex C.

Table 5.5. RCPs for 2D and 3D large room scenario and for different number of scatterers within the cluster.

	large room scenario									
	2D		3D		3D $N_{sc}=10$		3D $N_{sc}=15$		3D $N_{sc}=20$	
	mean	std	mean	std	mean	std	mean	std	mean	std
τ_{max} [ns]	302.77	25.04	256.99	42.86	263.67	40.26	262.85	42.18	264.60	43.96
σ_τ [ns]	75.40	10.13	54.52	10.07	63.91	12.19	62.67	11.86	63.12	12.49
σ_Ω [º]	42.78	11.89	47.15	12.02	42.52	8.44	41.79	8.53	40.45	7.45
$w_{DCIR}\left[\dfrac{rad}{\mu s}\right]$	10.13	3.26	15.67	5.22	12.21	3.48	12.08	3.42	11.66	3.34
Pr [%]	94.54	1.10	95.89	0.61	95.45	0.75	96.92	0.49	97.70	0.32
γ	1.22	0.05	1.16	0.04	1.19	0.04	1.09	0.04	1.01	0.04

Comparing the obtained values from the 2D case with the 3D one, the main difference observeed is the decrease of the delay spread. Despite this difference, which is also reflected on the maximum delay (due to its dependency), angle spread presents also some variation between the two models, being 9.3% higher in the 3D model than in the 2D one. It is observed that for the small room scenario the difference in this RCP is much higher (36.2%) than for this one. This can be explained by the different room lengths of the scenarios. Moreover, when a large-sized room is assumed, the influence of considering a 3D model is less than in a small-sized room. It is also worthwhile to notice that the scattering shape used to simulate the 2D case was a circle in opposition to the spheroid for the 3D one.

(a) CIR

(b) Azimuth PDAP

(c) Elevation PDAP

(d) Full PDAP
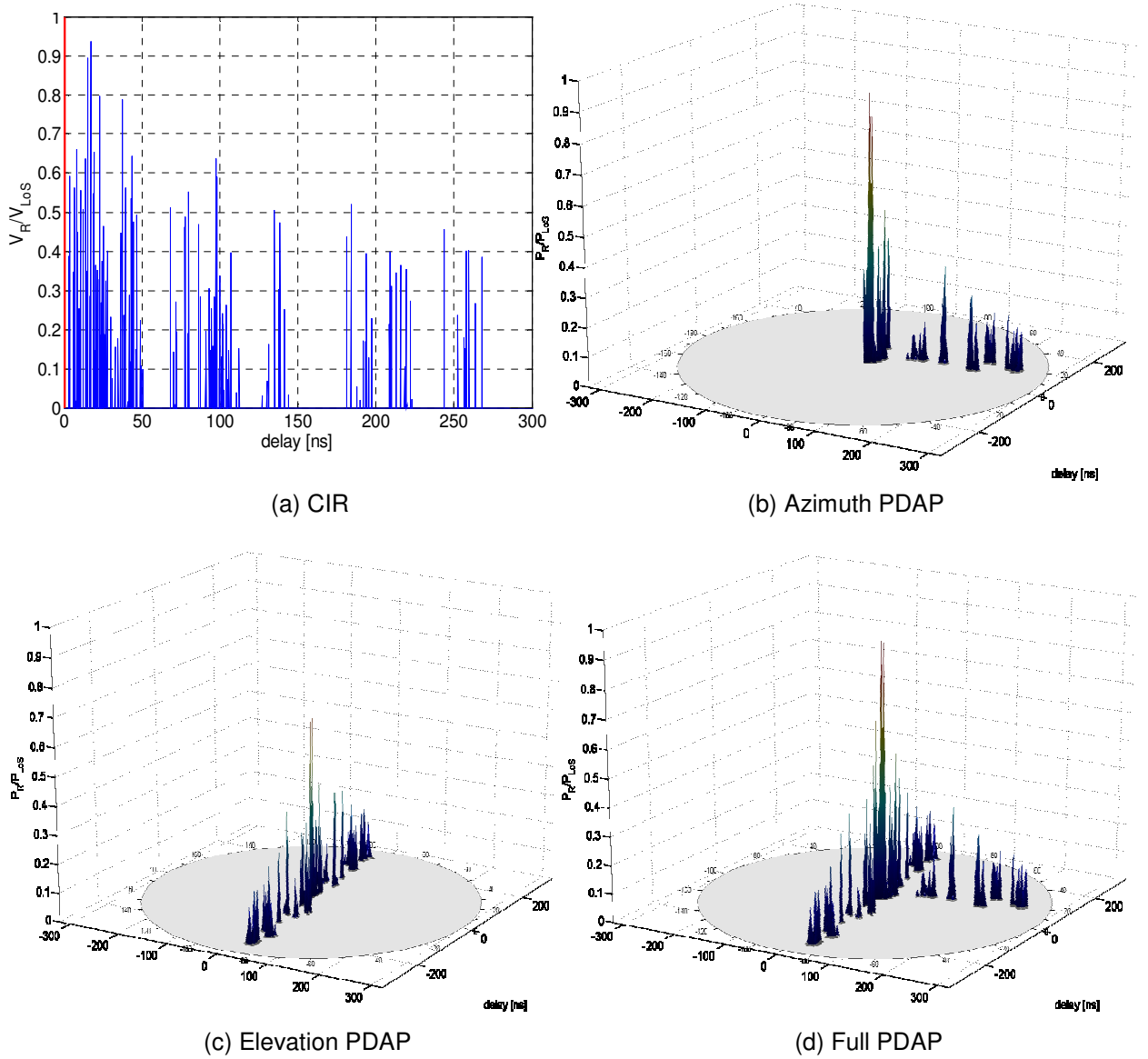
Figure 5.6. CIR and PDAPs for the large room scenario.

It is also possible to compare the variation of the RCPs when the density of scatterers within the cluster is changed. Simulations were performed with Tx/Rx antennas being $\lambda/2$ dipoles. Like the small room scenario, the delay spread stays constant, nevertheless for this specific type of scenario the angle spread presents a decreasing tendency, remaining almost constant due the characteristics of

the room and of the scattering region. Delay spread growth is more intense when the number of reflectors is small, and then this effect gradually saturates for a high number of scatterers, as shown in this variation.

Next, the variation of the α_{3dB} of antenna radiation pattern with dipoles and arrays of dipoles is analysed, which has a unique lobe in the vertical plane. Figure 5.7 and Figure 5.8 present the variation of the two main RCPs, angle spread and delay spread for the respective angles: 48º, 25.4º, 12.7º, 8.5º, 6.3º and 5.1º.
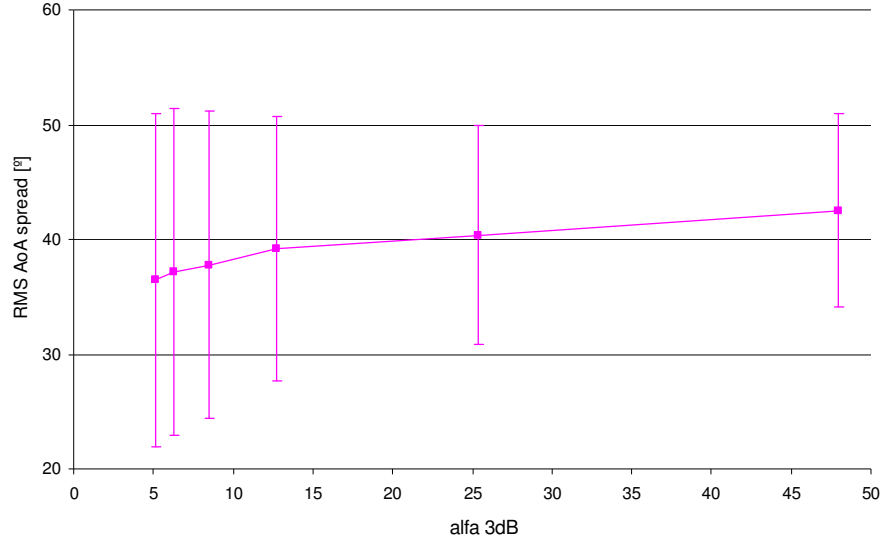
Figure 5.7. Angle Spread RCP for different α_{3dB} for the large room scenario.
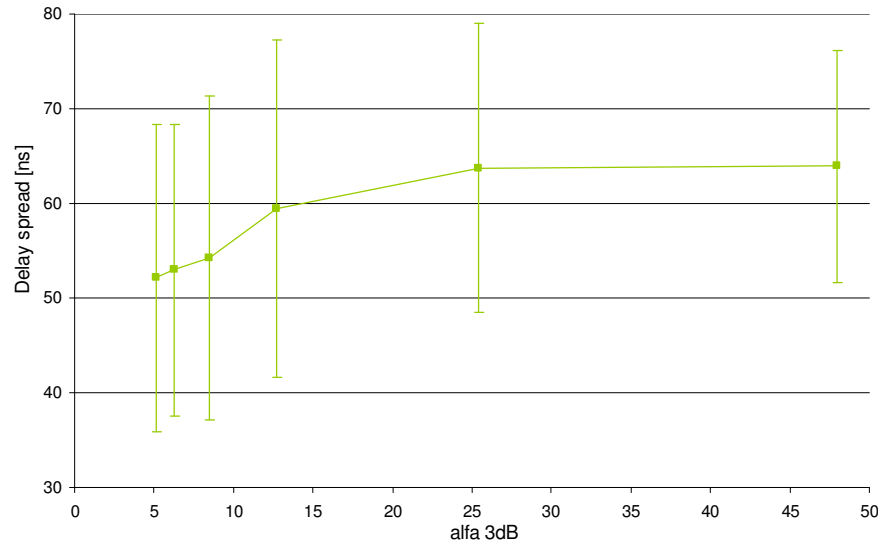
Figure 5.8. Delay Spread RCP for different α_{3dB} for the large room scenario.

When the beamwidth of the antennas radiation pattern takes smaller values, delay spread and AoA spread decrease, the delay spread presenting a more decreasing behaviour than the AoA one. More specifically, from the case of a $\lambda/2$ dipole to an array of 10 $\lambda/2$ dipoles, delay spread decreases approximately 18% and AoA spread 14%. Since narrowing the beamwidth implies a higher directivity antenna, angle spread and delay spread go down.

In the analysis of the influence of Rx sensitivity in RCPs, te whole set of RCPs is presented in Annex B. Figure 5.9 presents the two most interesting RCPs to analyse. When Rx sensitivity takes higher values, delay spread decreases. Rx sensitivity influences the number of MPCs that are detected by the Rx. When lower values of Rx sensitivity are assumed, all the MPCs are detected even the ones with lower power. However, when it is considered higher values, just the MPCs with high power (which corresponds mainly to the interfering objects that are near the Rx) are detected by the Rx.
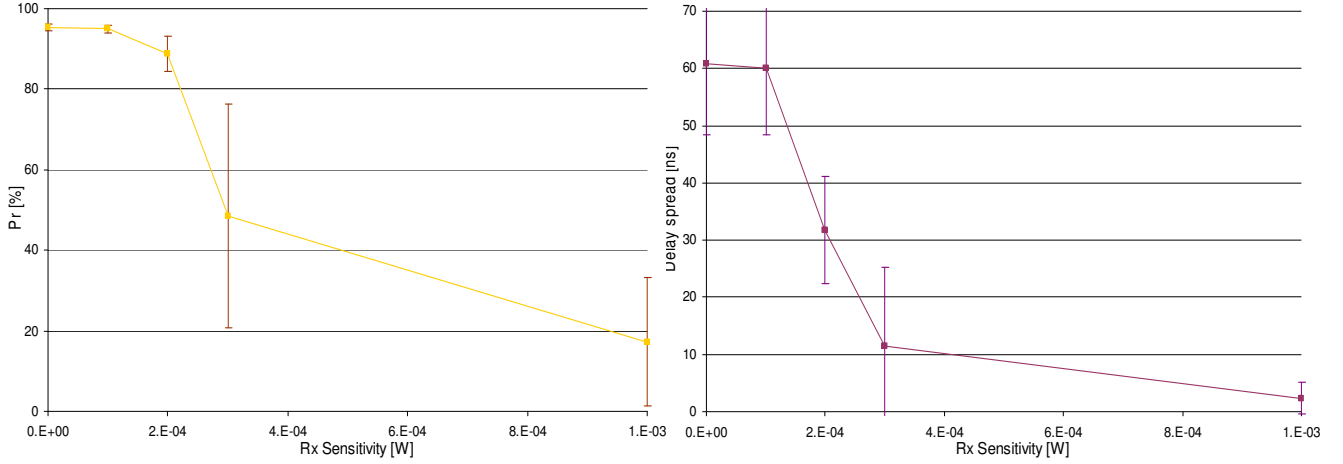
Figure 5.9. RCPs for the large room scenario with different Rx sensitivity.

Obviously, this causes a dramatically decreases on the delay spread. The received power due to single bounce relative to LoS proves that less MPCs are detected when lower values of Rx sensitivity are considered. This difference is very relevant, 78%, between the two limit values for the considered interval. From this variation, it is also concluded that 10^{-3} W of Rx sensitivity is the limit value in which the Rx starts not to detect any MPC. In the limit, just the MPC due to LoS is detected being the only one considered in the received signal.

Concerning the variation of system time resolution, again, one presents the plot of two RCPs, Figure 5.10 as the others are present on Annex B.
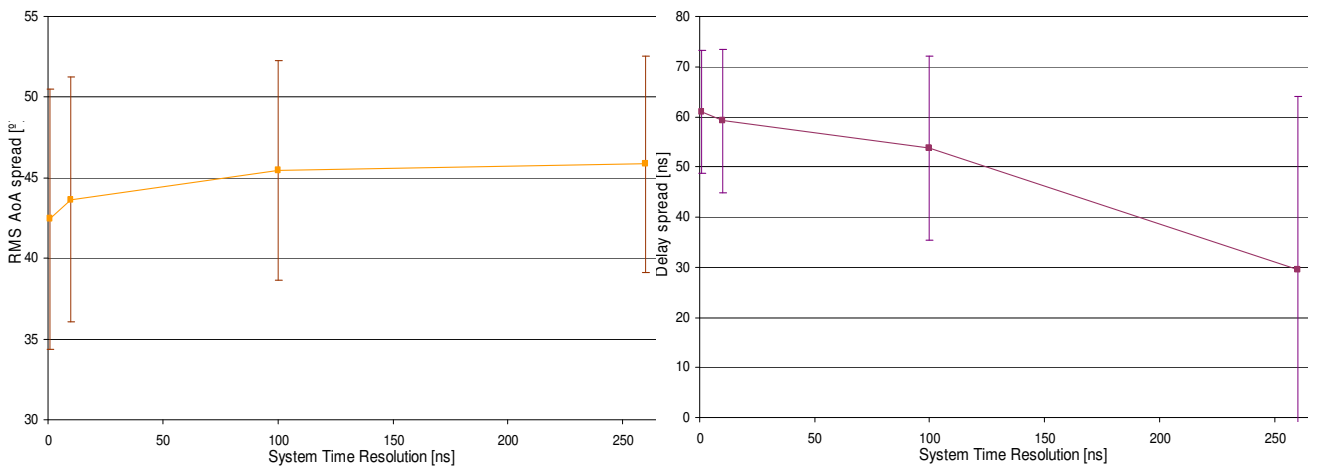
Figure 5.10. RCPs for the large room scenario with different system time resolution.

The higher time resolution of the system means that more MPCs can be distinguished at the Rx.

Angle spread and delay spread presents different behaviours when the system time resolution is higher.

From 1ns of system time resolution to the one UMTS has, 260ns, angle spread increases but the difference is not more than 10%. This means that system time resolution has not a great influence in angle spread, like the variation in the Rx sensitivity. On the other hand,, delay spread presents a decreasing behaviour; for the time resolution of 260ns is 50% less than for 1ns, however, the standard deviation of this parameter is very high. This fact leads to the conclusion that the mean value of this system time resolution cannot be reliable. Also, from the values presented on Annex B, as expected, the received power due to single bounce relative to LoS is almost the same, , because system time resolution just defines the gap in which MPCs are summed up.

Finally, the street scenario is analysed, obtaining the values presented in Table 5.6. Great differences on delay spread and maximum delay are seen from the 2D case to the 3D one. Moreover, a 2D street scenario with the same characteristics was also simulated, but with a street width factor of 1.5. Even though, the street width factor introduced is not able to enlarge the maximum delay and delay spread as much as 3D MPCs that exists in a real environment. Only with a street width factor of 2, similar values are obtained for the 3D case of maximum delay and delay spread. AoA spread value is also higher in the 3D case, because the differences on the considered scattering shape, ellipsoid in the 3D case and ellipse in the 2D one.

Concerning the comparison of the RCPs for a different density of scatterers within the cluster with Tx/Rx antennas being $\lambda/2$ dipoles, like for the large room scenario, delay spread and AoA spread have almost the same values, being constant, because with a high number of reflectors and in high dimension environments, the effect of growth on these RCPs saturates. Considering twice the value of scatterers within the cluster, represent only an increase of 2% on the received power due to single bounce relative to LoS. This also illustrates the previous fact.

Table 5.6. RCPs for 2D and 3D street scenario and for different number of scatterers within the cluster.

	street scenario									
	2D		3D		3D $N_{sc}=10$		3D $N_{sc}=15$		3D $N_{sc}=20$	
	mean	std	mean	std	mean	std	mean	std	mean	std
τ_{max} [ns]	19.85	5.82	47.05	7.91	48.17	8.23	48.32	9.49	48.94	7.35
σ_τ [ns]	5.15	1.66	12.69	2.52	11.85	2.21	11.81	2.39	11.89	2.31
σ_Ω [º]	14.05	5.26	26.87	4.45	26.17	4.26	26.46	17.99	26.02	7.80
$w_{DCIR} \left[\dfrac{rad}{\mu s} \right]$	51.47	22.57	38.06	8.03	42.50	8.31	40.00	40.25	39.08	11.98
Pr [%]	96.81	0.56	96.64	0.34	95.42	0.60	96.91	0.32	97.65	0.31

| γ | 1.24 | 0.04 | 1.26 | 0.02 | 1.33 | 0.03 | 1.25 | 0.03 | 1.19 | 0.03 |

As expected, average power decay presents a negative slope with a higher number of reflectors. The channel richness, which is an indication of relevant AoA per relevant time unit, decreases due to the increase of the delay spread. In this specific case, channel richness slightly decreases due to the small variation of the angle spread.

5.3   MIMO Channel

When considering a MIMO system, the correlation between links between input and output antennas must be analysed. A larger decorrelation enables a greater gain in capacity, despite of its dependency on the time resolution of the Rx. Correlation between links is also related with the deployment and the number of scatterers in the propagation environment. Simulations have been performed for two different time resolutions values: 260 and 0.1 ns. The time resolution of 260 ns is the time resolution of UMTS. Also, the spatial separation between antennas and their number has a great influence on correlation. For the purpose of this study, a 4×4 MIMO system was simulated, with spacing between antennas equal to λ. The mean values of correlation between links, calculated from (2.23), averaged over 50 simulations, are presented in Table 5.7.

As expected, the correlation between links for all analysed scenarios is lower in the case of 0.1 ns time resolution than in the 260 ns one. The higher time resolution of the system means that more MPCs can be distinguished at the Rx, which leads to a higher decorrelation between links.

The reference room scenario is the one that presents the highest correlation between links from all the scenarios. This can be explained by the lower angular spread presented in this scenario. A larger angular spread in the radio channel allows for a higher decorrelation between subchannels in MIMO. The differences between correlation in the two small rooms are not related with the angular spread (because the value of this RCP is similar for both scenarios), but with the density of scatterers and the deployment of clusters in the scenarios, despite the small difference. Comparing the large room scenario with the street one, the first has a larger angular spread than the second one, which is reflected in the mean values of correlation between links. The mean values of correlation between links present a considerable difference between the small- and medium-size rooms and the high dimension scenarios (like the large room and street). This is expected, since the interfering objects are more disperse, more delocalised (due the high dimensions of the scenarios) than in the small rooms, resulting in more decorrelation between the different subchannels of the MIMO system.

Concerning the comparison between 3D and 2D models on correlation between links for a 4×4 MIMO system, one observes small differences between the mean values of correlation. Nevertheless, the 2D model presents more decorrelation between links than the 3D one. The street scenario is the one for which the 3D model presents better results in what concerns decorrelation.

Figure 5.11 shows an example of correlation between particular links for the large room scenario, when CIRs are spaced by 0.1 ns, while other plots for other scenarios and parameters can be found in

Annex D.

Table 5.7. Mean values of correlation between links.

	correlation between links									
	reference room		small normal room		small office room		large room		street	
	0.1ns	260ns	0.1ns	260ns	0.1ns	260ns	0.1ns	260ns	0.1ns	260ns
3D model	0.85	0.97	0.62	0.95	0.57	0.93	0.31	0.95	0.36	0.96
2D model	0.85	0.98	0.58	0.95	N/A		0.26	0.94	0.53	0.96

Correlation is symmetric, which was predictable, because axes contain CIRs between the same pairs of input and output antennas. Moreover, the value of correlation for the diagonal of the plane is always equal to 1, since it is the correlation between the same CIRs. If the distance between transmit antennas increases, correlation goes down.

It can be concluded that higher values of the mean correlation between links can be obtained for higher system time resolutions. It is also worthwhile to notice that spacing between antennas was set equal to λ. This leads to the conclusion that in a MIMO system a separation between antennas larger than λ, mainly in small indoor environments, is vital to obtain higher values of decorrelation between links, mainly in small indoor environments.
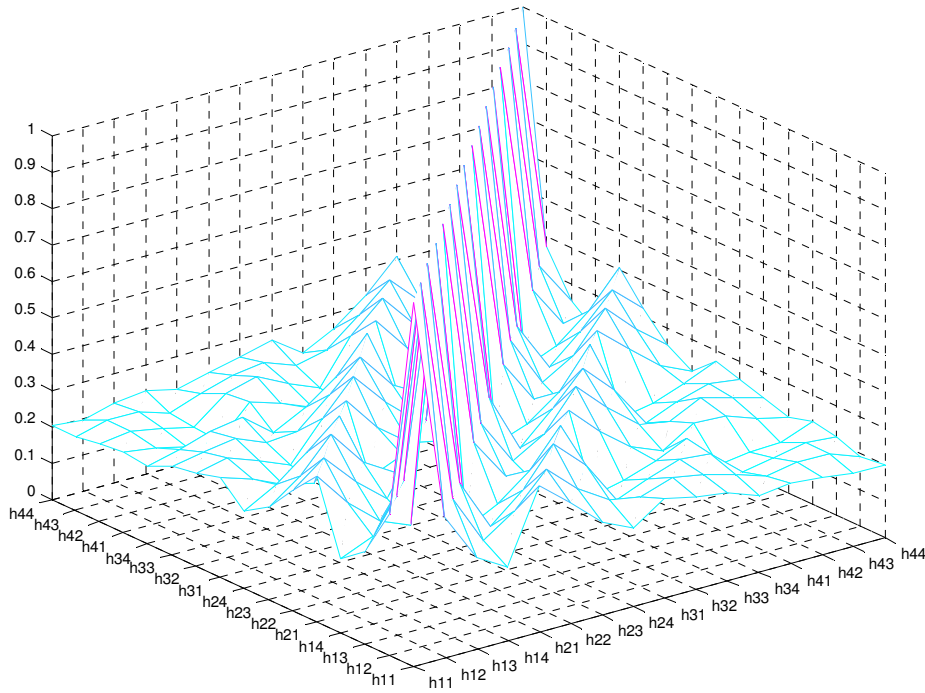

Figure 5.11. Correlation between links for the large room scenario with 0.1 ns of time resolution.

5.4 MIMO Capacity Gain

The main feature of a MIMO system, which distinguishes itself from other systems, is the fact of having multiple antennas on Rx and Tx. For the different scenarios, the 3D approach is compared with the 2D one, in which simulations are performed with a varying number of antennas on input and output ends of the radio link. The gain of capacity was calculated based on (2.27) for the two time resolutions, 0.1 and 260 ns and an asymmetric and symmetric numbers of input and output of antennas.

As expected, an increase of the number of antennas leads always to a growth of capacity gain, since more antennas allow to establish more subchannels in the MIMO system. This results in achieving a higher advantage of the system. Moreover, the capacity gain grows more in the case of higher time resolution for all scenarios.

Annex E presents the full set of results and comparisons of the obtained capacity gains for all the considered scenarios and for the two system time resolutions. Figure 5.12 shows, for the street scenario and 260 ns system time resolution, all the obtained capacity gains: MIMO capacity, minimum MIMO capacity, maximum MIMO capacity, SISO capacity and the relative MIMO gain. It can be concluded that asymmetric antennas configurations present small capacity gain differences when compared with symmetric ones. For example, the 8×8 MIMO system presents almost the same capacity gain than the 16×8 one. One can observe the differences concerning MIMO capacity minimum gain (when all subchannels are totally dependent) and MIMO capacity maximum gain (when there is no correlation between parallel paths and it is assumed that the signal is propagating without path loss). The 16×16 MIMO system presents the maximum difference between maximum and minimum capacity, almost 30 bps/Hz.
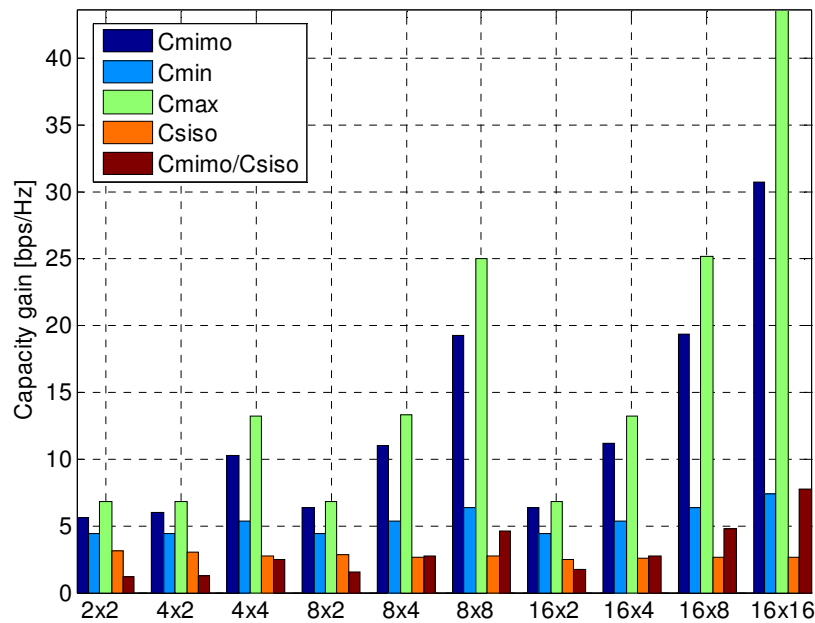

Figure 5.12. MIMO gain for the street scenario for a time resolution of 260 ns.

Figure 5.13 shows the comparison among scenarios, in what concerns MIMO capacity gain (for 260

ns of system time resolution). The greatest advantage of a MIMO system is observed for the small room scenarios, in particular for the small office room, which is the scenario with the highest capacity gain in all MIMO systems, because a 3D environment is much more important in small room scenarios. It is also relevant to point out the difference on the MIMO capacity gain between small-sized office and normal room. Despite the former type of room has only one more MPC than the latter type (which is irrelevant in a SISO channel or even in a 2×2 MIMO system), when is analysed a 16×16 MIMO system, the difference in terms of MIMO capacity gain cannot be neglected. Moreover, the office room scenario presents a MIMO capacity gain 12% higher than the normal room scenario. The reference room is the scenario with the worst results, which is due to the highest correlation between links, previously explained. Only for the highest number of input and output antennas, namely for the 8×8 MIMO system, one sees significant differences for the different scenarios in MIMO capacity.
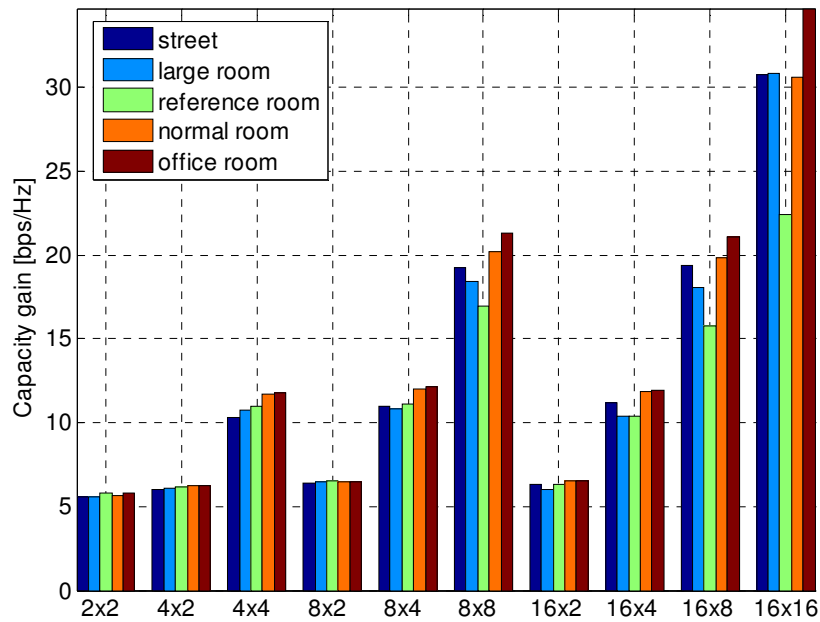
Figure 5.13. MIMO gain for the different scenarios, for a time resolution of 260 ns.

For the system time resolution of 0.1 ns (the plot is presented in Annex E) the office room scenario presents also the highest capacity gain. Nevertheless, the large room scenario, in this case, presents a higher capacity gain than the remaining ones. For this time resolution, the difference between capacity gain of the reference room scenario is smaller than in the 260 ns case.

Table 5.8 shows the comparison between the two models, for the two system time resolutions and for symmetric and asymmetric MIMO systems, concerning the relative MIMO gain. It is also worth while to notice that the small office room scenario could not be analysed in the 2D model, since this scenario was not contemplated in [Mack07]. When a MIMO system consists of only 2 antennas at input and output, the relative MIMO gains are almost the same, varying between 1.39 and 1.52 for the 0.1ns of system time resolution. This difference among scenarios is more visible when a higher number of antennas is deployed.

Figure 5.14 presents for 0.1 ns of system time resolution the difference observed (in percentage), in the relative MIMO gain, between the 3D and the 2D models. The street scenario is the one in which the best results are obtained in comparison with the 2D model, for different antennas configurations, achieving over than 20% for the 16×16 MIMO system. For the same size of the MIMO system, the reference room is characterised by a relative MIMO gain equal to 10.6, which is 14.4% higher in the case of the 3D model instead of the 2D one.

Table 5.8. Relative MIMO capacity gain for various scenarios and for both models.

		reference room		normal room		office room		large room		street	
		0.1ns	260ns	0.1ns	260ns	0.1ns	260ns	0.1ns	260ns	0.1ns	260ns
2×2	3D	1.52	1.52	1.39	1.24	1.43	1.31	1.59	1.49	1.58	1.19
	2D	1.47	1.32	1.39	1.3	*N/A*		1.55	1.44	1.46	1.29
	3D to 2D [%]	3.29	13.16	0	-4.84			2.52	3.36	7.59	-8.40
4×2	3D	1.71	1.69	1.56	1.4	1.61	1.47	1.78	1.68	1.76	1.28
	2D	1.62	1.46	1.55	1.44	*N/A*		1.75	1.55	1.65	1.43
	3D to 2D [%]	5.26	13.61	0.64	-2.86			1.69	7.74	6.25	-11.7
4×4	3D	3.47	3.3	3.1	2.74	3.31	2.94	3.58	3.17	3.59	2.5
	2D	3.18	2.61	3.07	2.7	*N/A*		3.66	3.21	3.12	2.58
	3D to 2D [%]	8.36	20.91	0.97	1.46			-2.23	-1.26	13.09	-3.20
8×2	3D	1.92	1.9	1.76	1.51	1.77	1.6	1.98	1.9	1.95	1.54
	2D	1.79	1.58	1.73	1.6	*N/A*		2	1.74	1.81	1.56
	3D to 2D [%]	6.77	16.84	1.70	-5.96			-1.01	8.42	7.18	-1.30

	3D	3.64	3.42	3.26	2.87	3.49	3.12	3.77	3.3	3.8	2.7
8×4	2D	3.34	2.72	3.2	2.8	*N/A*		3.91	3.36	3.27	2.68
	3D to 2D [%]	8.24	20.47	1.84	2.44			-3.71	-1.82	13.95	0.74
	3D	6.5	5.52	5.76	4.92	6.43	5.59	7.03	5.78	6.82	4.63
8×8	2D	5.71	4.14	5.56	4.43	*N/A*		6.95	5.72	5.67	4.34
	3D to 2D [%]	12.15	25	3.47	9.96			1.14	1.04	16.86	6.26
	3D	2.12	2.04	1.91	1.65	1.93	1.74	2.15	1.93	2.17	1.69
16×2	2D	1.92	1.61	1.86	1.67	*N/A*		2.22	1.93	1.9	1.61
	3D to 2D [%]	9.43	21.08	2.62	-1.21			-3.26	0	12.44	4.73
	3D	3.76	3.38	3.3	2.95	3.63	3.2	3.92	3.31	3.9	2.77
16×4	2D	3.38	2.63	3.22	2.73	*N/A*		4.04	3.48	3.31	2.63
	3D to 2D [%]	10.11	22.19	2.42	7.46			-3.06	-5.14	15.13	5.05
	3D	6.53	5.26	5.79	4.9	6.57	5.56	7.15	5.75	6.93	4.78
16×8	2D	5.68	3.95	5.56	4.32	*N/A*		7.08	5.71	5.69	4.28
	3D to 2D [%]	13.02	24.90	3.97	11.84			0.98	0.70	17.89	10.46
	3D	10.59	7.58	9.27	7.42	11	9.23	12.46	9.78	11.57	7.76
16×16	2D	9.07	5.63	9.02	6.43	*N/A*		11.62	9.09	9.19	6.84
	3D to 2D [%]	14.35	25.73	2.70	13.34			6.74	7.06	20.57	11.86

Small normal and large room scenarios are the ones with the smallest differences between the two models, the last one being even worse than the 2D model for some MIMO systems. For the 8×4 MIMO system the relative MIMO gain of the 3D model is 3.7% lower than the 2D one.

In the case of system time resolution of 260 ns (the plot is presented in Annex E), the reference room scenario is the one with the highest difference on the relative MIMO gain, which is confirmed by the correlation analysis. In fact, the relative MIMO gain for the 16×16 MIMO system equals 10.6 for the 3D model and is 25.7% higher than in the 2D one. Remaining scenarios presents also benefits on the relative MIMO gain when the 3D model is considered despite the poor results in some antennas configurations. Still, for higher MIMO systems configurations and for both system time resolutions, the 3D model presents better results for all the considered scenarios than the 2D one, since the 3D approach exploits better the advantages of MIMO systems.
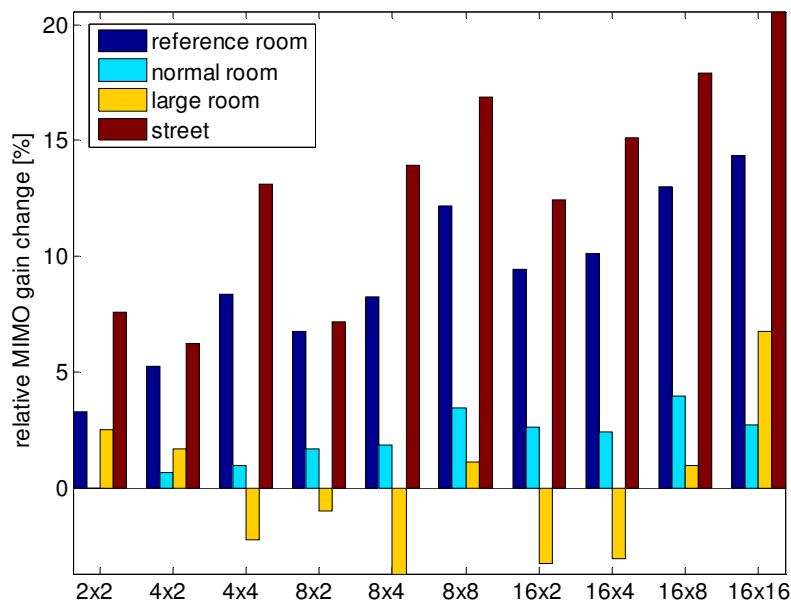

Figure 5.14. Difference in relative MIMO gain between 3D and 2D model for time resolution of 0.1 ns.

Chapter 6

Conclusions

This chapter finalises this work, summarising conclusions and pointing out aspects to be developed in future work.

The aim of this work was to develop a 3D single bounce radio channel model for a MIMO system and to investigate the influence of considering a 3D environment on several scenarios, namely in indoor ones, that emulate different situations in mobile communications. As only single bounce was accounted for (which fulfils the purpose of this work), just specular reflection was assumed for single bounce reflections. First, an algorithm of 3D single bounce was developed and implemented in a simulator written in C++. Then, the input parameters for the scenarios for this model were picked, partially from [Koko05], [Mack07] and from the values available in the literature. Finally, some research related to SISO and MIMO systems for 3D SB was performed and compared to 2D SB approach.

The main advantage of a GBSB model is simplicity. This model has been extended by GROW, who suggested grouping scatterers in clusters, which allows to emulate a real behaviour of the radio channel. Scatterers are described in a random way, which increases similarity to real conditions. [Koko05] implemented the MIMO radio channel model for the GBSB model and then [Mack07] introduced MB on the previous developed model. Taking these models as a starting point, the 3D GBSB channel model was developed. The simplicity and efficiency of the geometrically based model was preserved.

The simulator implements the 3D GBSB model and supports any antenna type the user wants, since any antenna radiation pattern can be deployed with input horizontal and vertical planes files. Unfortunately, the model does not consider propagation phenomenon like diffraction, Doppler's effect which is a drawback. Also, MB is not taken into account, which is a substantial constraint of the model. Nevertheless, 3D GBSB model serves perfectly for the purposes of this work.

In the simulator, the spatio-temporal and power parameters of the SISO channel and their statistics, like maximum, minimum, mean value and standard deviation, can be calculated. The MIMO system can be simulated by using any number of input and output antennas and the result of simulations is the set of CIRs for each particular link. Also, some additional Matlab script files are generated during simulations, which allow to see the created or loaded environment and their scattering region, to plot the CIR of the scenario and their PDAPs (azimuth, elevation and full PDAP), and to calculate the correlation properties of the MIMO system. The MIMO capacity and relative capacity gain are calculated by an external script prepared in Matlab.

To fulfil the scope of this master thesis, the motivation and the overview of the thesis are described, Chapter 1. Then, the basic concepts in this thesis are pointed out, i.e., UMTS, MIMO, and MIMO channel models, channel models being the main aspects in Chapter 2. In Chapter 3, the strategy is defined concerning how to develop the 3D Single Bounce Channel Model, based on the 2D GBSBCM. So, the output of this chapter is the 3D model. The scenarios of study are also analysed in Chapter 3. The description of the tool, to simulate physical radio link between multiple input and output antennas, considering 3D single bounce – the 3D simulator – is presented in Chapter 4. Finally, the analyse of the considered scenarios is done in Chapter 5, according to three aspects: SISO channel (the outputs are the RCPs for different variations), MIMO channel (correlation between links) and then, MIMO capacity gain (with the comparison between 3D and 2D models concerning relative MIMO capacity

gain).

In what concerns the results analysis, first, the assessment of the simulator for the reference scenario (the medium-sized room) is done, by comparing the values of the RCPs (in this case, the delay spread, the AoA spread and the received power due to single bounce), with a different number of clusters and scatterers, with measured results. It is concluded that the right number of scatterers and the cluster density of this scenario is 5 clusters with 2 scatterers.

Then, a group of simulations was performed for different scenarios concerning only the SISO radio channel. For small-sized rooms, as expected, the difference between office room RCPs and normal room ones is very small, however, the fact that the office room scenarios has an extra MPC due the reflection on the roof is shown with more 7% of received power due to single bounce. Comparing the RCPs for this scenario, in the normal case, between 2D and 3D model, it is shown that the latter increases AoA spread, this difference being the main one between the models. This is also expected, since the scenario under consideration is a small-sized room (length ~ 6m) and the 3D environment is now accounted for.

Afterwards, a set of tests were performed in order to analyse the variation of the RCPs when one changes the density of scatterers within the cluster, Tx position and room dimensions. Several conclusions can be taken from this study. From the first one, delay spread stays almost with no variation when the density of scatterers is changed within the cluster and an increase in the AoA spread and the received power due to single bounce is observed. From the second one, Tx position has influence on the RCPs, however the small differences are for the small normal room scenario. From the third one, enlarging room dimensions increases the delay spread on the one hand, but decreases the angular spread, channel richness and the received power due single bounce on the other.

Concerning the large room scenario, one compares the 2D model with the 3D one, a decrease on the delay spread is observed, as well an increase in the AoA spread and in the channel richness. A study of RCPs concerning these variations is done: α_{3dB}, Rx sensitivity and system time resolution. It can be concluded that when α_{3dB} decreases, delay spread and AoA spread decreases too, since Tx antenna is becoming more directive. Rx sensitivity influences the number of MPCs that are detected by the Rx. When higher values are considered, just the MPCs with high power (which corresponds mainly to the interfering objects that are near the Rx) are detected by the Rx. This causes, a highly decrease on delay spread and in the received power due single bounce relative to LoS. Finally, system time resolution influences RCPs, in the sense that a higher the time resolution of the system means that more MPCs can be distinguished at the Rx, which follows in higher values of delay spread. It is also concluded that system time resolution has not a great influence in angle spread RCP. The same happens to the received power due to single bounce relative to LoS, because system time resolution defines only the gap in which MPCs are summed up.

Concerning the SISO channel and the street scenario, largedifferences on delay spread and maximum delay are observed from the 2D case to the 3D one. Only with a street width factor of 2 in the 2D

model, maximum delay and delay spread can be enlarged as 3D MPCs that exist in a real environment.

As expected, it is the small-sized rooms that present the highest values for the AoA spread (in particular the small office room), despite for wider scenarios the clusters are more disperse in the environment, cluster density of these scenarios is higher reducing the mean value of this RCP.

In order to analyse the MIMO channel of the 3D model, a study concerning the correlation between links for system time resolution of 0.1 and 260 ns is performed. Some conclusions can be pointed out in which correlation dependes on a few aspects:

- spatial separation between antennas in antenna array,
- time separation between arriving MPCs at the Rx (i.e., time resolution of the Rx),
- channel richness of the radio channel,
- type of scenario.

Independently of the scenario, decorrelation between subchannels in a MIMO system is higher when spacing between antennas is greater and also increases when the time resolution of the system is higher since more MPCs can be distinguished at the Rx. It is also proved that correlation between links is lower when the channel richness of the radio channel is higher since the multipath phenomenon is also higher, increasing the number of MPCs.

From correlation mean values, it can be also concluded that small indoor environments should have a higher spacing between antennas, higher than λ, in order to increase the decorrelation among the MIMO subchannels. This effect is not so relevant in large dimensions environments since the interfering objects are more disperse, more delocalised in the space.

Regarding the analysis of the MIMO capacity gain and its relative gain for the considered scenarios for system time resolution of 0.1 and 260 ns and for different antennas configurations, the relative capacity gain of a MIMO system is mainly regulated by the dimension of the antenna set. The number of MIMO antennas and spacing between them are the main factors. System time resolution influences also MIMO capacity gain. In fact, the capacity gain grows more in the case of higher time resolution for all scenarios. From this study it can be taken too that asymmetric antennas configurations present small capacity gain differences compared with symmetric ones.

The greatest advantage of a MIMO system is observed for the small room scenarios, in particular for the small office room, which is the scenario with the highest capacity gain in all MIMO systems. This happens because a 3D environment is much more important in small dimensions scenarios.

For 0.1 ns of system time resolution the difference observed, in the relative MIMO gain, between the 3D and 2D model is for the street scenario over than 20% for the 16×16 MIMO system. In fact, this is the scenario in which the best results are obtained in comparison with the 2D model, for different antennas configurations. In the case of system time resolution of 260 ns, the reference room scenario is the one with the highest difference on the relative MIMO gain, which is confirmed by the correlation analysis. In fact, the relative MIMO gain for 16×16 MIMO system equals 10.6 for the 3D model and is 25.7% higher than in the 2D one. These facts are regarded as main results of the 3D GBSB model,

since the radio environment in these scenarios can be more accurately simulated.

It is shown that for higher MIMO systems configurations and for both system time resolutions, the 3D model presents better results for all the considered scenarios than the 2D one, as expected, since a 3D approach exploits better the advantages of MIMO systems.

Considering the radio channel model, in future work, some improvements can be done in order to approximate the model to real conditions. For instance and despite the fact that in real life, propagation is dominated by single bounce, neglecting MB MPCs is insufficient [HoMC06] for modelling MIMO systems performance. Moreover, the influence of MB is stronger in indoor environments (like the ones considered in the work) due channel richness and Tx-Rx short distances. So, it is fundamental to consider MB reflections.

New types of scenarios and shapes of scattering region can be implemented and accounted for in the simulator. The following shapes are already included in the simulator: sphere, spheroid and ellipsoid. The option to have many overlaying and different shapes in one environment can be also a possible improvement.

Also, many objects in indoor environments (which have many obstacles) can change their position during transmission and stop to exist, which can be emulated by the movement of clusters and scatterers and by clusters lifetime.

Finally and concerning antennas, in a real MIMO system the antennas are not ideally isolated and mutual coupling between them should be accounted for, since the developed model considers an ideal (and inexistent in reality) situation in this aspect.

Annex A. User's manual

The configuration input file is prepared in XML, in a tree structure where each input parameter has a unique path. Having such a structure of the input file not only helps to add new input parameters easily, but also allows to organise them into a hierarchic structure. The user just has to introduce the wanted values according to the specifications of each parameter, as described next. The input parameters are divided into three main groups: simulator, system and environment. The first group handles with the simulator parameters:

```
<simulator>
        <projectName>test</projectName>            % name of the scenario
        <scenarioType>Micro-cell</scenarioType>    % type of the scenario
        <runNumber>1</runNumber>                    % number of simulator runs
        <environmentMask>2</environmentMask>        % 0: no change; 1: randomize coefficients
                                                    % 2: randomize positions of scatterers
        <maxPath>1000</maxPath>                     % maximum path length [m]
        <angleRes>1</angleRes>                      % angle resolution
</simulator>
```

Then, the following group defines the system parameters, like the carrier frequency but also the MIMO system parameters:

```
<system>
        <frequency>2000000000</frequency>          % carrier frequency [Hz]
        <maxDelay>0.000002</maxDelay>              % system maximum delay [s]
        <timeRes>0.000000000001</timeRes>          % time resolution [s]
        <rxSensitivity>0</rxSensitivity>           % sensitivity [V/m]
        <modeTxPower>1</modeTxPower>               % mode Tx power
                                                   % 0: each Tx antenna feed by Tx power
                                                   % 1: all Tx antennas feed by Tx power
        <txPower>1</txPower>                        % Tx power [W]
        <AlignedAntennas>1</AlignedAntennas>       % Aligned antennas; 0: No, 1: Yes
        <txNumber>1</txNumber>                      % number of Tx antennas
        <rxNumber>1</rxNumber>                      % number of Rx antennas
        <rxRandGen>0</rxRandGen>                    % Rx position generated randomly
                                                   % 0: No, 1: Yes
        <antennaSpacingX>0</antennaSpacingX>       % X- spacing between antennas [m]
        <antennaSpacingY>0</antennaSpacingY>       % Y- spacing between antennas [m]
        <antennaSpacingZ>0.15</antennaSpacingZ>    % Z- spacing between antennas [m]
        <tx1>
                <radiation>antenna.xml</radiation> % file with Tx radiation pattern information
                <x>15</x>                           % X- position of Tx
```

```
            <y>10</y>                          % Y- position of Tx
            <z>10</z>                          % Z- position of Tx
      </tx1>
      <rx1>
            <radiation>antenna.xml</radiation>  % file with Rx radiation pattern information
            <x>40</x>                          % X- position of Rx
            <y>35</y>                          % Y- position of Rx
            <z>50</z>                          % Z- position of Rx
      </rx1>
</system>
```

The last group handles with the environment parameters, like the scattering region, the dimensions of the environment:

```
<environment>
      <deep>50</deep>                          % X- dimension [m]
      <width>50</width>                        % Y- dimension [m]
      <height>50</height>                      % Z- dimension [m]
      <shapeType>3</shapeType>                 % Shape type; 3: sphere, 4:ellipsoid
      <sphere>                                 % Sphere centre position
            <x>25</x>
            <y>25</y>
            <z>25</z>
            <r>25</r>                          % Radius of the sphere [m]
      </sphere>
      <elipsoide>                              % Ellipsoid centre position
            <x>15</x>
            <y>30</y>
            <z>15</z>
            <a>30</a>                          % Dimension of the y axis of the ellipsoid
            <b>10</b>                          % Dimension of the x axis of the ellipsoid
            <c>10</c>                          % Dimension of the z axis of the ellipsoid
      </elipsoide>
      <los>1</los>                             % 1: LoS, 0: NLoS
      <rClst>1</rClst>                         % Cluster radius [m]
      <layer1>                                 % parameters for SB environment
            <environmentFile>test_1.xml</environmentFile>
            <loadEnvironment>0</loadEnvironment>% 1: Load, 0: do not load
            <clstDensity>0.00015</clstDensity> % Cluster density [m$^{-3}$]
            <sctrNumber>2</sctrNumber>         % Number of scatterers within the cluster
      </layer1>
</environment>
```

The antenna configuration file, which includes the information about the type of Tx/Rx antennas, is also presented in detail:

<antenna>

<mode>2</mode>	% Antenna type; 1: Real 2D antenna patterns
	% 2: $\lambda/2$ dipoles, 3: array of $\lambda/2$ dipoles
<file>antena1.txt</file>	% name of the real 2D antenna pattern file
<na>1</na>	% number of dipoles in the array
<da>0.149896</da>	% distance between the dipoles [m]
<delta>0</delta>	% array phase shift [rad]
<r_patternRotationH>0</r_patternRotationH>	% Horizontal antenna rotation [deg]
<r_patternRotationV>0</r_patternRotationV>	% Vertical antenna rotation [deg]

</antenna>

It is worth while to notice that when the user wants to load the layout of the environment from a previous created XML file, the name of the file should be introduced in the path <environmentFile> and should be at the route of the simulator. The same happens, when the user wants to use the first antenna type, a real 2D antenna pattern. The file should be found at the route of the simulator folder.

Annex B. Radio channel parameters for various variations

This annex includes tables with the RCPs for different tests, done in the small normal and large room scenarios. In the first one, presented in Table B. 1, the density of scatterers within the cluster is changed. One presentes the results of the RCPs, Table B. 2, for three different Tx antennas radiation patterns. These "real" radiation patterns were obtained from antennas manufactures and used by companies in this segment. Figure B. 1 shows the used antennas radiation patterns. Then, for the large room scenario, one consideres the variation of the RCPs when it is changed Rx sensitivity, Table B. 3. Finally, in the same scenario one presents how the RCPs vary with different values of system time resolution, Table B. 4.

Table B. 1. RCPs for the small normal room for different number of scatterers within the cluster.

	N_{sc}									
	2		4		6		8		10	
	mean	std	mean	std	mean	std	mean	std	mean	std
τ_{max} [ns]	17.87	2.98	19.43	2.75	19.62	2.62	20.39	2.48	20.68	2.45
σ_τ [ns]	4.83	1.14	4.93	0.95	4.71	0.82	4.73	0.84	4.65	0.78
σ_Ω [º]	65.78	9.05	74.02	8.29	76.47	8.87	78.62	7.08	78.89	6.87
$w_{DCIR} \left[\dfrac{rad}{\mu s}\right]$	255.17	87.79	273.48	69.23	293.99	71.67	301.55	74.62	305.94	64.59
$P_{Rx[dB]}$	2.30	2.11	5.46	1.63	7.52	1.44	8.72	1.11	9.82	1.15
Pr [%]	62.33	10.96	77.20	6.74	84.46	4.43	87.88	2.81	90.32	2.40
γ	0.93	0.31	0.40	0.30	0.01	0.29	-0.24	0.24	-0.48	0.25

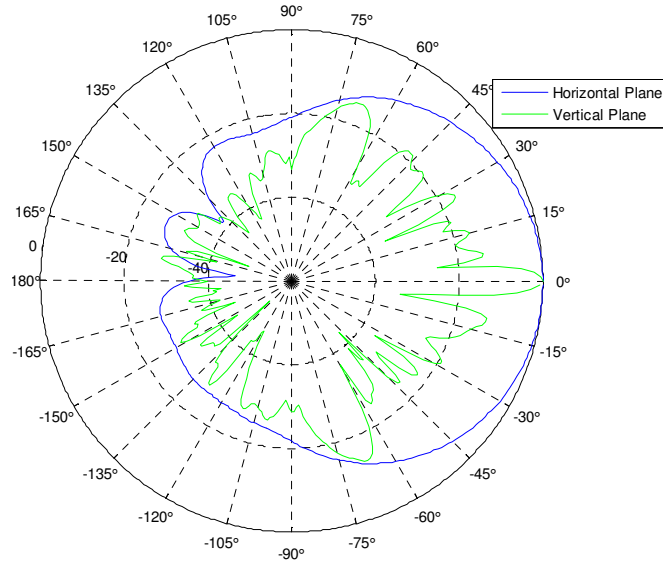Table B. 2. RCPs for the small room with different Tx antennas radiation patterns.

Variation in Tx antennas radiation patterns						
	Radiation Pattern 1		Radiation Pattern 2		Radiation Pattern 3	
	mean	std	mean	std	mean	std
τ_{max} [ns]	17.87	3.06	17.94	2.97	18	3.46
σ_τ [ns]	3.13	1.14	3.22	1.2	3.35	1.16
σ_Ω [º]	56.2	16.4	58.59	19.03	61.64	16.88
$W_{DCIR} \left[\dfrac{rad}{\mu s} \right]$	352.75	181.31	349.22	151.16	355.4	151.56
$P_{Rx[dB]}$	-1.36	4.92	-1.32	5.15	-0.43	4.23
Pr [%]	44.48	21.81	45.33	20.52	48.45	20.21
γ	1.28	0.48	1.27	0.46	1.21	0.46
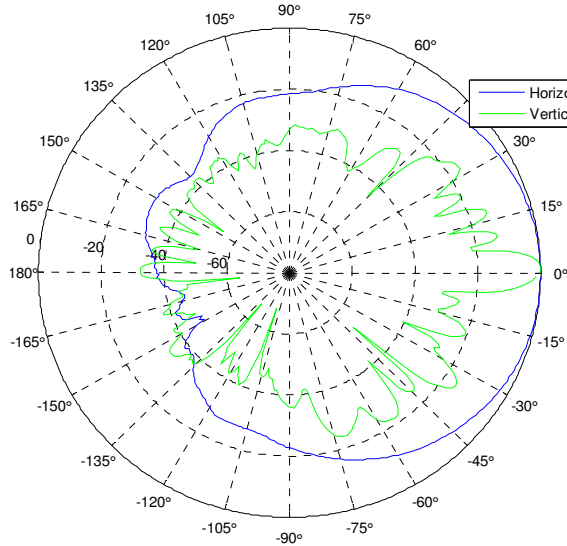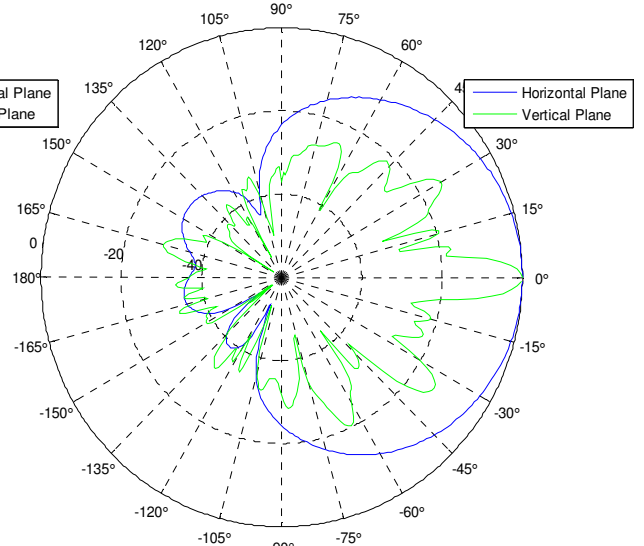
(a) Radiation Pattern 1   (b) Radiation Pattern 2

(c) Radiation Pattern 3

Figure B. 1. Three Tx antennas radiation patterns used in simulations.

Table B. 3. RCPs for large room with different values of Rx sensitivity.

	Rx Sensitivity [W]									
	0		10^{-4}		2×10^{-4}		3×10^{-4}		10^{-3}	
	mean	std	mean	std	mean	std	mean	std	mean	std
τ_{max} [ns]	253.36	40.09	257.78	37.30	111.45	37.72	28.72	32.26	8.09	7.89
σ_τ [ns]	60.78	12.46	60.01	11.65	31.72	9.35	11.56	13.65	2.32	2.79
σ_Ω [º]	43.33	8.39	41.30	7.98	41.53	7.68	49.64	7.31	50.09	6.63
$w_{DCIR} \left[\dfrac{rad}{\mu s} \right]$	13.07	4.17	12.43	3.24	25.36	15.52	761.7	2955.54	3029.2	6759.7
$P_{Rx[dB]}$	13.21	0.74	12.86	0.81	9.29	1.79	-1.88	8.7	-10.39	8.89
Pr [%]	95.37	0.78	95.00	0.91	88.82	4.37	48.41	27.76	17.26	15.94
γ	1.19	0.04	1.21	0.04	1.41	0.09	1.78	0.14	1.94	0.06

Table B. 4. RCPs for the large room scenario with different values of system time resolution.

| | System time resolution [ns] | | | | | | | |
| | 1 | | 10 | | 100 | | 260 | |
	mean	std	mean	std	mean	std	mean	std
τ_{max} [ns]	255.69	41.73	251.5	42.72	208	47.28	159.9	126.51
σ_τ [ns]	61.01	12.27	59.16	14.26	53.8	18.34	29.48	34.54
σ_Ω [º]	42.45	8.06	43.64	7.58	45.47	6.79	45.87	6.71
$w_{DCIR}\left[\dfrac{rad}{\mu s}\right]$	12.77	4.21	13.71	4.43	16.89	7.52	∞	N/A
$P_{Rx[dB]}$	13.35	0.83	13.31	1.57	12.48	3.38	11.25	4.85
Pr [%]	95.51	0.82	95.28	1.6	93.16	6.07	89.37	12.82
γ	1.18	0.04	1.18	0.09	1.23	0.18	1.29	0.24

Annex C. CIRs and PDAPs for various scenarios

The present annex includes CIRs and the Power Delay Angle Profiles (PDAPs) for the considered scenarios. Each profile has particular characteristics, distinctive for the various scenarios. For example, small room scenarios have less MPCs (despite higher cluster density) in comparison with large room and street scenarios, which is well reflected in the CIR plot. PDAPs were created separately, for azimuth and elevation angle and finally for the resultant AoA.
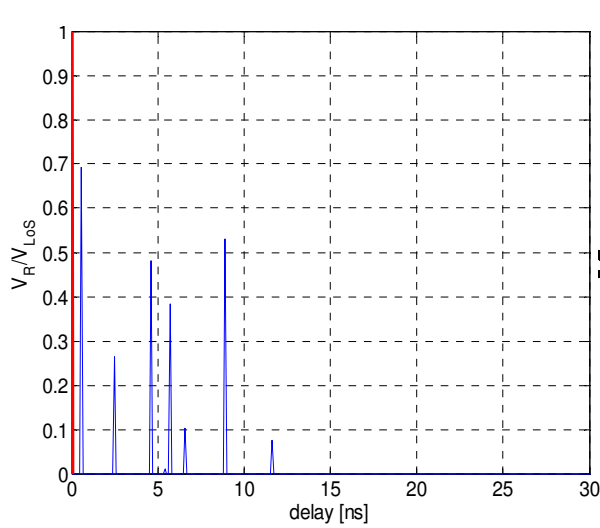
(a) CIR
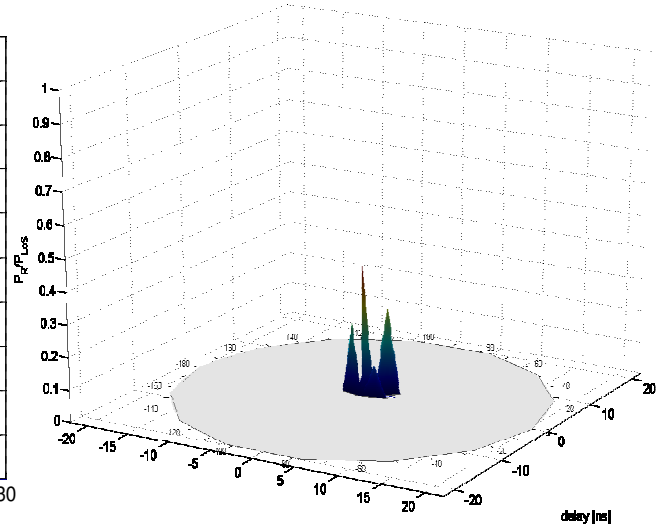
(b) Azimuth PDAP
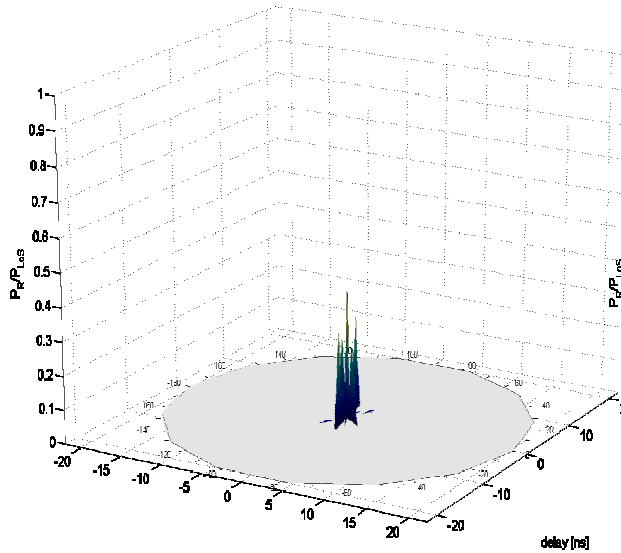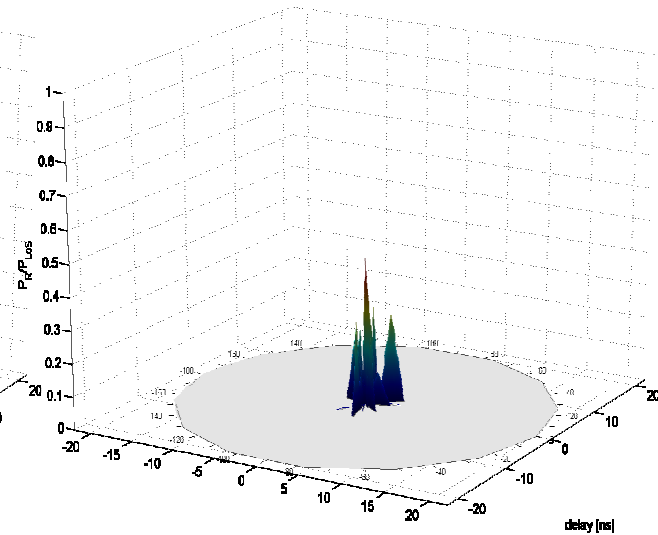
(c) Elevation PDAP

(d) Full PDAP

Figure C. 1. CIR and PDAPs for the small normal room scenario.
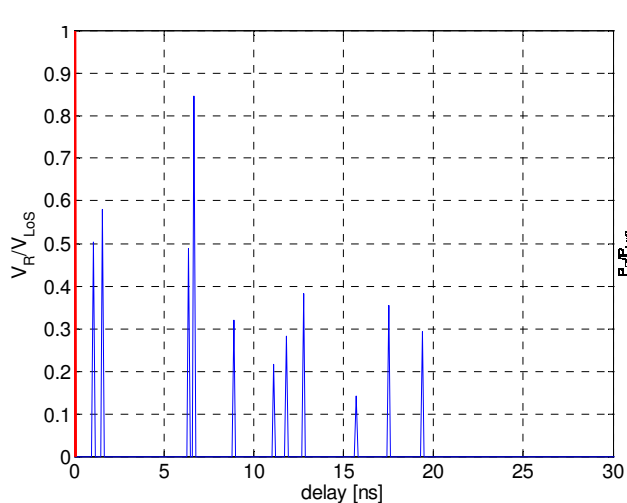
(a) CIR
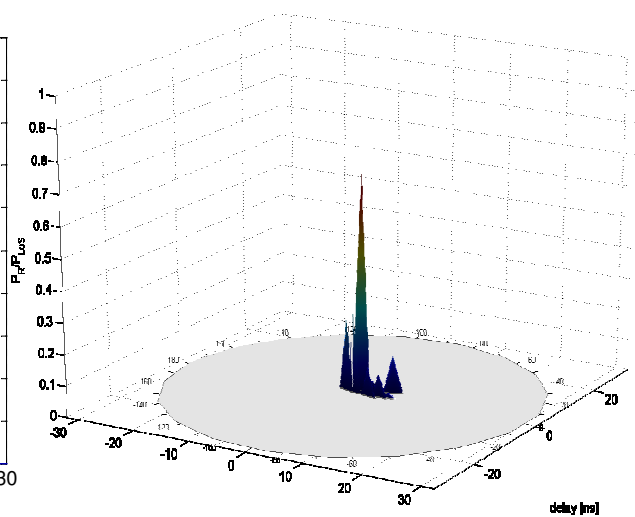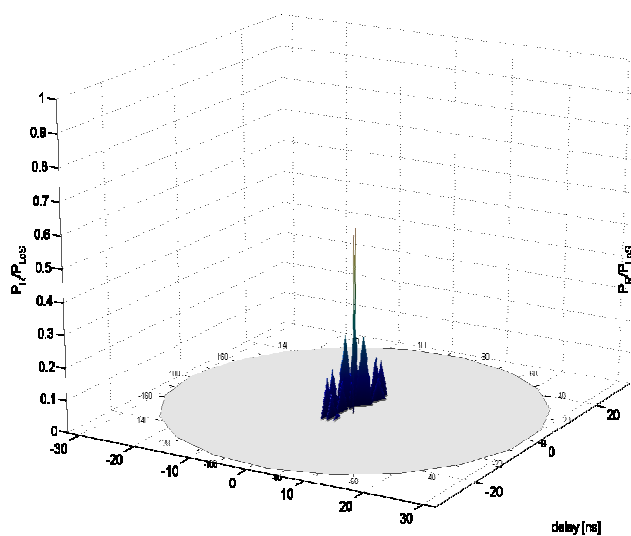
(b) Azimuth PDAP
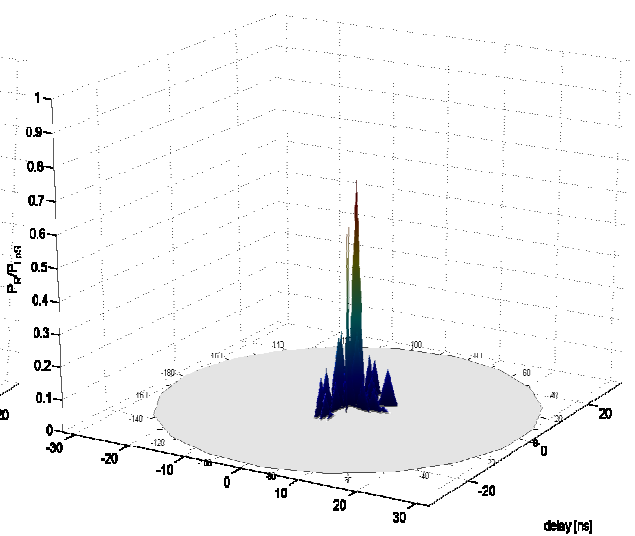
(c) Elevation PDAP

(d) Full PDAP

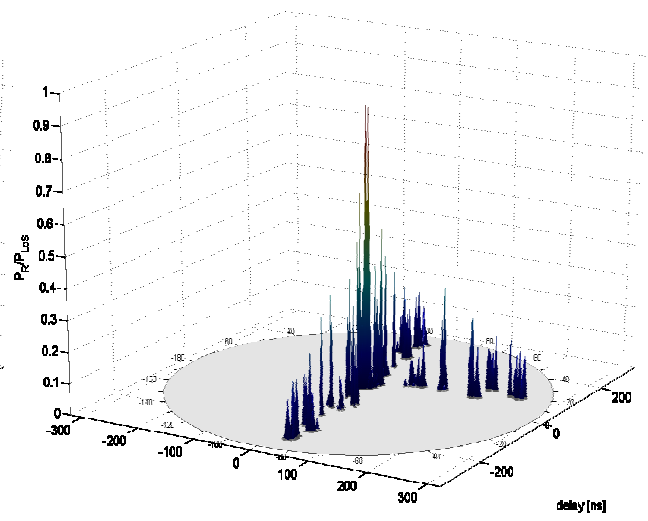Figure C. 2. CIR and PDAPs for the small office room.
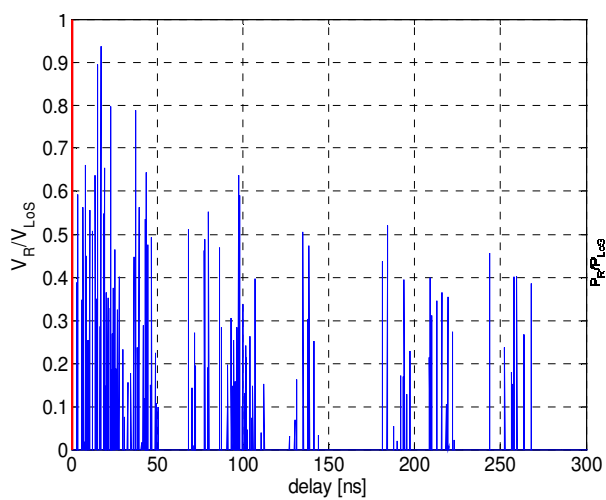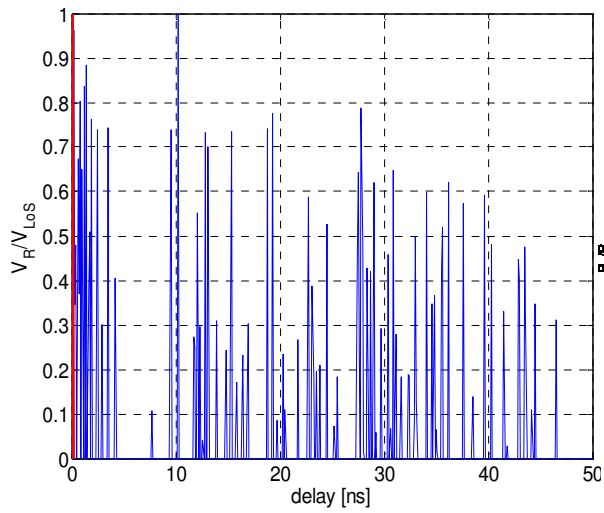

(a) CIR
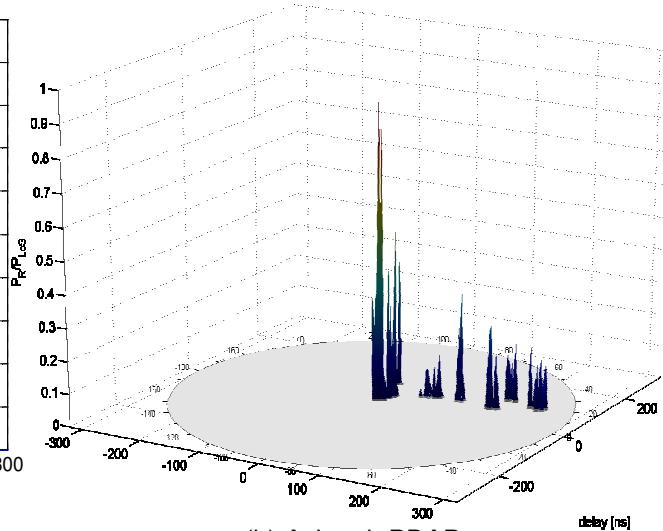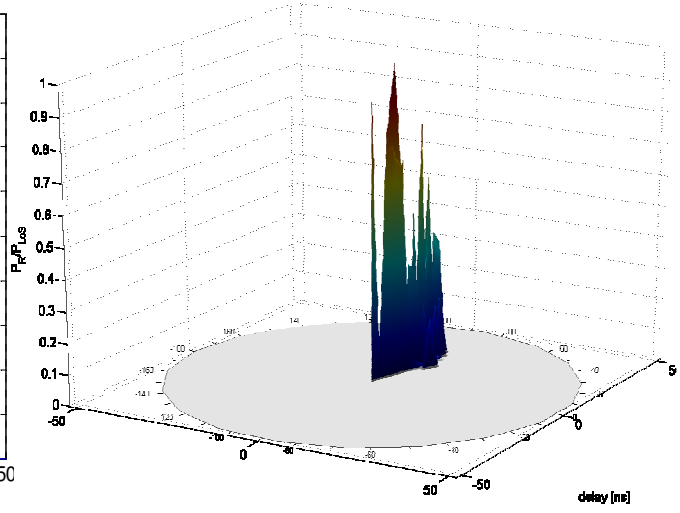

(b) Azimuth PDAP
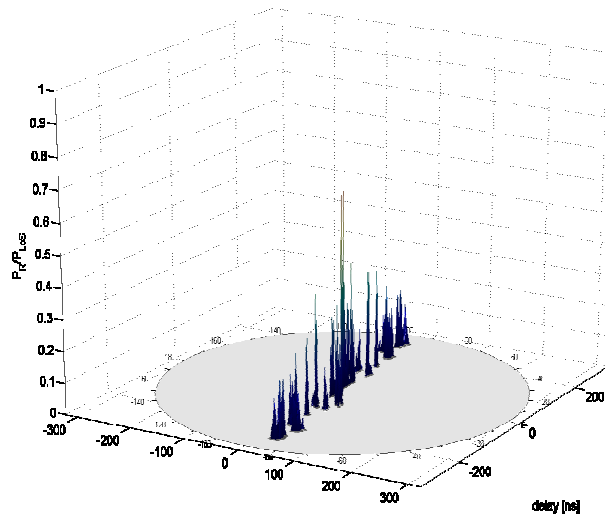
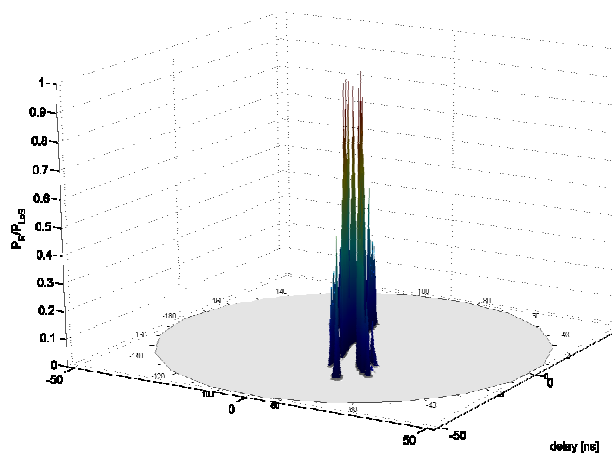(c) Elevation PDAP

(d) Full PDAP

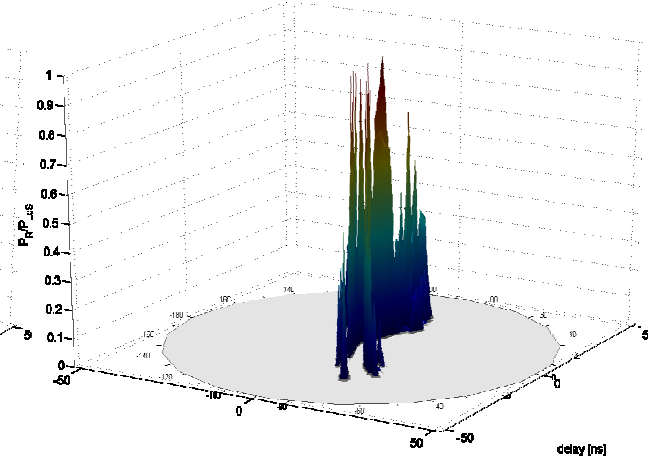Figure C. 3. CIR and PDAPs for the large room scenario.

(a) CIR

(b) Azimuth PDAP

(c) Elevation PDAP

(d) Full PDAP

Figure C. 4. CIR and PDAPs for the street scenario.

Annex D. Correlation between links

The following graphs consist of correlation between all pairs of input and output antennas for the different scenarios. The simulations were performed for two different values of system time resolution: 0.1 and 260 ns. Obtained values of correlation coefficients were averaged over 50 simulations.
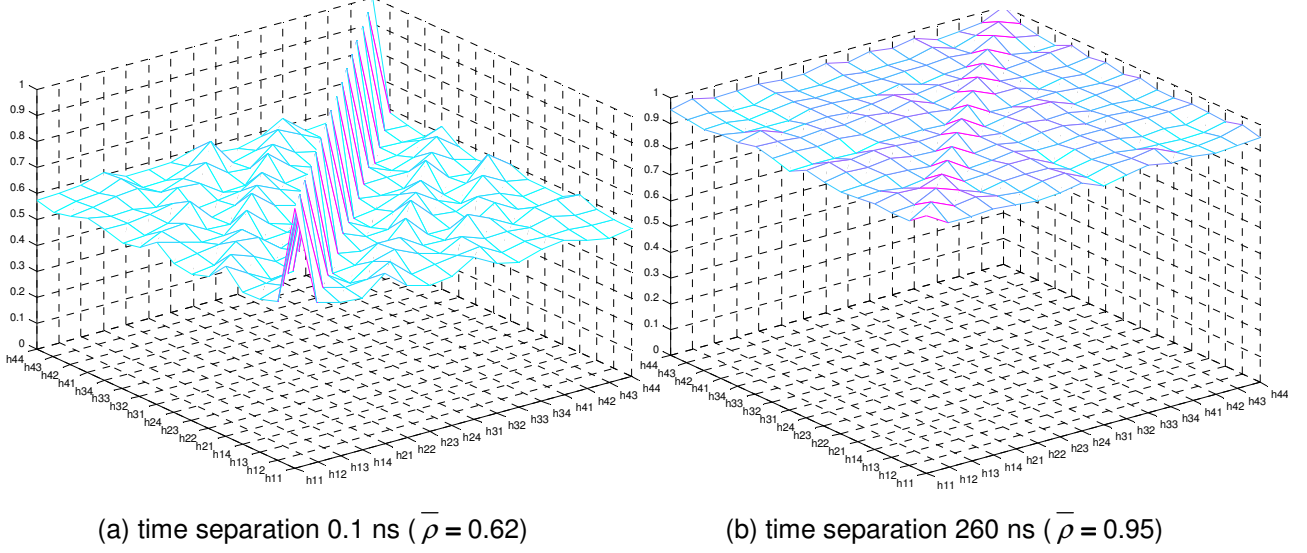

(a) time separation 0.1 ns ($\overline{\rho} = 0.62$)   (b) time separation 260 ns ($\overline{\rho} = 0.95$)

Figure D. 1. Correlation between links for the small normal room scenario.

(a) time separation 0.1 ns ($\overline{\rho} = 0.31$)   (b) time separation 260 ns ($\overline{\rho} = 0.95$)
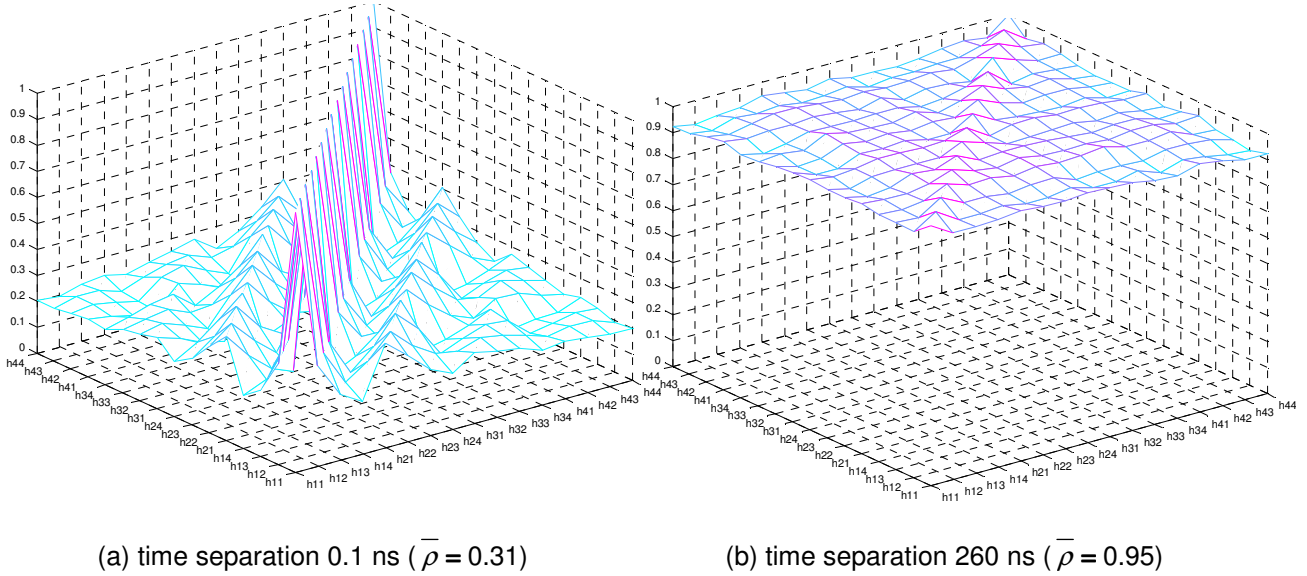
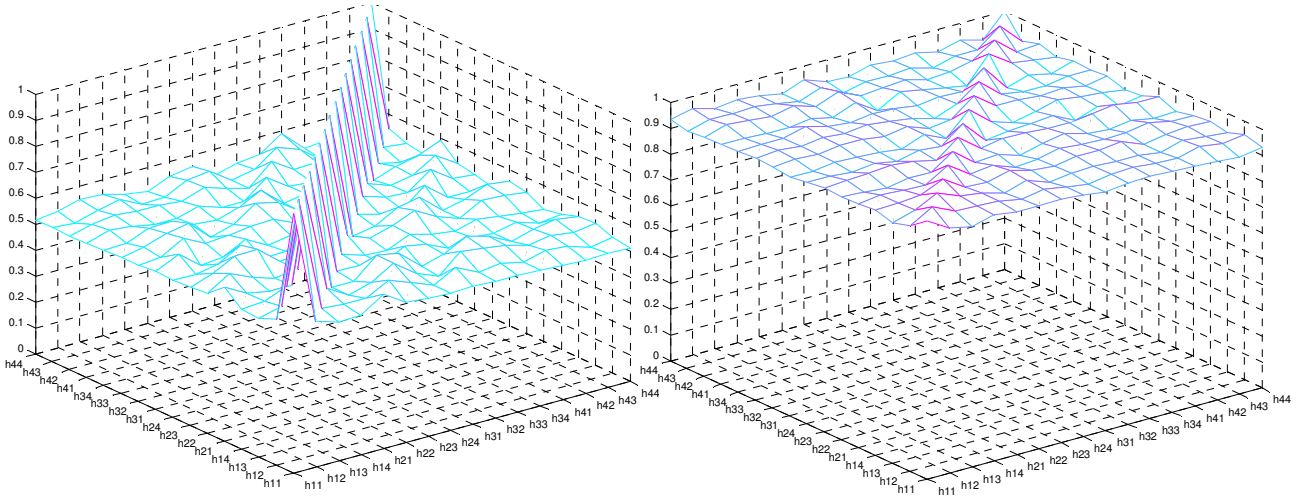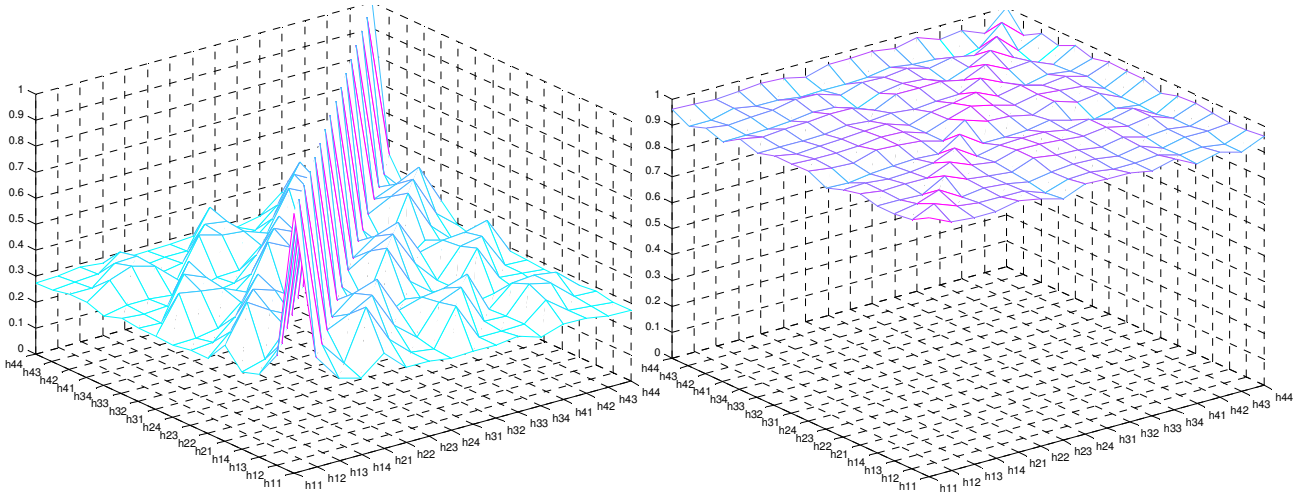Figure D. 2. Correlation between links for the large room scenario.

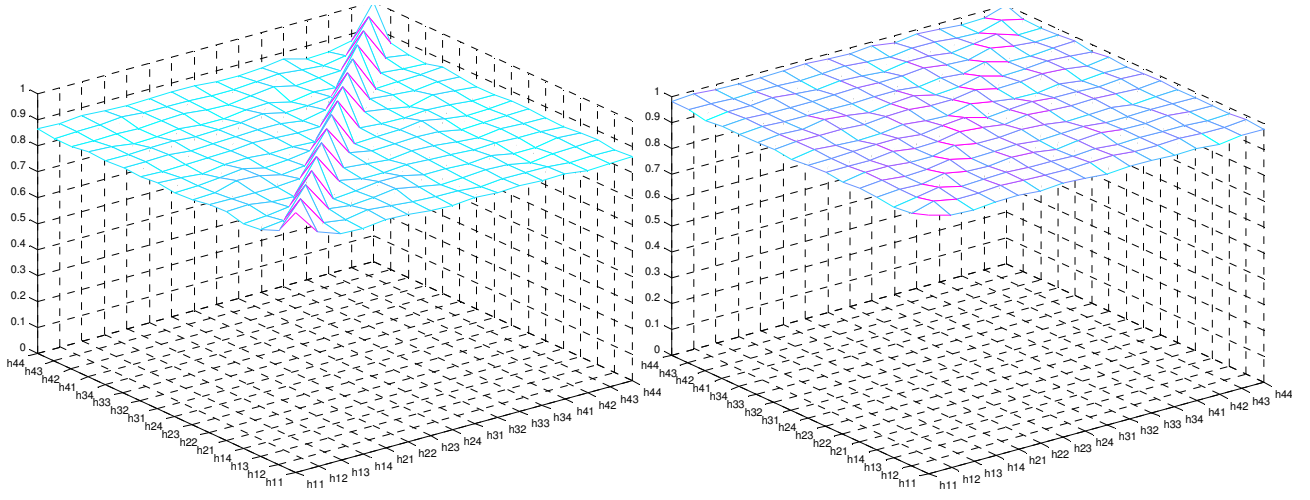(a) time separation 0.1 ns ($\bar{\rho} = 0.57$)   (b) time separation 260 ns ($\bar{\rho} = 0.93$)

Figure D. 3. Correlation between links for the small office room scenario.

(a) time separation 0.1 ns ($\bar{\rho} = 0.36$)   (b) time separation 260 ns ($\bar{\rho} = 0.96$)

Figure D. 4. Correlation between links for the street scenario.

(a) time separation 0.1 ns ($\bar{\rho} = 0.85$)   (b) time separation 260 ns ($\bar{\rho} = 0.97$)

Figure D. 5. Correlation between links for the reference room scenario.

Annex E. MIMO capacity gain

This annex presents the calculated values of the MIMO capacity gain, maximum and minimum capacity gain, SISO capacity gain and the relative MIMO capacity gain for all the considered scenarios and for different antennas configurations. One also presents the comparison between the 3D model and the 2D one in what concerns MIMO capacity gain, Table E. 1, for the two values of system time resolution: 0.1 and 260 ns.

Table E. 1. MIMO capacity gain for various scenarios and for the two models.

		reference room		normal room		office room		large room		street	
		0.1ns	260ns	0.1ns	260ns	0.1ns	260ns	0.1ns	260ns	0.1ns	260ns
2×2	3D	5.72	5.81	5.64	5.62	5.81	5.79	5.72	5.57	5.65	5.61
	2D	5.7	5.69	5.66	5.65	N/A		5.56	5.76	5.6	5.64
	3D to 2D [%]	0.35	2.07	-0.35	-0.53			2.80	-3.41	0.88	-0.53
4×2	3D	6.21	6.2	6.13	6.22	6.27	6.22	6.16	6.11	6.07	6
	2D	6.12	6.11	6.13	6.11	N/A		6.09	6.08	6.11	6.11
	3D to 2D [%]	1.45	1.45	0	1.77			1.14	0.49	-0.66	-1.83
4×4	3D	11.53	11	11.45	11.67	12	11.78	11.29	10.71	11.27	10.27
	2D	10.84	10.01	11.07	10.52	N/A		11.51	11.28	10.63	10.22
	3D to 2D [%]	5.98	9.00	3.32	9.85			-1.95	-5.32	5.68	0.49
8×2	3D	6.53	6.52	6.52	6.46	6.56	6.49	6.42	6.43	6.38	6.38
	2D	6.38	6.29	6.43	6.4	N/A		6.48	6.43	6.36	6.34
	3D to 2D [%]	2.30	3.53	1.38	0.93			-0.93	0	0.31	0.63

|											
8×4	3D	11.79	11.09	11.76	12.01	12.3	12.13	11.58	10.8	11.6	11
	2D	11.12	10.22	11.3	10.73	N/A		11.88	11.49	10.9	10.43
	3D to 2D [%]	5.68	7.84	3.91	10.66			-2.59	-6.39	6.03	5.18
8×8	3D	20.38	16.95	20.12	20.19	22.25	21.3	20.87	18.44	20.2	19.22
	2D	18.43	15.24	19.05	16.49	N/A		20.9	19.33	18.47	16.69
	3D to 2D [%]	9.57	10.09	5.32	18.33			-0.14	-4.83	8.56	13.16
16×2	3D	6.45	6.3	6.48	6.54	6.56	6.51	6.24	6.03	6.27	6.32
	2D	6.13	5.82	6.31	6.18	N/A		6.39	6.27	6.06	5.97
	3D to 2D [%]	4.96	7.62	2.62	5.50			-2.40	-3.98	3.35	5.54
16×4	3D	11.54	10.41	11.5	11.85	12.27	11.93	11.39	10.35	11.32	11.16
	2D	10.74	9.45	10.98	10.14	N/A		11.7	11.33	10.57	9.88
	3D to 2D [%]	6.93	9.22	4.52	14.43			-2.72	-9.47	6.63	11.47
16×8	3D	19.95	15.75	19.82	19.86	22.2	21.07	20.68	18.07	19.94	19.36
	2D	17.99	14.31	18.75	15.85	N/A		20.8	19.01	18.2	16.17
	3D to 2D [%]	9.82	9.14	5.40	20.19			-0.58	-5.20	8.73	16.48
16×16	3D	32.45	22.43	32.33	30.6	37.7	34.7	35.7	30.8	33.03	30.76
	2D	28.64	20.57	30.3	23.68	N/A		34.53	30.86	30.35	26.63
	3D to 2D [%]	11.74	8.29	6.28	22.61			3.28	-0.19	8.11	13.43
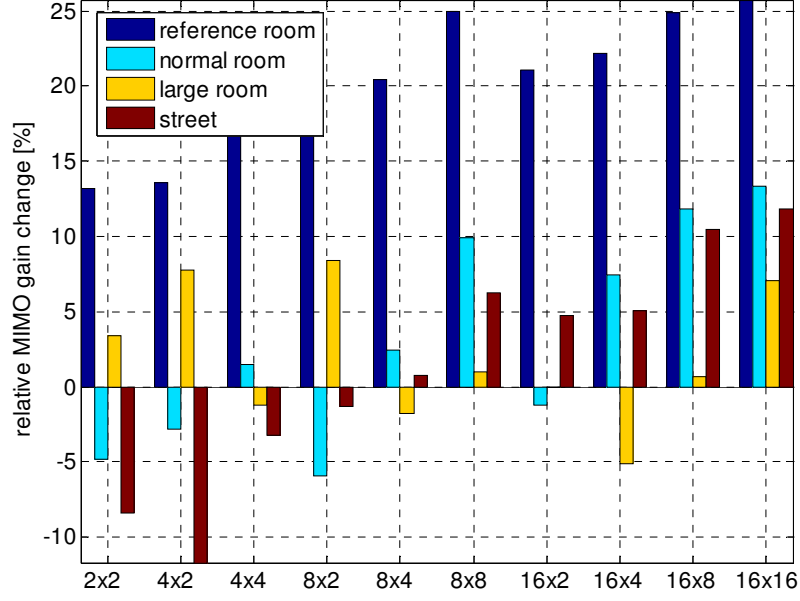
Figure E. 1. Difference in relative MIMO gain between 3D and 2D model for a time resolution of 260ns.
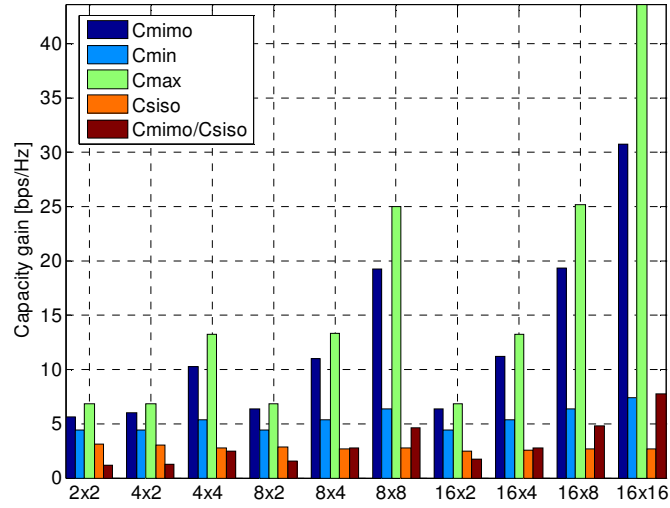

Figure E. 2. MIMO gain for the street scenario for a time resolution of 0.1ns.
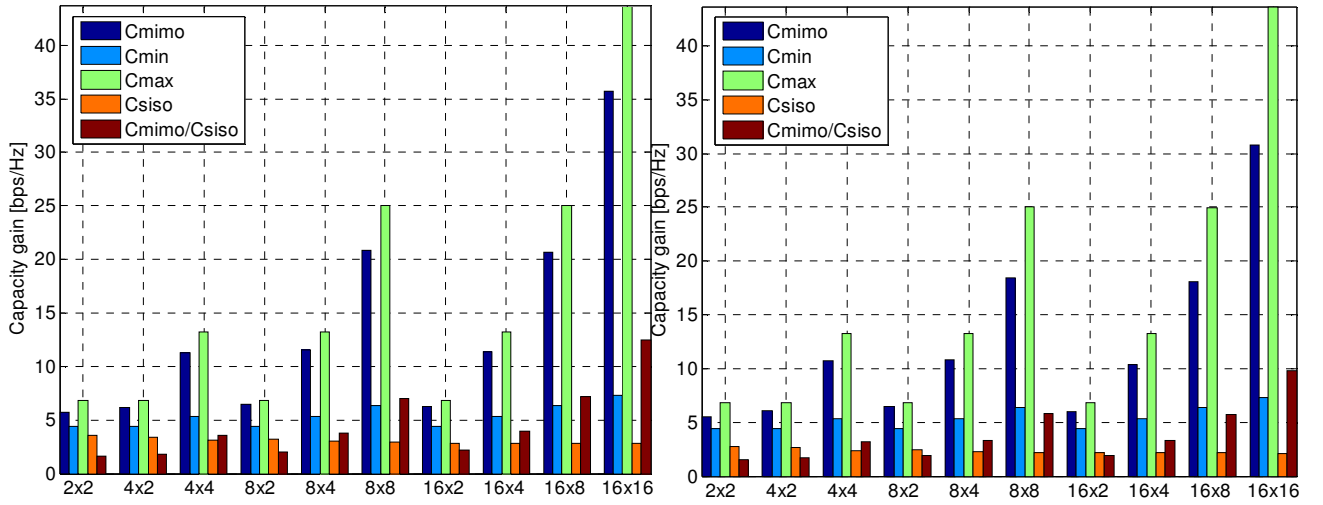

Figure E. 3. MIMO gain for the large room scenario for a time resolution of 0.1 and 260 ns, respectively.
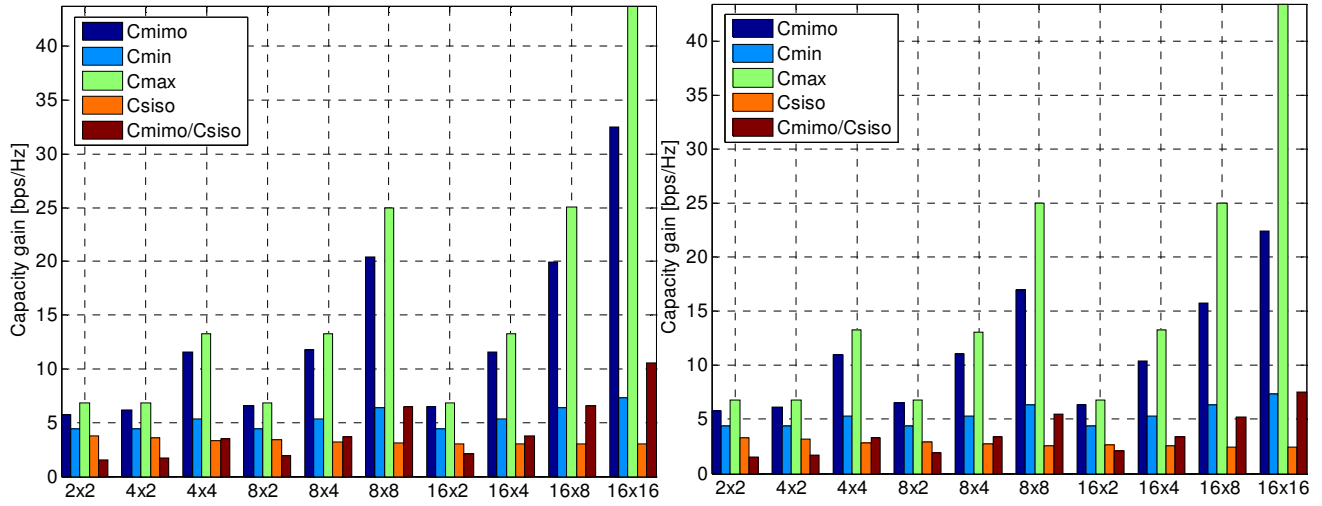
Figure E. 4. MIMO gain for the reference room scenario for a time resolution of 0.1 and 260 ns, respectively.
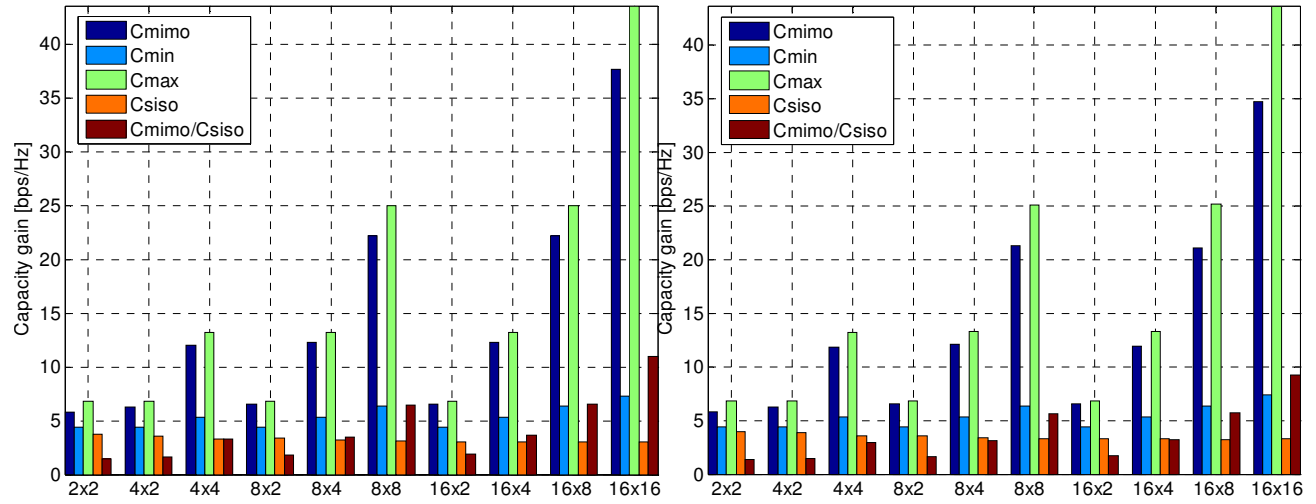

Figure E. 5. MIMO gain for the small office room scenario for a time resolution of 0.1 and 260 ns, respectively.
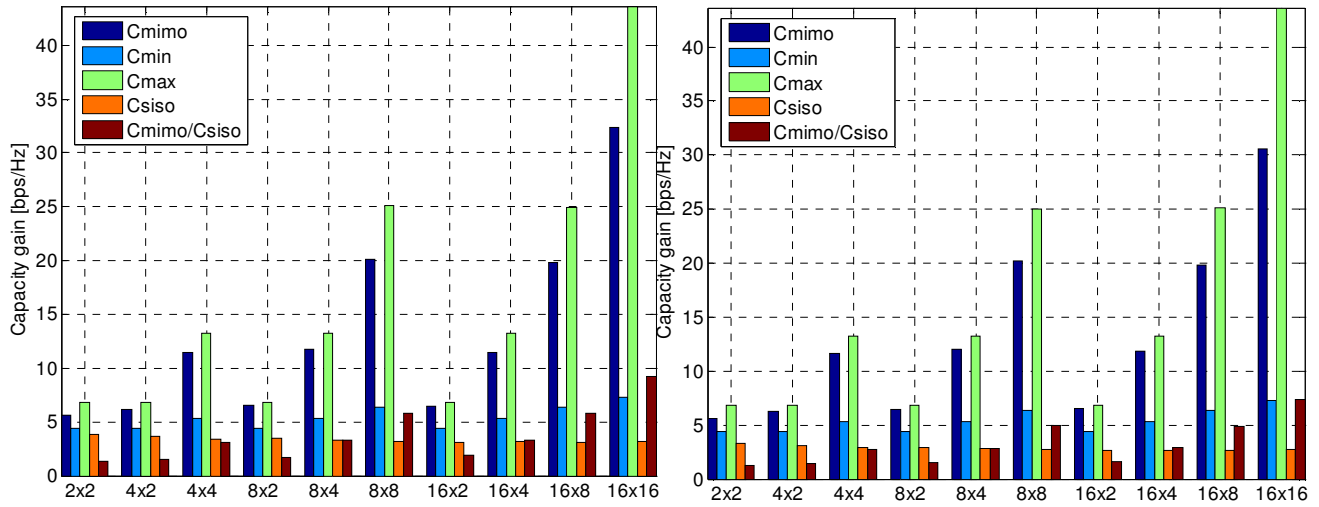

Figure E. 6. MIMO gain for the small normal room scenario for a time resolution of 0.1 and 260 ns, respectively.
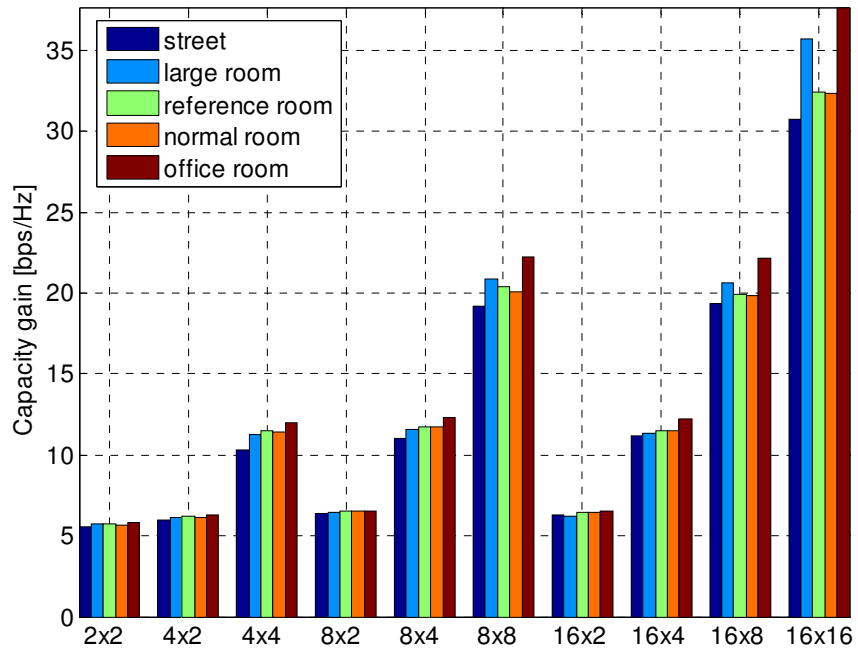
Figure E. 7. MIMO gain for a time resolution of 0.1 ns for the different scenarios.

References

[3GPP08]   http://www.3gpp.org/, Feb. 2008.

[ABBC07]   Almers,P., Bonek,E., Burr,A., Czink,N., Debbah,M., Degli-Esposti,V., Hofstetter,H., Kyosti,P., Laurenson,D., Matz,G., Molisch,A.F., Oestges,C. and Ozcelik,H., "Survey of Channel and Radio Propagation Models for Wireless MIMO Systems", *EURASIP Journal on Wireless Communications and Networking*, Vol. 2007, No. 19070, 2007.

[ATEM02]   Almers,P., Tufvesson,F., Edfors,O. and Molisch,A., "Measured Capacity gain using waterfilling in frequency selective MIMO channels", in *Proc. of PIMRC'02 - 13th IEEE International Symposium on Personal, Indoor and Mobile Radio Communications*, Lisbon, Portugal, Sep. 2002.

[Burr03]   Burr,A., "Capacity bounds and estimates for the finite scatterers MIMO wireless channel", *IEEE Journal on Selected Areas in Communications*, Vol. 21, No. 5, June 2003, pp. 812-818.

[ChFV00]   Chizhik,D., Foschini,G.J. and Valenzuela,R.A., "Capacities of Multi-Element Transmit and Receive Antennas: Correlations and Keyholes", *Electronic Letters*, Vol. 36, No. 13, June 2000, pp. 1099-1100.

[Corr01]   Correia,L.M. (ed.), *Wireless Flexible Personalised Communications (COST 259 Final Report)*, John Wiley, Chichester, UK, 2001.

[Corr06]   Correia,L.M. (ed.), *Mobile Broadband Multimedia Networks*, Academic Press, London, UK, 2006.

[Corr08]   Correia,L.M., *Mobile Communication Systems* (in Portuguese), Course Notes, IST-TUL, Lisbon, Portugal, 2008.

[CWTN07]   Czink,N., Wyne,S.R.T., Tufvesson,F., Nuutien,J.P., Ylitalo,J., Bonek,E., Molisch,A.F., "Tracking Time-Variant Cluster Parameters in MIMO Channel Measurements", in *Proc. of CNC'07 - Communications and Networking in China*, Shanghai, China, Aug. 2007.

[Czin07]   Czink,N., *The Random-Cluster Model – A Stochastic MIMO Channel Model for Broadband Wireless Communication Systems of the 3rd Generation and Beyond*, PhD Thesis, TU Vienna, Dec. 2007.

[DeMu05]   Debbah,M. and Muller,R.R., "MIMO channel modeling and the principle of maximum entropy", IEEE Transactions on Information Theory, Vol. 51, No. 5, May 2005, pp. 1667-1690.

[Dziu04]   Dziunikowski,W., Multiple-Input Multiple-Output (MIMO) Antenna Systems, in Chandran,S. (ed.), Adaptive Antenna Arrays, Springer, Berlin, Germany, 2004.

[ErHS01]   Erceg,V., Hari,K.V.S. and Smith,M.S., Channel models for fixed wireless applications, IEEE 802.16 Broadband Wireless Access Working Group, Contribution IEEE 802.16.3c-01 29r4, 2001, (http://www.nari.ee.ethz.ch/commth/pubs/p/EHSB01).

[ErSK04]   Erceg,V., Schumacher,L. and Kyritsi,P., TGn channel models, Tech. Rep. IEEE P802.11, Wireless LANs, Garden Grove, CA, USA, 2004, (http://www.802wirelessworld.com/8802).

[FoGa98]   Foschini,G.J. and Gans,M.J., "On Limits of Wireless Communications in a Fading Environment when Using Multiple Antennas", *Wireless Personal Communication*, Vol. 6, No. 3, Autumn 1998, pp. 311-335.

[GCFP01]   Gil,F., Claro,A.R., Ferreira,J.M., Pardelinha,C. and Correia,L.M., "A 3D Interpolation Method for Base-Station-Antenna Radiation Patterns", *IEEE Antennas and Propagation Magazine*, Vol. 43, No. 2, April 2001.

[GiCo06]   Gil,J.M. and Correia,L.M., "Comparing Adaptive Beamforming in Micro- and Macro-Cells", *IEEE Transactions on Antennas and Propagation*, Vol. 54, No. 2, Feb. 2006, pp. 629-637.

[HoMC06]   Hofstetter,H., Molisch,A.F. and Czink,N., "A twin-cluster MIMO channel model", in Proc. EuCAP 2006 - The European Conference on Antennas and Propagation, Nice, France, Nov. 2006.

[HoTo04]   Holma,H. and Toskala,A. (eds.), *WCDMA for UMTS*, John Wiley, Chichester, UK, 2004.

[HoTo06]   Holma,H. and Toskala,A., *HSDPA/HSUPA for UMTS* (1st Edition), John Wiley & Sons, Chichester, UK, 2006.

[ISTW08]   http://www.ist-winner.org/, February 2008.

[Koko05]   Kokoszkiewicz,H., MIMO Geometrically Based Channel Model, M. Sc. Thesis, IST-TUL, Lisbon, Portugal, 2005.

[KuMC08]   Kuipers,B.W.M., Mackowiak,M., Correia,L.M., *Evaluating Geometrically Based Multiple Bounce Channel Models*, WPMC 2008, Ivalo, Finland, Sep. 2008.

[Lee73]   Lee,W.C.Y., "Effects on correlation between two mobile base-station antennas", IEEE Transactions on Communications, Vol. COM-21, No. 11, Nov. 1973, pp. 1214-1224.

[Mack07]   Mackowiak,M., *Geometrically Based Multibounce MIMO Channel Models,* M. Sc. Thesis, IST-TUL, Lisbon, Portugal, 2007.

[MaCo04]   Marques,M.G. and Correia,L.M., *A Wideband Directional Channel Model for Mobile Communication Systems*, in Chandran,S. (ed.), *Adaptive Antenna Arrays*, Springer, Berlin, Germany, 2004.

[MKLH03]   A.F.Molisch, A.Kuchar, J.Laurila, K.Hugl, and R.Schmalenberger, "Geometry-based directional model for mobile radio channels – principles and implementation", *European Transactions on Telecommunications*, Vol. 14, No. 4, 2003, pp. 351-359.

[MKLH99]   Molisch,A.F., Kuchar,A., Laurila,J., Hugl,K. and Bonek,E., "Efficient Implementation of a Geometry-Based Directional Model for Mobile Radio Channels", in Proc. VTC'99 Fall - 50th IEEE Vehicular Technology Conference, Amsterdam, Netherlands, Sep. 1999.

[Moli05]   Molisch,A.F., *Wireless Communications*, John Wiley, Chichester, UK, 2005.

[MPSF08]   Mammasis, K., Pfann, E., Stewart, R.W. and Freeland,G., "Three-dimensional channel modelling using spherical statistics for smart antennas", Electronic Letters, Vol. 44, No. 2, January 2008.

[OeCl07]   Oestges,C. and Clerckx,B., *MIMO Wireless Communications*, Academic Press, Oxford, UK, 2007.

[OzCB05]   Ozcelik,H., Czink,N. and Bonek,E., "What Makes a Good MIMO Channel Model?", in Proc. of VTC'05 Spring - 61st IEEE Vehicular Technology Conference, Stockholm, Sweeden, June 2005.

[Pras98]   Prasad,R., *Universal Wireless Personal Communications*, Artech House, London, UK, 1998.

[Proa01]   Proakis, J.,G., *Digital Communications*, MacGraw Hill, New York, USA, 2001.

[SaVa87]   Saleh,A.M. and Valenzuela,R.A., "A Statistical Model for Indoor Multipath Propagation", IEEE Journal on Selected Areas in Communications, Vol. 5, No.2, Feb 1987, pp. 128-137.

[Saye02]   Sayeed,A.M., "Deconstructing multiantenna fading channels", IEEE Transactions on Signal Processing, Vol. 50, No. 10, Oct. 2002, pp. 2563-2579.

[SBMS04]   Schumacher,L., Berger,L.T., Ramiro-Moreno,J. and Sorensen,T.B., Propagation Characterisation and MIMO Channel Modeling for 3G, in Chandran,S. (ed.), Adaptive Antenna Arrays, Springer, Berlin, Germany, 2004

[Suzu77]   "A statistical model for urban radio propagation", IEEE Transactions on Communications, Vol. 25, No. 7, July 1977, pp. 673-680.

[Svan02]   Svantesson,T., "A Double-Bounce Channel Model for Multi-Polarized MIMO Systems", in Proc. VTC 2002 Fall - 56th IEEE Vehicular Technology Conference, Vancouver, Canada, Sep. 2002.

[SZSM06]   Shafi,M., Zhang,M., Smith, P.J., Moustakas,A.L., Molisch,A.F., "The Impact of Elevation Angle on MIMO Capacity", IEEE ICC 2006, pp. 4155-4160.

[UMTS07]   http://www.umts-forum.org, October 2007.

[WHOB06]   Weichselberger,W., Herdin,M., Ozcelik,H. and Bonek,E., "A stochastic MIMO channel model with joint correlation of both link ends", IEEE Transactions on Wireless Communications, Vol. 5, No. 1, Jan. 2006, pp. 90-99.

[WiMF06b]   "Mobile WiMAX – Part II: A Comparative Analysis", WiMAX Forum, May 2006.

[YLCP04]   Yu,K., Li,Q., Cheung,D. and Prettie,C., "On the tap and cluster angular spreads of indoor WLAN channels", *Proceedings of IEEE Vehicular Technology Conference*, Milano, Italy, May 2004.

[ZwFW02]   Zwick,T., Fischer,C. and Wiesbeck,W., "A stochastic multipath channel model including path directions for indoor environments", IEEE Journal on Selected Areas in Communications, Vol. 20, No. 6, Aug. 2002, pp. 1178-1192.